NAVAL POSTGRADUATE SCHOOL

Monterey, California

THESIS

ANALYSIS OF THE TIP LEAKAGE FLOW FIELD IN
AN AXIAL TURBINE

by

C. Scott Anderson

June 1999

Thesis Advisor: Garth V. Hobson

Approved for public release; distribution is unlimited.

19991213 015

REPORT DOCUMENTATION PAGE

Form Approved
OMB No. 0704-0188

1. AGENCY USE ONLY *(Leave blank)*	2. REPORT DATE June 1999	3. REPORT TYPE AND DATES COVERED Engineer's Thesis

4. TITLE AND SUBTITLE ANALYSIS OF THE TIP LEAKAGE FLOW FIELD IN AN AXIAL TURBINE	5. FUNDING NUMBERS Contract Number N00421-4219WA016220
6. AUTHOR(S) Anderson, C. Scott	
7. PERFORMING ORGANIZATION NAME(S) AND ADDRESS(ES) Naval Postgraduate School Monterey, CA 93943-5000	8. PERFORMING ORGANIZATION REPORT NUMBER
9. SPONSORING / MONITORING AGENCY NAME(S) AND ADDRESS(ES) Commander, Naval Air Systems Command, AIR 4.4 Bldg. 2272, 47123 Buse Rd., Patuxent River, MD 20670	10.SPONSORING/MONITORING AGENCY REPORT NUMBER

11. SUPPLEMENTARY NOTES
The views expressed in this thesis are those of the author and do not reflect the official policy or position of the Department of Defense or the U.S. Government.

12a. DISTRIBUTION / AVAILABILITY STATEMENT Approved for public release; distribution is unlimited.	12b. DISTRIBUTION CODE

13. ABSTRACT

Comparisons of experimental laser-Doppler-velocimetry measurements using the Naval Postgraduate School cold-flow turbine test rig were made with 3D viscous computational fluid dynamics flow solutions. The turbine tested was the first stage of the Pratt and Whitney designed High Pressure Fuel Turbopump for the Space Shuttle Main Engine. The laser anemometer was modified to incorporate a field stop, which acted as a spatial filter to limit reception of undesired blade reflections. The laser measurements were made in the endwall region of the test turbine, at three axial locations, and at three radial depths. For each location, absolute flow angle, axial and tangential velocity ratios, turbulence intensities and correlation coefficients were measured. The computational effort encompassed modeling a single blade passage of both the stator and the rotor and computing flow solutions of the stage using NASA software. Exit plane and endwall flow property profiles showed good agreement when compared with experimental data. A quasi-three-dimensional flow analysis of stator wake/rotor flow interaction was completed to investigate the unsteady effects neglected when "plane averaging" flow properties between blade rows during the full three-dimensional simulation.

14. SUBJECT TERMS Laser Doppler Velocimetry, Computational Fluid Dynamics, Annular Turbine Endwall Region Flow Analysis	15. NUMBER OF PAGES 189
	16. PRICE CODE

17. SECURITY CLASSIFICATION OF REPORT Unclassified	1. SECURITY CLASSIFICATION OF THIS PAGE Unclassified	19. SECURITY CLASSIFICATION OF ABSTRACT Unclassified	20. LIMITATION OF ABSTRACT UL

NSN 7540-01-280-5500

Standard Form 298 (Rev. 2-89)
Prescribed by ANSI Std 239-18

ANALYSIS OF THE TIP LEAKAGE FLOW FIELD IN AN AXIAL TURBINE

C. Scott Anderson
Commander, United States Navy
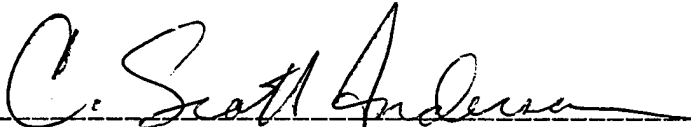B.S., United States Naval Academy, 1983

Submitted in partial fulfillment of the
requirements for the degree of

AERONAUTICAL ENGINEER

From the

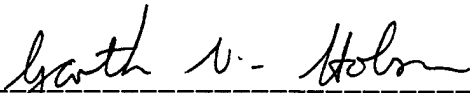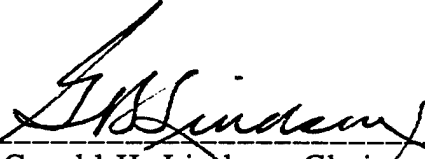**NAVAL POSTGRADUATE SCHOOL**
June 1999

Author: _____
C. Scott Anderson

Approved by: _____
Garth V. Hobson, Thesis Advisor

_____
Raymond P. Shreeve, Second Reader

_____
Gerald H. Lindsey, Chairman
Department of Aeronautics and Astronautics

iii

ABSTRACT

Comparisons of experimental laser-Doppler-velocimetry measurements using the Naval Postgraduate School cold-flow turbine test rig were made with 3D viscous computational fluid dynamics flow solutions. The turbine tested was the first stage of the Pratt and Whitney designed High Pressure Fuel Turbopump for the Space Shuttle Main Engine. The laser anemometer was modified to incorporate a field stop, which acted as a spatial filter to limit reception of undesired blade reflections. The laser measurements were made in the endwall region of the test turbine, at three axial locations, and at three radial depths. For each location, absolute flow angle, axial and tangential velocity ratios, turbulence intensities and correlation coefficients were measured. The computational effort encompassed modeling a single blade passage of both the stator and the rotor and computing flow solutions of the stage using NASA software. Exit plane and endwall flow property profiles showed good agreement when compared with experimental data. A quasi-three-dimensional flow analysis of stator wake/rotor flow interaction was completed to investigate the unsteady effects neglected when "plane averaging" flow properties between blade rows during the full three-dimensional simulation.

TABLE OF CONTENTS

LIST OF FIGURES

xiii

LIST OF TABLES

LIST OF SYMBOLS

α	Absolute flow angle
θ	Tangential direction
r	Radial direction
z	Axial direction
T_z	Axial turbulence intensity
T_θ	Tangential turbulence intensity
X_z	Non-dimensional mean axial velocity
X_θ	Non-dimensional mean tangential velocity
c_{mz}	Mean axial velocity
$c_{m\theta}$	Mean tangential velocity
c'_z	Fluctuating axial velocity
c'_θ	Fluctuating tangential velocity
$c_{\theta z}$	Correlation coefficient
ρ	Density
u	Axial velocity (CFD)
v	Tangential velocity (CFD)
w	Radial velocity (CFD)
e	Specific internal energy
k	Kinetic energy of turbulent fluctuations per unit mass
ω	Rate of dissipation per unit turbulence kinetic energy
μ	Molecular viscosity
μ_T	Eddy viscosity
Re	Reynolds number
Re_T	Turbulent Reynolds number
M	Mach number
c_t	Tip chord
C_p	Specific heat at constant pressure
T_{01}	Total freestream temperature

I. INTRODUCTION

A. PURPOSE

The purpose of the present study was to help assess new computer-analysis methods for turbomachinery flow fields by obtaining experimental measurements, performing computational predictions, and comparing the results. In particular the endwall and tip leakage flows of a turbine were examined so that losses associated with these flows could be quantified.

B. OVERVIEW

The turbine used in the study was the first stage turbine of the Space Shuttle Main Engine (SSME) High-Pressure Fuel TurboPump (HPFTP) Alternate Turbopump Development model, designed by Pratt and Whitney, and shown in Figure 1.
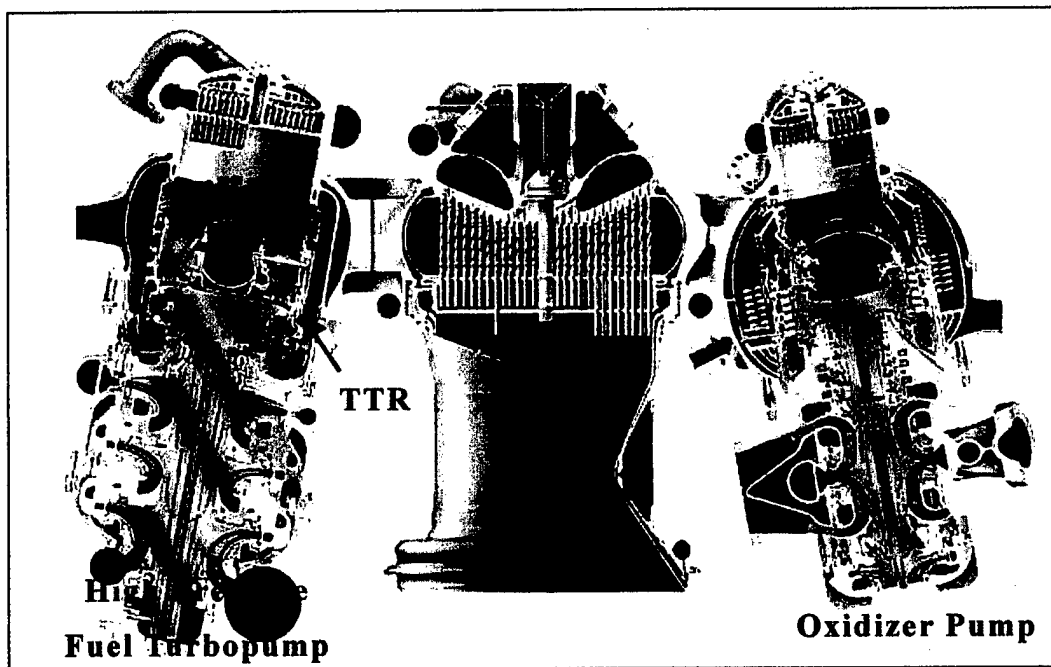
Figure 1. Space Shuttle Main Engine Cutaway [Ref. 1]

The SSME HPFTP, as described by Sutton in [Ref.2], consisted of a two stage axial flow turbine of the reaction-impulse type which, when installed, was driven by a steam/hydrogen gas mixture and drove a three stage liquid hydrogen pump. The turbine was designed to operate with an inlet temperature and pressure of 1900 °R and 5200 psia respectively. At 37,000 RPM, the pump produced 73,000 shaft horsepower.

The SSME HPFTP was experimentally tested in the Turbine Test Rig (TTR) of the Turbopropulsion Laboratory (TPL) at the Naval Postgraduate School (NPS). Laser Doppler velocimetry (LDV) was used to measure flow field velocity. The laser powering the LDV was an Argon Ion Lexel model rated at four Watts. The two-component LDV setup was capable of velocity measurements in the axial and circumferential or tangential directions. LDV measurements were made in the rotor endwall region at a total of nine locations composed of three depths at each of three axial locations. Measurements were performed using cold compressed air to drive the turbine at 5,000 RPM.

Complementary Computational Fluid Dynamic (CFD) flow predictions were made using 3D grid generation and viscous flow solver computer codes developed by Dr. Chima of the NASA Glenn Research Center. The flow solutions were computed using both the NPS CRAY Y-MP 94 supercomputer and a multi-processor Silicon Graphics workstation. A turbine stage composed of stator, rotor and tip gap grids was built using Turbomachinery C-Grid (TCGRID) [Ref. 3]. The combined grid flow solution was computed using the SWIFT program [Ref. 4]. The code permitted relative rotation of the stator and rotor grids, and incorporated multiple turbulence models. To begin an investigation of flow unsteadiness, a quasi-3D analysis was performed using the RVCQ3D code [Ref. 5] modified to permit non-averaged periodic upstream boundary conditions on the rotor grid.

2

Experimental and computational results were analyzed, and compared, where possible. In the exit plane, test results from previous Cobra Probe survey experiments [Ref. 6] were compared with computational predictions. In the endwall region LDV measurements were compared with computational predictions.

C. BACKGROUND

The evolution of turbomachinery design has been driven by the need for increased propulsive engine power, efficiency and reliability. A significant portion of the power/efficiency loss that occurs in modern engine designs is due to turbine tip leakage and secondary flows in the endwall region. For further performance improvements, a thorough knowledge of these complex flows is necessary. To this end, two objectives must be met: 1) accurate experimental measurement of the critical turbomachinery flow fields, and 2) development of validated computer software for modeling and simulation to use during design.

1. LDV Experimental Measurement

Few measurement techniques are able to determine the unsteady and complex flows within turbomachinery. The measurement of flow between blades of a spinning rotor requires a non-intrusive sensor capable of measuring velocity at locations, which are known precisely, to thousandths of an inch. LDV has emerged as the most useful technique, capitalizing on the inherent precision of the directed laser beams, and the development of extremely fast digital acquisition/processing systems. Although the first LDV measurements within turbomachinery were completed over 20 years ago [Ref. 7], reports of axial turbine flow field measurements are limited. The most comprehensive was a two-part report by Zaccaria and Lakshminarayana [Refs. 8 and 9] in which LDV measurements were taken at mid-span, both within and downstream of the

3

rotor passage of a single stage turbine, with an emphasis on the stator wake/rotor flow field interaction.

The NPS TPL cold-flow turbine test facility was designed and constructed for the purpose of making LDV measurements in the turbine blade tip gap region. Several previous students have worked and reported on this project. Studevan [Ref. 10] initiated the design and, in 1993, installed the first stage turbine of the SSME HPFTP (acquired from Pratt and Whitney), the inlet ducting, and the dynamometer. Rutkowski [Ref. 11] completed installation of the turbine itself, and added instrumentation to initiate mapping of turbine performance. Greco [Ref. 12] integrated a PC-based data acquisition system and optical window for future LDV measurements, and performed a cobra-probe exit flow survey to complete a mapping of the turbine performance characteristics. Southward [Ref. 13] installed the LDV system and obtained initial LDV measurements. McKee [Ref. 6] performed additional LDV measurements and Cobra probe surveys at the first stage rotor exit plane for comparison with CFD solutions.

2. Computational Fluid Dynamics (CFD)

CFD is the numerical representation of the fundamental equations governing fluid flow and the "marching" of these equations, in time and/or space, to obtain a complete numerical description of the flow field of interest. In 1947, Kopal, who compiled solution tables of supersonic flow over sharp cones using a "primitive digital computer", completed the first major example of CFD work [Ref. 14]. In the 1950's and 1960's the first "generation" of CFD solutions were necessary to solve the high-speed, high-temperature reentry body problem. The complexity of this problem required the use of high-speed digital computers. The ensuing exponential increase in digital computer processing speed has allowed CFD to emerge as a "third dimension" in fluid dynamics, an intermediate

4

between pure theory and pure experiment [Ref. 14]. Since certain aspects of the flow, such as turbulence, are modeled by equations based on empirical data, the accuracy of the solution is subject not only to truncation error and computer accuracy, but also the accuracy of empirical based models.

Turbomachinery flow is both complex and relatively inaccessible to physical measurements. CFD codes have been developed to specifically address turbomachinery flow. NASA Lewis Research Center, now NASA Glenn, developed the series of codes used during the present work. Rutkowski [Ref. 11] used TCGRID and RVC3D to develop a relatively coarse 3D solution of the SSME HPFTP stator blade. Greco [Ref. 12] developed the adjacent rotor grid solution using the same software. McKee [Ref. 6], combined the stator and rotor grids, incorporated a step in the outer casing, and developed a relatively coarse grid solution for the stage using the SWIFT flow solver with the Baldwin-Lomax turbulence model.

II. DESCRIPTION OF EXPERIMENTAL FACILITY AND FLOW SOLVERS

A.   TURBINE TEST RIG

Laser Doppler velocimetry measurements were made within the axial turbine of the Turbine Test Rig at the Turbopropulsion Laboratory shown in Figure 2.
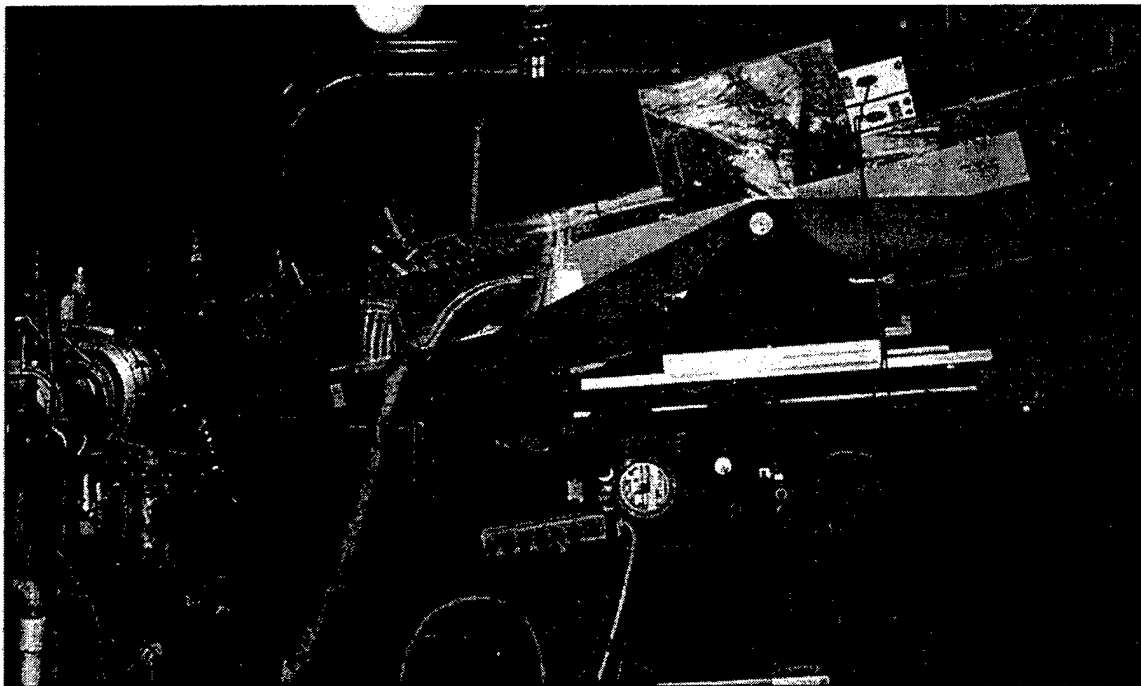
Figure 2. Turbine Test Rig and Laser Doppler Velocimeter

The experimental apparatus consisted of an air supply system, the test turbine, laser and optics, instrumentation, and two data acquisition systems.

1.   Air Supply System

The air to drive the test turbine was supplied by an Allis-Chalmers twelve-stage axial compressor driven by a 1250 horsepower electric motor. Torque from the motor was transmitted to the compressor via a

7

hydraulic coupling and mechanical gearbox. The compressor was operated at a constant 12,000 RPM, providing a maximum airflow rate of 10,000 CFM. Both the electric motor and the hydraulic coupling were rebuilt prior to commencing turbine testing. The compressor air was cooled via an air/water heat exchanger and then routed via 8-10 in. steel piping, which incorporated a mass flow measurement orifice, to the turbine test cell. A schematic of the air supply system is shown in Figure 3. [Ref. 13] Within the test cell, the air entered a plenum chamber and passed through a honeycomb/screen arrangement upstream of the turbine. With a constant supply of compressor air, flow rate through the turbine was controlled by manually adjusting two electrically-driven dump valves and a single electrically-driven supply valve from a control console in a room adjacent to the test cell.
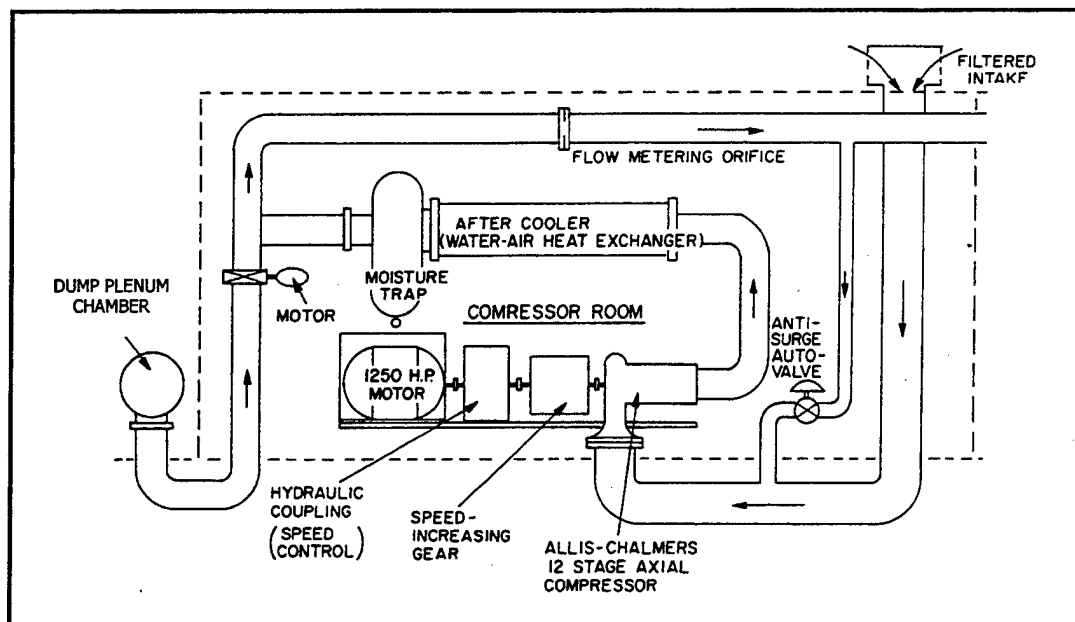
Figure 3. Air Supply System

8

2. Test Turbine

The turbine, housed within an explosion-proofed test cell, was the first stage of the SSME HPFTP 'Alternate Turbine Development' model, designed, manufactured, and provided by Pratt and Whitney. The controlled air supply flowed axially through the turbine inlet strut assembly into the first stage stator. The 52 stator blades, each with a metal turning angle of approximately 70°, imposed a counter-clockwise (CCW) swirl to the airflow looking aft. The swirling flow was then turned toward the clockwise (CW) direction by the spinning rotor blades and exhausted into the test cell. The power generated by the spinning rotor was absorbed by a water dynamometer. The turbine shaft was supported by two bearings within a common housing, which was rebuilt by McKee [Ref. 6] prior to his testing. The turbine was operated in the configuration shown in Figure 4 without the movable backpressure plate, throttle guide rod and shaft cover described by Greco [Ref. 12].
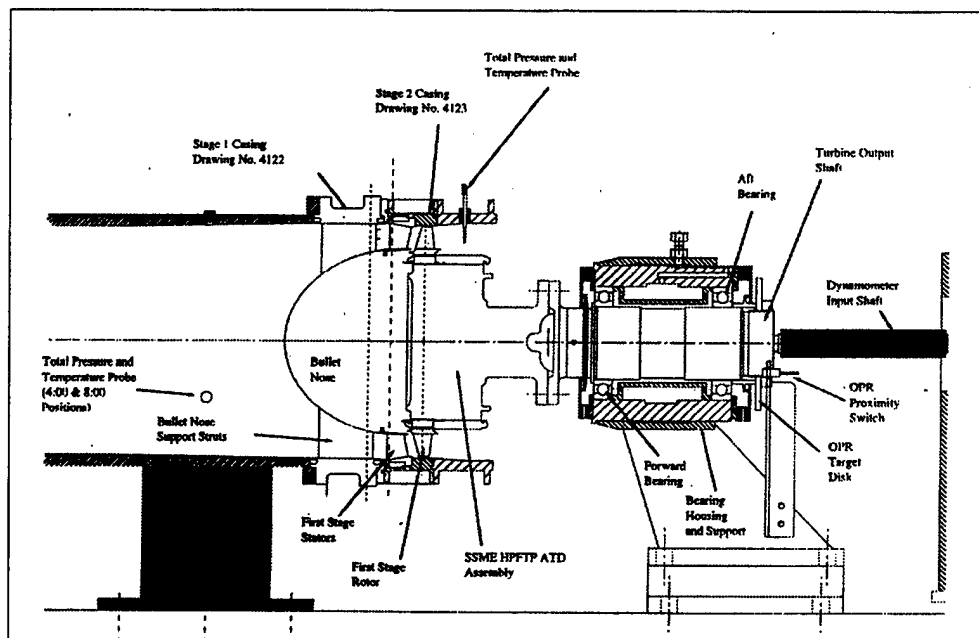
Figure 4. Schematic of the Turbine Test Rig

The turbine casing, previously modified as reported by Greco [Ref. 12], incorporated a LDV window, within which the three-hole vented plug described by Southward [Ref. 13], was installed. The rotor blade tip gap was 0.045 inches, vice 0.02 inches reported by Southward, due to machining necessary during the previous rebuild.

3. Laser and Optics

The laser was a Lexel model 95, Argon-Ion, four-beam (blue-green) system rated at four Watts. The TSI Model 9100-7 laser and associated optics assembly was mounted on a traverse table system (TTS), and was set up in a back-scatter configuration capable of measuring axial and tangential components of velocity within the turbine. Prior to testing, the laser and optics were disassembled, cleaned, and re-aligned. During reassembly, a field-stop was installed in the receiving optics, to act as a spatial filter for the returning signal, shown in Figure 5.
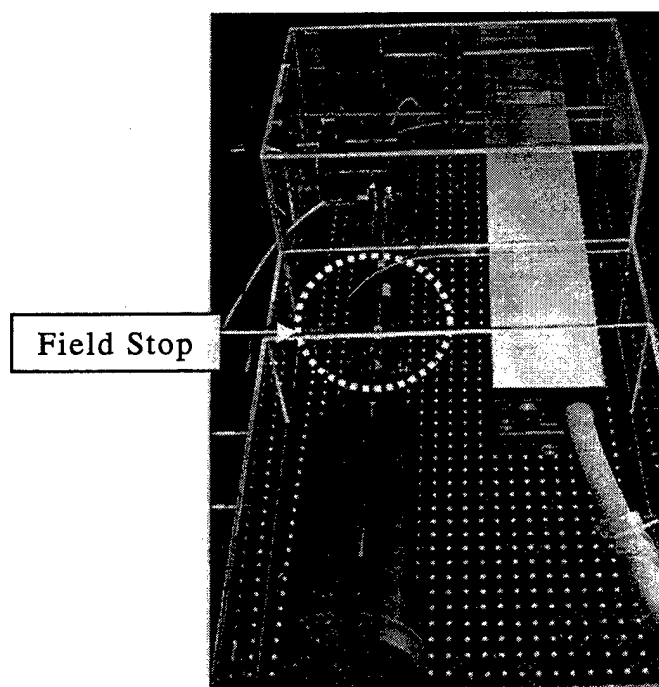
Figure 5. Laser and Optics with Field Stop Installed

Anhydrous glycerin was used for seeding with the setup described by McKee [Ref. 6].

4.   Instrumentation

The TTR was instrumented with sensors to measure or monitor the following properties:

- Air mass flow rate through the turbine
- Total temperatures and pressures at the turbine inlet and exit
- Turbine RPM
- Dynamometer torque
- Dynamometer cooling water inlet and exit temperatures
- Turbine bearing temperatures and vibration levels.

Measurement of turbine shaft horsepower was computed using three different techniques, to allow a crosscheck of the instrumentation calibrations. For a detailed description of the instrumentation setup see references 10, 12, and 13.

5.   Data Acquisition/Reduction

Data acquisition was controlled from two consoles located in control rooms adjacent to the test cell.

At the first console in the upper control room, LDV signals were processed. These signals were routed from photomultipliers at the end of the receiving optics, through frequency shifters, and correlated with Once Per Revolution (OPR) signal data from the Rotating Machinery Resolver (RMR) within the Intelligent Flow Analyzer (IFA), TSI Model 750. The IFA 750 signal was received by the 486 Personal Computer (PC) loaded with PHASE software. The PHASE software provided sub programs for data acquisition, data reduction and TTS control. The PHASE menus for data acquisition were set up as shown in APPENDIX E. A more detailed

description of the PHASE software may be found in the PHASE Software Manual [Ref.15].

At the second console in the lower control room, non-LDV data were processed. This console incorporated a 486 PC, which ran LABVIEW software virtual instruments (vi) developed by Greco [Ref. 12] and described by Southward [Ref. 13]. The programs were 'TTR_TEST.vi' and 'SSME_TTR.vi' for real-time and performance data, respectively.

B.   COMPUTATIONAL FLUID DYNAMICS

The CFD solutions were performed by running NASA FORTRAN software, with user-generated input files, on either the NPS CRAY Y-MP 94 supercomputer or a single or multi-processor Unix-based workstation. The grid generation software used included Grids about Airfoils using Poisson's Equations (GRAPE) modified for cascades, referred to as GRAPE2, and Turbomachinery C-GRID (TCGRID). The flow solvers used were Rotor Viscous Code Quasi-3D (RVCQ3D) and SWIFT. Additional MATLAB and FORTRAN programs were written for analysis of results and are included in APPENDIX J.

1.   Grid Generation Software

a.   GRAPE2

The GRAPE2 code [Ref. 16], developed by Chima of NASA Glenn, was a modified version of GRAPE [Ref. 17] written by Sorenson of NASA Ames. The baseline code generated 'C' and 'O' type 2D structured grids by solving Poisson's equation. The modification, named GRAPE2, permitted "flexing" of the 2D grids to accommodate annular sheets with radius changes (as are required in turbomachinery), and incorporated periodic outer boundaries. The program mapped an orthogonal "computational space" grid onto an inner body in "physical

12

space" defined in either Cartesian (x, y) or cylindrical-like (m, θ, r) coordinates where radius (r) was constant.

b.   TCGRID

TCGRID was a three-dimensional grid generation code developed by Chima [Ref. 3] of NASA Glenn specifically for turbomachinery blades. The code generated multi-block grids which were combinations of 'C' grids around blades and 'O' grids in tip or hub gaps as well as 'H' grids for inlet or exit extensions. The code, based on GRAPE, first generated two-dimensional, blade-to-blade 'C' grids at spanwise locations, then stacked and clustered the 'C' grids to form a three-dimensional grid. Hub and casing geometry's were specified in (z, r) coordinates.

The code accepted user-defined FORTRAN namelist input files to specify grid parameters and outputted files in PLOT3D format compatible with the SWIFT flow solver. A more detailed description of the grid generator software can be found in the TCGRID User's Manuals [Refs. 18 and 3].

The 'Multix.f' utility routine was a separately coded program by Chima, which was used to combine stator and rotor blade rows to form a stage grid.

2.   Flow Solver Software

a.   RVCQ3D

RVCQ3D was a quasi-three-dimensional flow solving code [Ref. 5] developed by Chima for analysis of inviscid and viscous blade-to-blade flows in turbomachinery. The code accepted GRAPE2 output and accounted for annular radius and axial stream surface thickness variations as well as blade row rotation. The code solved the thin-layer Navier-Stokes equations for flow through a single blade row; it also incorporated

13

the Baldwin-Lomax, Cebeci-Smith and k-ω turbulence models. A more detailed description of the code may be found in the RVCQ3D User's manual [Ref. 5].

The baseline code, which accepted only constant initial inlet boundary conditions, was modified to accept an inlet profile by modifying the 'bcio' and 'qin' subroutines as shown in APPENDIX J. From the upstream stator wake q-vector [defined as fluxes of mass, momentum and energy], interpolated distributions of total pressure (P_0), total temperature (T_0), tangential velocity (v) and flow angle (α), were calculated and used to initiate the solution. Inlet P_0, T_0, v and exit static pressure were held fixed allowing all other quantities to float, particularly the downstream flow properties which were extrapolated using Giles' type characteristic boundary conditions. Initial modification, referred to as RVCQ3Dmod1, permitted solutions of stationary wakes only. Additional modification was initiated to permit transiting of the wake profile across the inlet plane to solve the unsteady case. For unsteady calculations, Δt will be specified as globally constant with magnitude determined by specifying the CFL number.

b.   SWIFT

SWIFT was a 3D flow solver developed by Chima [Ref. 4] to analyze multiple turbomachinery blade rows simultaneously. The code accepted TCGRID output and solved the thin-layer Navier Stokes equations using a multi-stage explicit Runge-Kutta scheme. Turbulent flow was simulated with the Baldwin-Lomax, Wilcox fully turbulent k-ω, or low Re# k-ω models. Convergence was accelerated using a spatially varying time step computed from a user-defined CFL number and implicit residual smoothing. Between blade rows, computational grids were overlapped by one cell to allow two-way communications of flow properties. At the grid boundaries, the flow information was integrated

14

circumferentially and then averaged to create the boundary condition for the neighboring grid, using the options defined in APPENDIX B [Ref. 20]. Inlet and exit boundary conditions were also specified using parameters defined in APPENDIX B. ·

The user-specified flow parameters were divided between two input files, a grid index file and a namelist file. Grid parameters were read from 'fort.1', a PLOT3D-formatted file, and restarts used 'fort.2' files, renamed from the 'fort.3' q-file [i.e.-$(\rho, \rho u, \rho v, \rho w, e)^T$] solution. Runs using k-ω turbulence modeling additionally used the 'fort.7' restart file, renamed from the 'fort.8' solution file and formatted as: $(\mu_T, k, \omega, Re_T, \mu)^T$. For a more detailed description, see the SWIFT preliminary documentation [Ref. 4] and the RVC3D User's Manual [Ref. 21].

III. EXPERIMENTAL AND NUMERICAL ANALYSIS PROCEDURES

A. LDV EXPERIMENTS

Prior to commencing LDV measurements, several actions were completed to increase system reliability and measurement accuracy. The air supply system's 1250 HP electric motor and hydraulic coupling were rebuilt. The LDV system frequency shifters were rebuilt. The laser and optics system was disassembled, cleaned, aligned, and tuned; and during reassembly, a field stop was incorporated into the receiving optics to act as a spatial filter.

1. TTR and LDV System Operation and Data Acquisition

The TTR and LDV system operation procedures were governed by checklists, which were slightly modified from those reported by Southward [Ref. 13] and included in APPENDIX I. An overview of the checklist procedures is included below.

a. TTR and LDV System Pre-Start

The "TTR PRE-START" and "LDV SYSTEM OPERATION" checklists were completed to set up the hardware and software components of the turbine, laser, instrumentation and data acquisition systems. The air supply system was started and operated by the shop technician and required approximately two hours of warm-up prior to test measurements being taken. The LDV instrumentation system was powered up and calibrated from the lower control station. The LDV system was set up and used to make measurements with seeding external to the TTR, using Flow Information Display (FIND) software [Ref.23] (with the menu setup shown in APPENDIX E), to check LDV system integrity. Following checkout, the laser probe volume reference position was checked and

17

relocated as necessary using the procedure described by Southward [Ref. 13]. At the completion of the TTR/LDV pre-start procedures, the system was ready to operate. For a more detailed description of the system setup, refer to Southward [Ref. 13].

b.   TTR and LDV System Operation

Using the "TTR START CHECKLIST", the turbine was operated first at 1500 and 3000 RPM to checkout the system, and then at 5000 RPM for all the measurements. The "TTR_TEST.vi" LABVIEW program was run during all speed changes for real-time performance monitoring.

At 1500 RPM, the TTR performance measurements were recorded with "SSME_TTR.vi". The LDV data acquisition software, PHASE [Ref. 15], was operated from the test cell computer using the menu settings in APPENDIX E. LDV data were taken to gauge system performance using the forward hole and the center depth, shown in Figure 6.
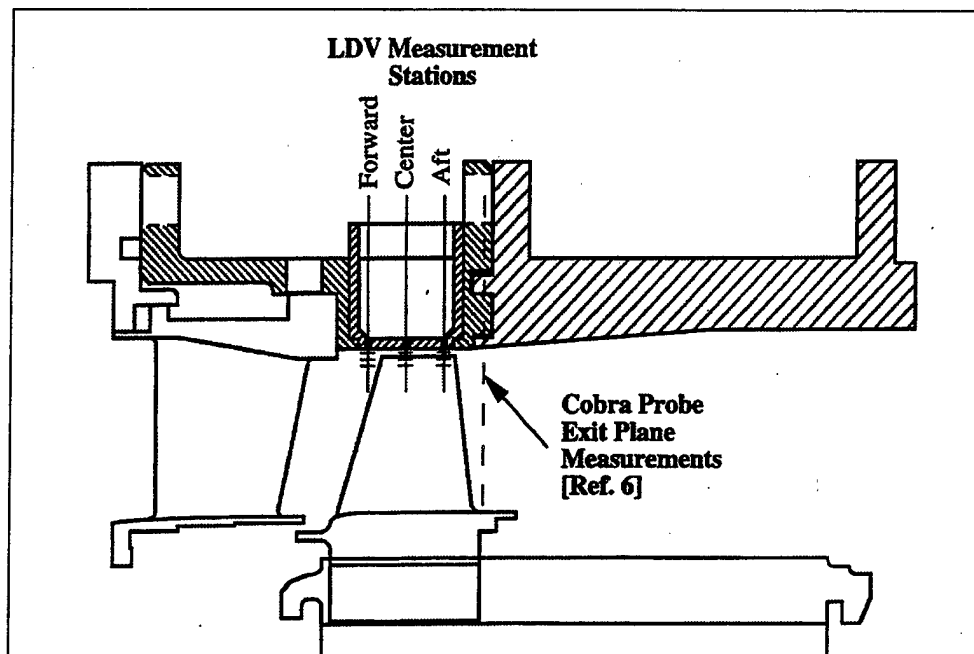
Figure 6. Probe Volume Measurement Locations (Meridional View)

At 3000 RPM, established as the maximum safe speed for personnel to be in the test cell for extended periods, the procedures followed at 1500 RPM were repeated. Once measurements were completed, control for the PHASE software was transferred to the computer in the remote upper control station, and measurements were repeated to check for consistency. Equipment setting changes within the test cell were made prior to increasing speed to 5000 RPM.

At 5000 RPM, TTR operation was checked and recorded as described above. LDV measurements were again obtained at the forward center location, to verify system performance and data repeatability, using the PHASE menu settings shown in APPENDIX E. The TTS was used to move the probe volume between the measurement locations shown in Table 1.

Position		Radial Location (% Blade Span)	Distance from Outer Wall (in.)	TTS Settings		
Axial	Radial			X	Y	Z
Forward (−0.16c$_t$)	Inner (fi)	88	0.1190	0.125	0.1837	−0.0284
	Center (fc)	93	0.0688	0.125	0.1329	−0.0205
	Outer (fo)	98	0.0187	0.125	0.0822	−0.0127
Center (0.35c$_t$)	Inner (ci)	88	0.1190	−0.125	0.1837	−0.0284
	Center (cc)	93	0.0688	−0.125	0.1329	−0.0205
	Outer (co)	98	0.0187	−0.125	0.0822	−0.0127
Aft (0.84c$_t$)	Inner (ai)	88	0.1190	−0.375	0.1837	−0.0284
	Center (ac)	93	0.0688	−0.375	0.1329	−0.0205
	Outer (ao)	98	0.0187	−0.375	0.0822	−0.0127

Table 1. LDV Measurement Positions

19

The probe volume measurement locations are physically shown relative to the stator/blades and outer casing step in Figure 6.

Using the probe volume dimensions from the TSI LDV Components Parts Description [Ref. 22] for the Model 9169-750 transmitting optics for the green beam wavelength, the probe volume is shown located at the outer position in the tip gap region (aft or center axial location) in Figure 7.
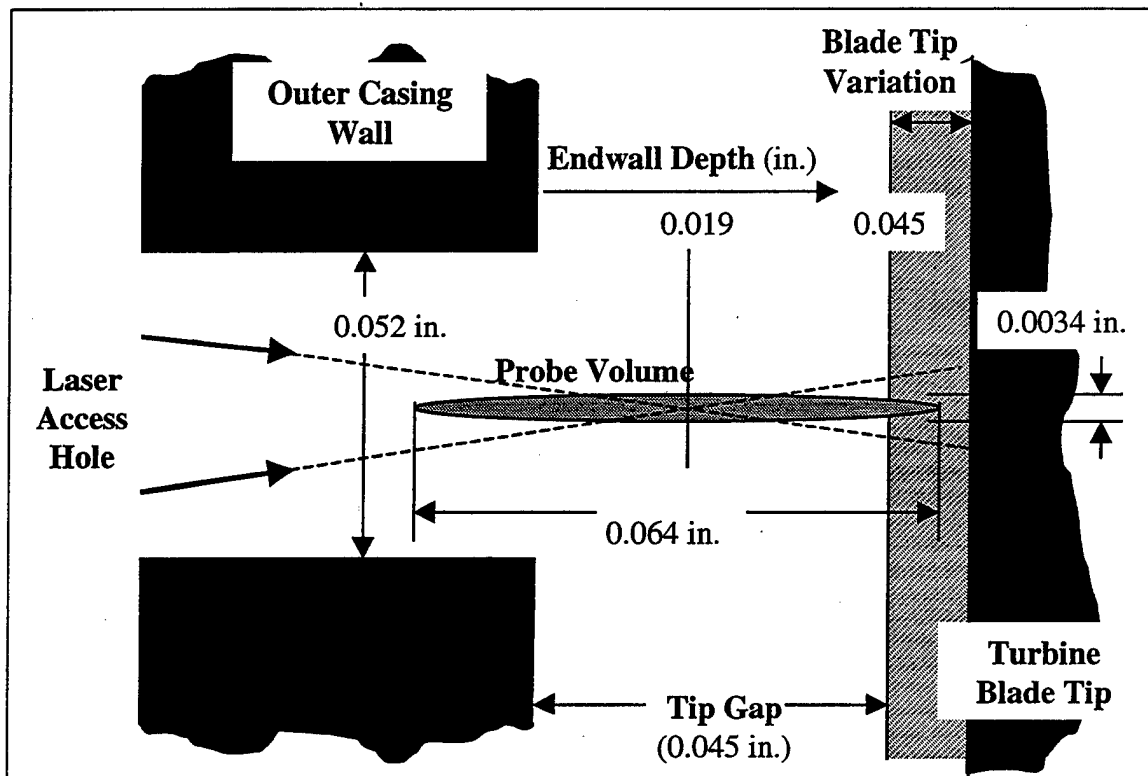
Figure 7. Probe Volume in Tip Gap Region (98% span)

The axial locations of the LDV measurements relative to the rotor blade tip are shown on Figure 8, which is a picture of the turbine outer casing with the three-hole vented plug removed.
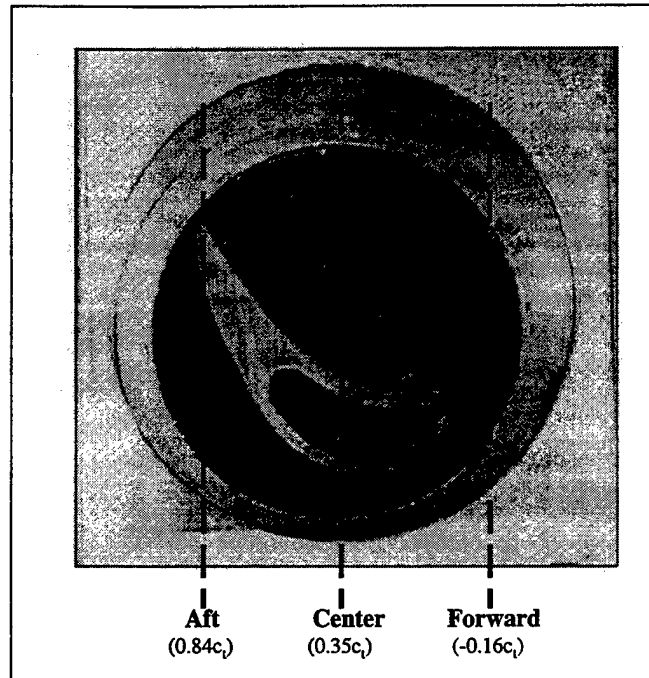
Figure 8. LDV Axial Measurement Locations (Plug Removed)

Measurements between the blades were determined to be a tradeoff of noise return, blade reflection, and seeding particle reflections. The procedure described below was constructed with the objective of minimizing blade and noise return, while maximizing valid particle return between blades:

- Seeding was turned off.
- Nominal laser power that ensured blade return was set (approx. 0.5 W).
- PHASE windowing was used to minimize blade return.
- IFA 750 frequency filtering was used in conjunction with frequency shifting to further minimize blade reflections without eliminating valid flow measurements.
- IFA 750 detection threshold was lowered until noise detected.
- Seeding was turned on.
- Unseeded flow statistics were compared with seeded flow statistics.
- Results were compared with previous measurements as available.

21

Seeding was periodically shut off to determine changes in measurement characteristics (e.g. data rates, frequencies, etc...). With the field stop installed, a higher laser power setting than Southward reported [Ref. 13] (0.5W vice 0.25W) was possible without saturating the photomultipliers.

c.   TTR and LDV System Shutdown

With measurements completed, the TTR and LDV systems were systematically shut down using the TTR and LDV Shutdown Checklists.

d.   Emergency Shutdown

The "TTR Emergency Shutdown Checklist" provided the most expeditious means of shutting off the supply air from driving the turbine, and was used to shutdown the system during a dynamometer shaft failure.

2.   LDV Data Acquisition and Reduction

LDV data were acquired using the PHASE data acquisition subprogram, which produced raw data files (*.R*) consisting of Doppler frequency information for each of the data points. With Once-Per-Revolution (OPR) input from the Rotating Machinery Resolver (RMR), the data were tagged with circumferential location. A window was defined for each of 50 rotor blade spaces and, within each, there were 72 bins, providing 0.1° angular resolution.

LDV data were reduced using the PHASE statistical analysis subprogram, where velocity (*.V*) and statistical (*.S*) files were created from the raw data files. During this process, the data from each of the 50 windows were averaged to create a single representative blade passage. Some data smoothing was incorporated by combining bins into groups of two, reducing the circumferential resolution to 0.2°.

The velocity and statistics files were modified into an ASCII-formatted file compatible with Microsoft EXCEL, using the 'Phase3.f' FORTRAN program included as an appendix in reference 13. The resulting files (*.C*) contained columns of angular location, mean axial velocity, mean tangential velocity, axial turbulence intensity, tangential turbulence intensity, flow angle, and correlation coefficient, which were computed as follows:

○   Non-Dimensional Mean Axial Velocity

$$X_z = \frac{c_{mz}}{\sqrt{2C_p T_{01}}}$$

○   Non-Dimensional Mean Tangential Velocity

$$X_\theta = \frac{c_{m\theta}}{\sqrt{2C_p T_{01}}}$$

○   Absolute Flow Angle

$$\alpha = 90 - \arctan\left(\frac{c_{mz}}{c_{m\theta}}\right)$$

○   Axial Turbulence Intensity

$$T_z = \frac{\sqrt{c'^2_z}}{c_{mz}}$$

○   .   Tangential Turbulence Intensity

$$T_\theta = \frac{\sqrt{c'^2_\theta}}{c_{m\theta}}$$

○   Correlation Coefficient

$$c_{\theta z} = \frac{\overline{c'_\theta c'_z}}{\sqrt{c'^2_z}\sqrt{c'^2_\theta}}$$

For each data run, 20,000 total data points were specified. Due to a DMA timeout limitation of 999 seconds within PHASE, this limit was not

23

always achieved, especially during measurements between blades due to low data rates.

B.   COMPUTATIONAL FLUID DYNAMICS

1.   Quasi-Three-Dimensional Calculations

A quasi-3D analysis was carried out to investigate the impact of an upstream translating stator wake on the rotor flow field at mid span. These flow field changes, and resulting blade pressure distributions, were evaluated to determine the periodic unsteady forces on the blades.

a.   Grid Construction

Using mid-span blade cuts, the quasi-3D viscous grids for the rotor and stator blades were constructed using GRAPE2. Standard namelist input files were used to define grid parameters, and these are included in APPENDIX C. The rotor inlet plane edge radius was set to zero to square off the inlet boundary for eventual interpolation with the stator exit plane. The stator and rotor "C" grids were dimensioned as 310x50 and 330x50, respectively, and are shown in Figure 9.
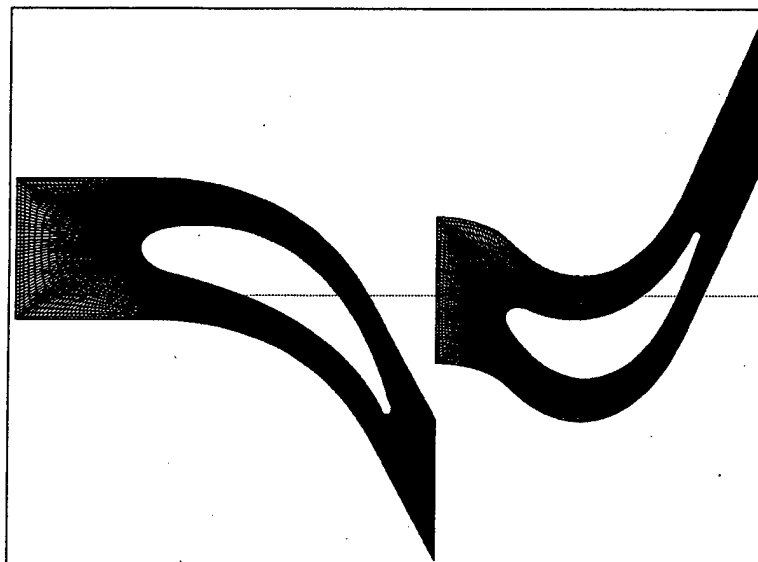
Figure 9. Quasi-3D Stator and Rotor Grids

24

b. Steady-State Baseline Flow Solutions

The RVCQ3D code was used to obtain a quasi-3D flow solution, using the GRAPE2 grids and steady (but not necessarily uniform) inlet boundary conditions. The boundary conditions were derived from a combination of Southward's experimental results [Ref. 13] and McKee's computational results [Ref. 6]. The solutions were run until steady state was demonstrated by the convergence history. An example is shown in Figure 10.
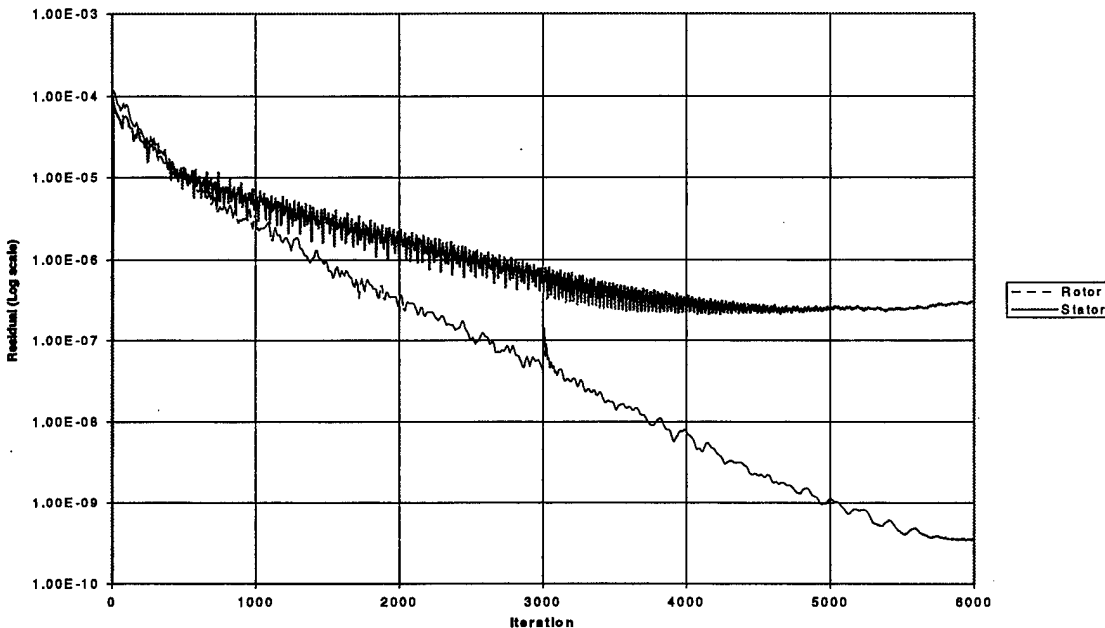
Figure 10. Quasi-3D Rotor and Stator Baseline Convergence History

The solution flow properties were viewed using FAST. The steady-state Mach number contours for the stator and rotor are shown in Figure 11 and Figure 12, respectively.

25
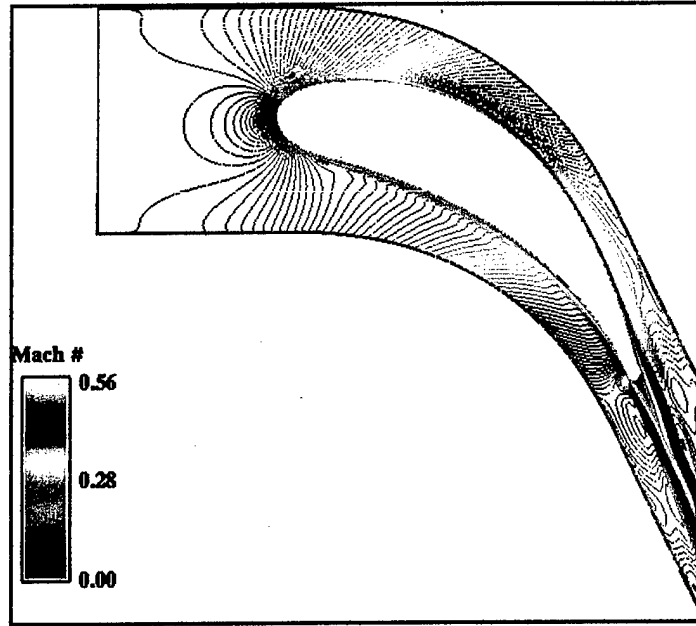
Figure 11. Quasi-3D Stator Baseline Flow Field Mach Number Contours
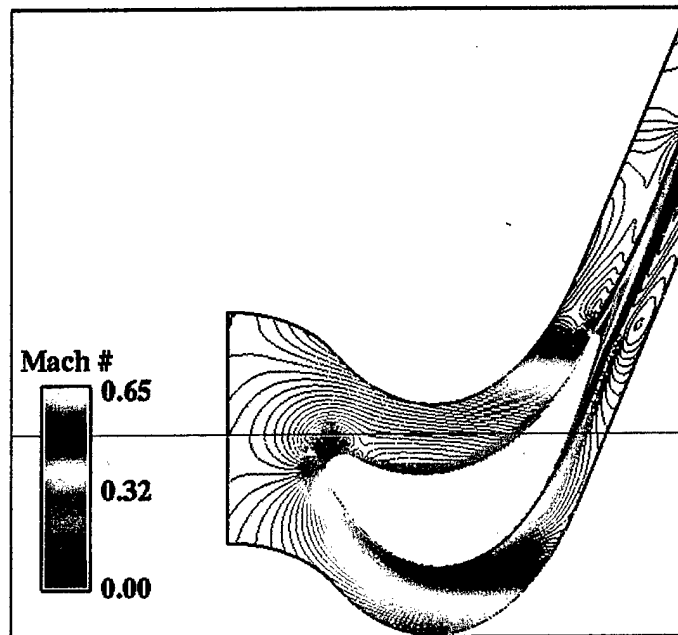
Figure 12. Quasi-3D Rotor Baseline Flow Field Mach Number Contours (Relative Frame)

The solutions clearly show the leading edge stagnation points, and the wakes at the grid exit boundaries. Note the nearly uniform Mach number distribution across the rotor inlet boundary. The rotor flow solution was used for comparison with non-uniform inlet calculations, as well as providing a restart file for the steady wake calculations. The stator flow solution was used to determine the wake profile as discussed below.

c.   Interpolation of the Stator Wake onto the Rotor Inlet

The stator wake profile was extracted from the stator solution file using the program 'qout.f' included in APPENDIX J. The stator wake non-dimensionalized 'q' vector profile is shown as Figure 13.
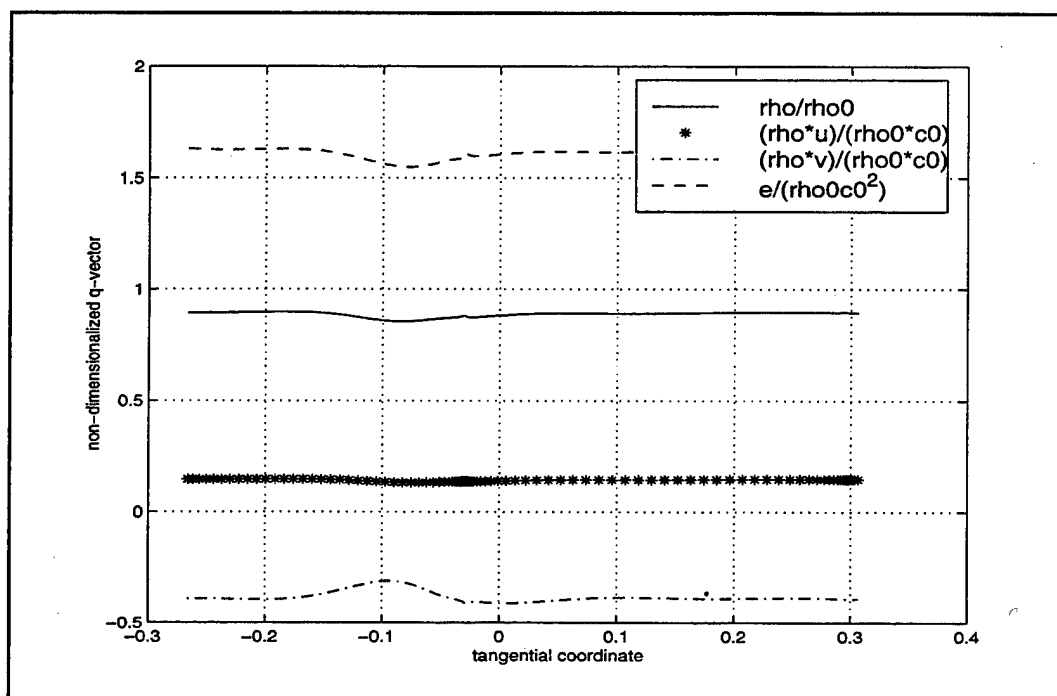
Figure 13. Quasi-3D Stator Wake 'q' Vector Profile

The stator wake distribution, defined at 99 unevenly distributed grid points, was interpolated onto 46 evenly distributed rotor inlet grid points, as shown in Figure 14, using a MATLAB program called 'wake_interpolation.m'. The program is included in APPENDIX J.
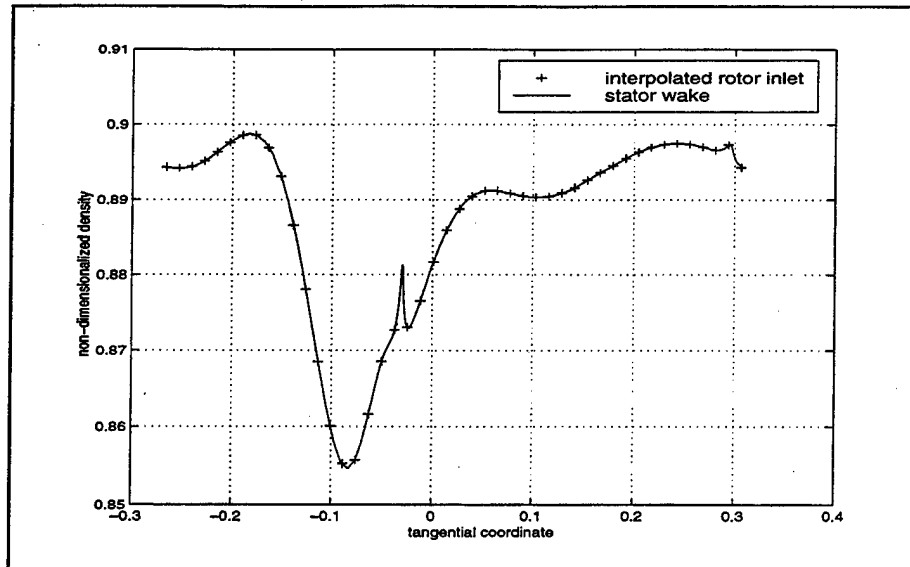
Figure 14. Interpolated Wake Profile for Non-Dimensionalized Density

d.   Movement of the Wake Profile

Using the 'wake_interpolation.m' code, the stator wake was translated to generate the six profiles shown in Figure 15.
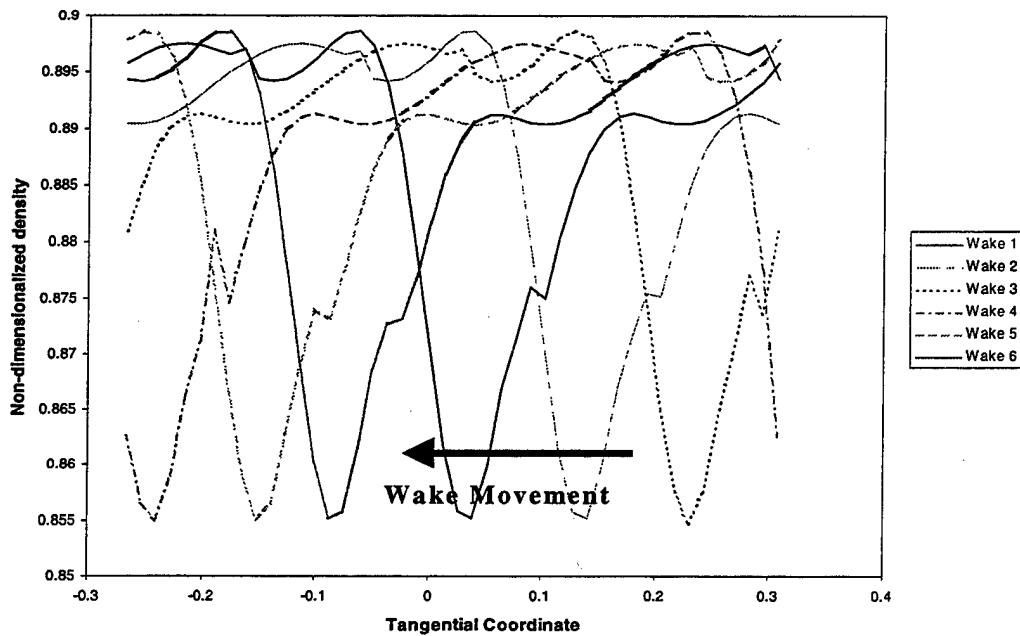
Figure 15. Rotor Inlet Wake Profiles

e.   Stationary Wake Inlet Profile Solutions

Flow solutions were determined for each of six wake
positions using RVCQ3D modified to accept stationary wake profiles as
inlet boundary conditions. The RVCQ3Dmod1 code is included in
APPENDIX J. The wake solutions were each determined as a restart from
the baseline rotor solution.

f.   Translating Wake Inlet Profile Solutions

The RVCQ3D code was additionally modified to calculate
flow solutions with a translating wake inlet boundary condition, but
converged, unsteady flow solutions were not obtained. The use of a
globally constant time step is recommended.

2.   Three-Dimensional Stage Calculations

The 3D analysis was completed in order to compare CFD results
with, 1) cobra probe data in the rotor exit plane, and 2) LDV
measurements in the tip gap/endwall region. The effort consisted of two
parts. The first part consisted of a boundary condition and turbulence
model analysis using the grid built by McKee [Ref. 6]. The second part
involved the construction of and attempted flow solution with a much
denser grid, referred to herein as the "fine grid". The purpose was to
improve exit plane agreement, as recommended by McKee [Ref. 6].

a. Grid Construction

The 3D grids necessary to construct the turbine stage passage were built using TCGRID version 204, described in reference 3. All grids were clustered for viscous flow. The grid parameters were defined separately for the rotor and stator, within namelist input files. The files are given in APPENDIX A.

The stator C-grid was built using the physical boundaries described by McKee [Ref. 6]. The grid dimensions, however, were modified to increase grid density throughout the blade row. The dimensions of the new stator grid were 218x46x84, as shown in Figure 16.
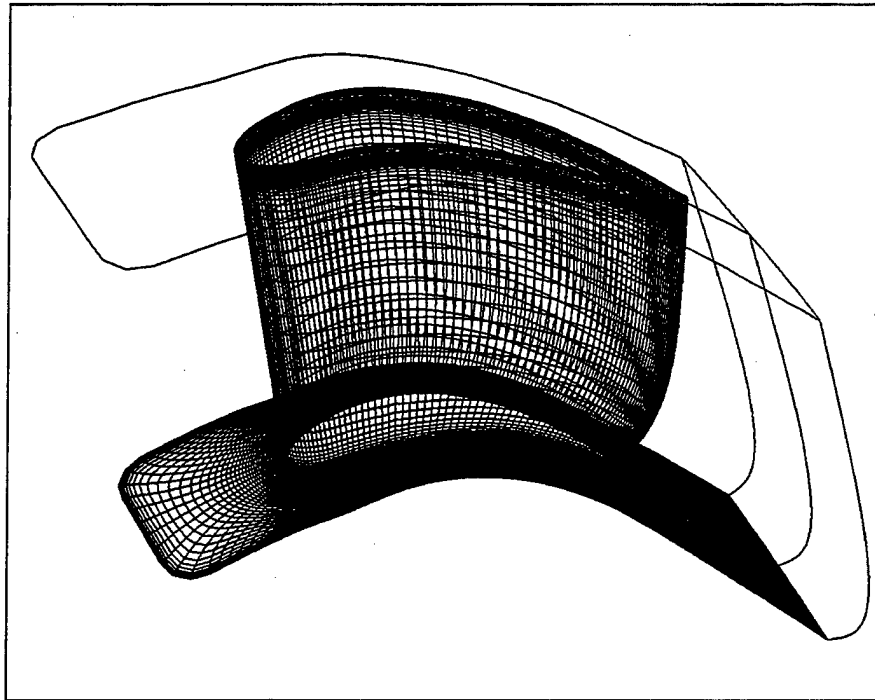
Figure 16. 3D Stator Grid

The rotor blade and tip gap grids were specified together, and their dimensions were increased appropriately. The number and placement of stator and rotor spanwise planes were required to be identical, for compatibility. The rotor grid, dimensioned as 318x46x84, is shown in Figure 17.

30
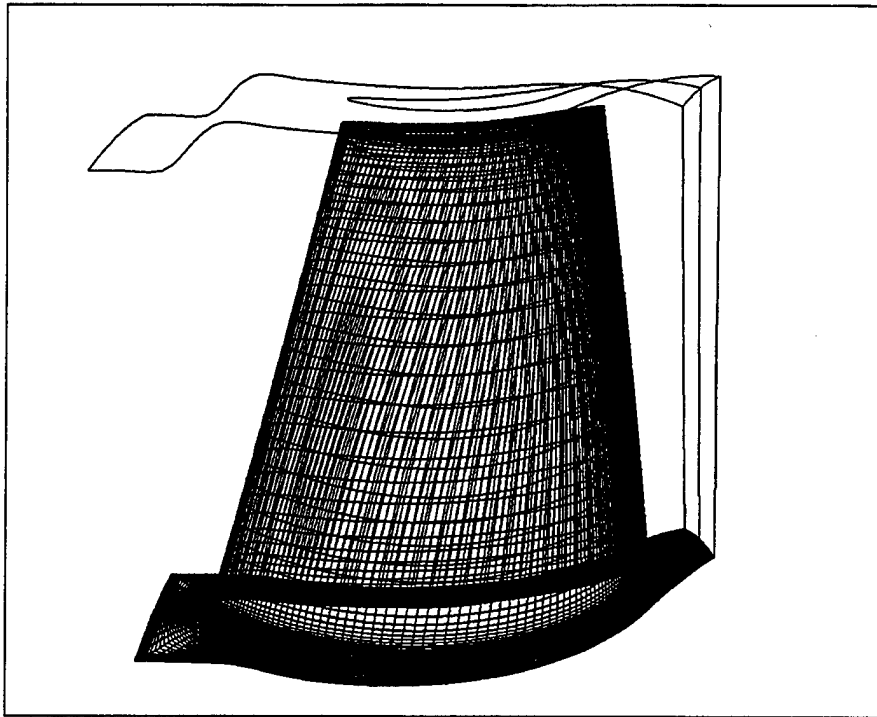
Figure 17. 3D Rotor Grid

The rotor grid physical boundaries were the same as those used by McKee [Ref. 6] except at the outer casing, where the step was modified to a ramp with a slope of approximately one. The more gradual transition was required due to the finer grid spacing; the original abrupt step (slope~100) caused grid plane overlap, and resulted in negative cell volumes. The modified outer casing step is shown as Figure 18.
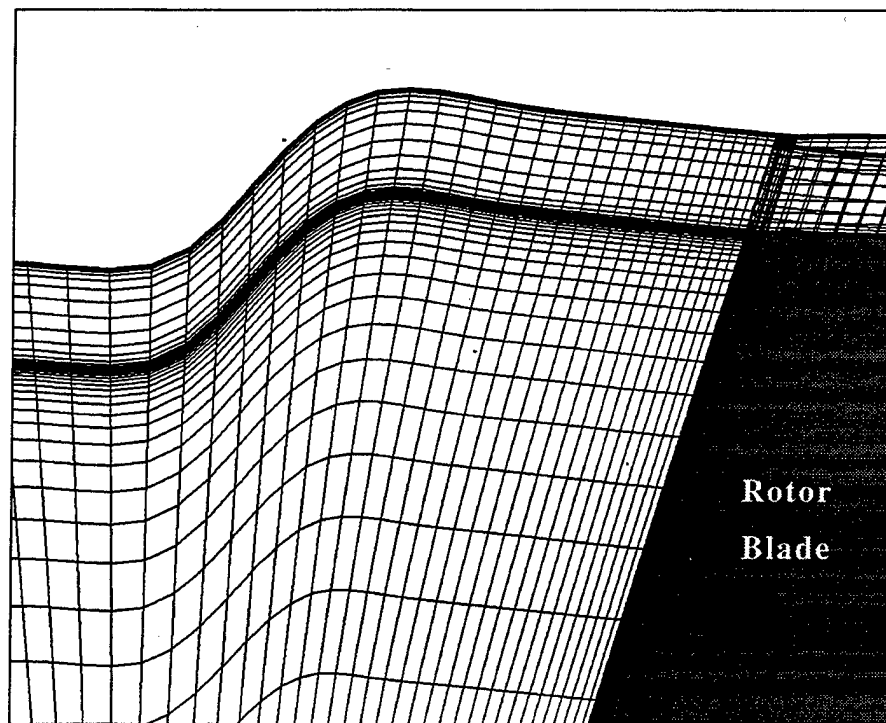
Figure 18. Modified Outer Casing Step

The tip gap was constructed as an O-grid, and dimensioned as 196x20x20, as shown in Figure 19.
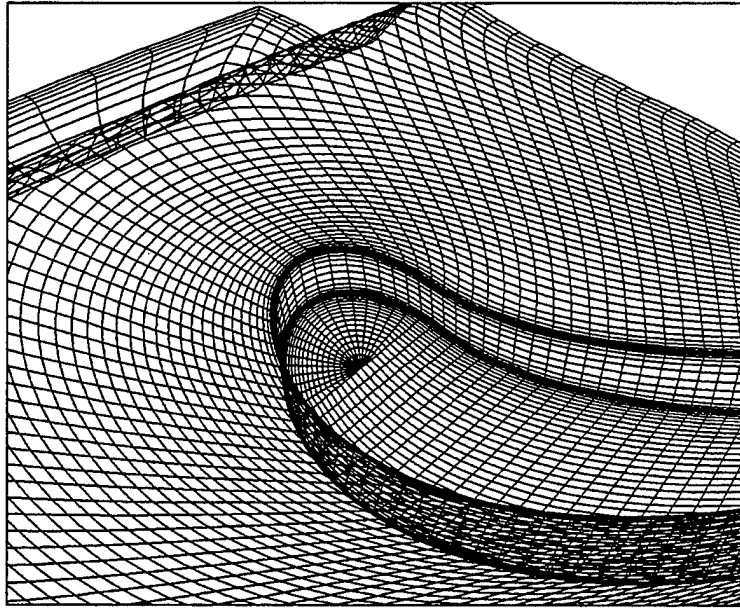
Figure 19. 3D Rotor Tip Gap Grid

Following a check for compatibility using FAST, the grids
were combined using 'multix.f'. The resulting turbine stage grid was
comprised of greater than two million points, and is shown in Figure 20.
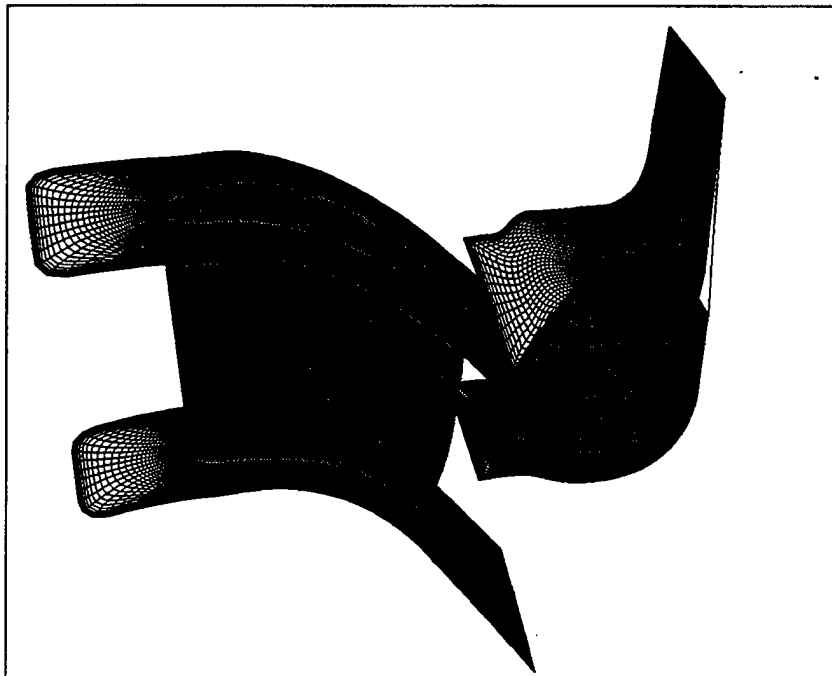
Figure 20 Combined First-Stage Stator and Rotor

b. Flow Solving

The flow solution for the combined grids generated by TCGRID was obtained by running the SWIFT program. The program required two input files to specify parameters. Flow solution parameters such as pressure ratios, temperatures, rotational speed and turbulence levels were specified in an input file, '*.in', shown in APPENDIX B. Grid interaction parameters were specified in the 'fort.10' file, also included in APPENDIX B.

During the solution, first-order viscosity was used to stabilize the computation. The first-order viscosity coefficient (AVISC1) was started at 1.0, then reduced in a schedule similar to that shown in Table 2.

AVISC1	Iterations
1.0	0-400
0.5	401-800
0.25	801-1200
0.125	1201-1600
0.062	1601-2000
0.031	2001-2400
0.016	2401-2800
0.008	2801-3200
0.004	3201-3600
0.002	3601-4000
0.001	4001-4400
0.0	4401-End

Table 2. SWIFT First Order Viscosity (AVISC1) Schedule

IV. RESULTS AND DISCUSSION

A. EXPERIMENTAL RESULTS

LDV familiarization and data runs were conducted during 38 hours of operation of the NPS TPL turbine test rig. Data were taken at a nominal speed of 5000 RPM, at three radial depths, in three axial locations using the procedures outlined above. The data are presented with tangential direction (θ) plotted on the horizontal axis, where a blade-to-blade passage was 7.2°. The center of the blade-to-blade passage occurred at approximately $\theta=0°$, as determined with a stationary rotor.

1. Coincidence Window

The LDV processor could be operated in either the 'Random' or 'Coincidence', mode as selected in the PHASE data acquisition subprogram menu. All data runs were made in the coincidence mode, and the coincidence window size was specified ultimately to limit the window to correlate green and blue channel data to a single particle. Test data were obtained with the coincidence window set at 1μsec, 1msec and 0.1 seconds, in order to determine the effect of window size and to compare with data taken by Southward at 0.1 seconds [Ref. 13]. Figure 21 to Figure 24 below show data at each of the coincidence window settings, at the forward center (fc) measurement position.
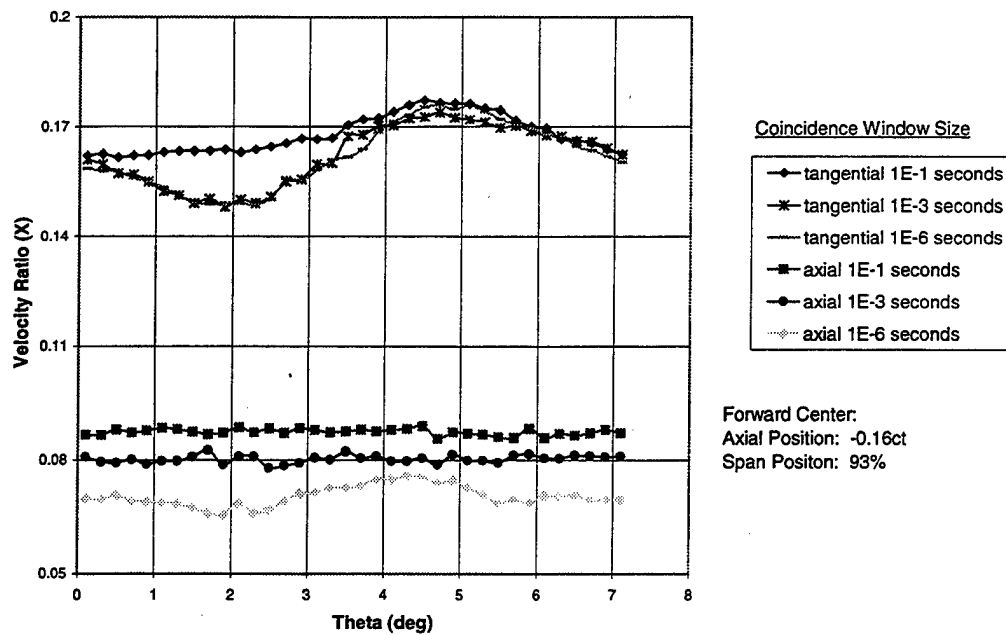
Figure 21. Effect of Concidence Window Size on Velocity Ratio
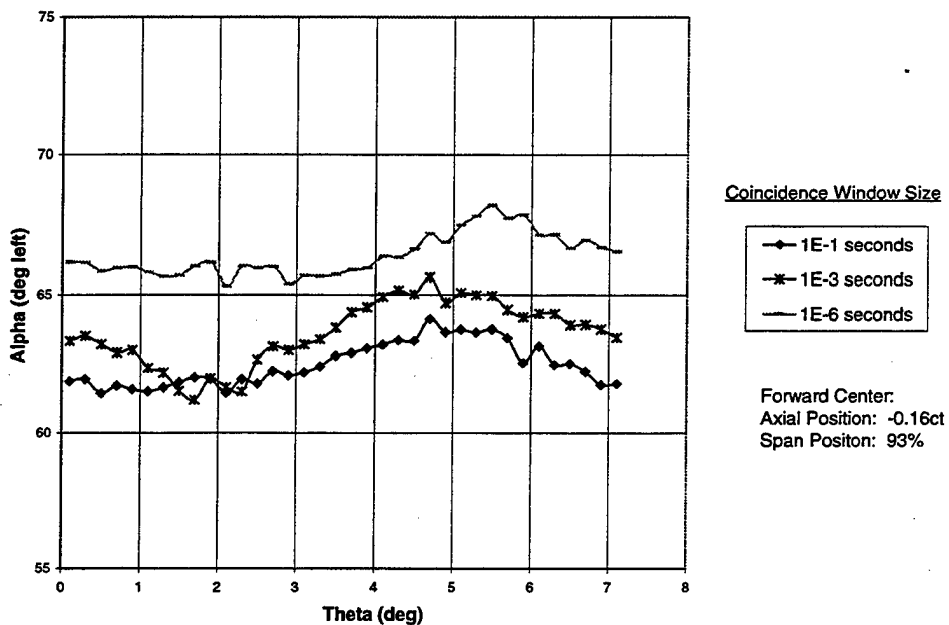
Figure 22. Effect of Concidence Window Size on Flow Angle

36
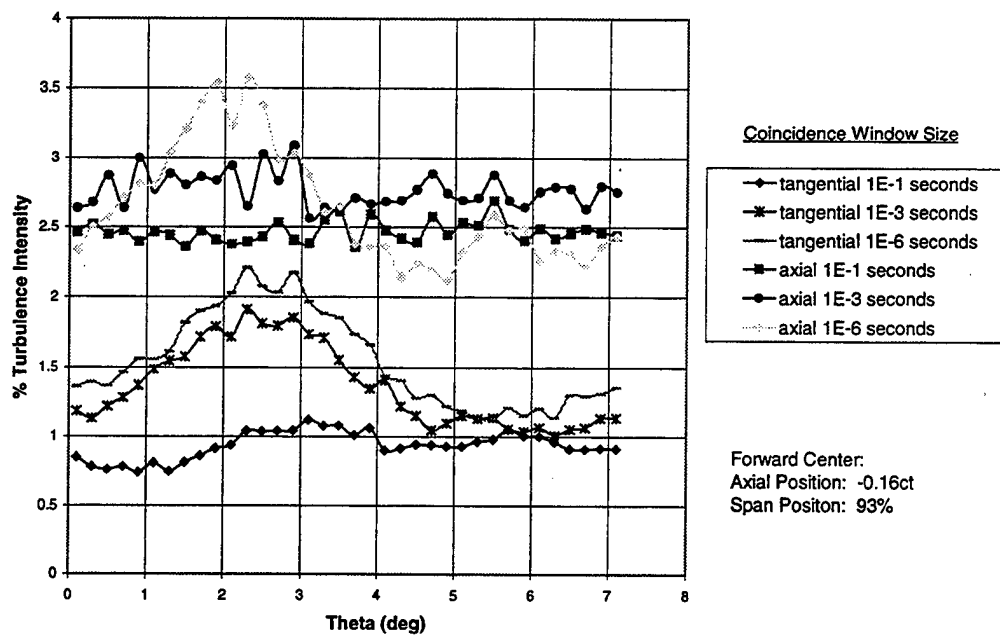
Figure 23. Effect of Concidence Window Size on Turbulence Intensity
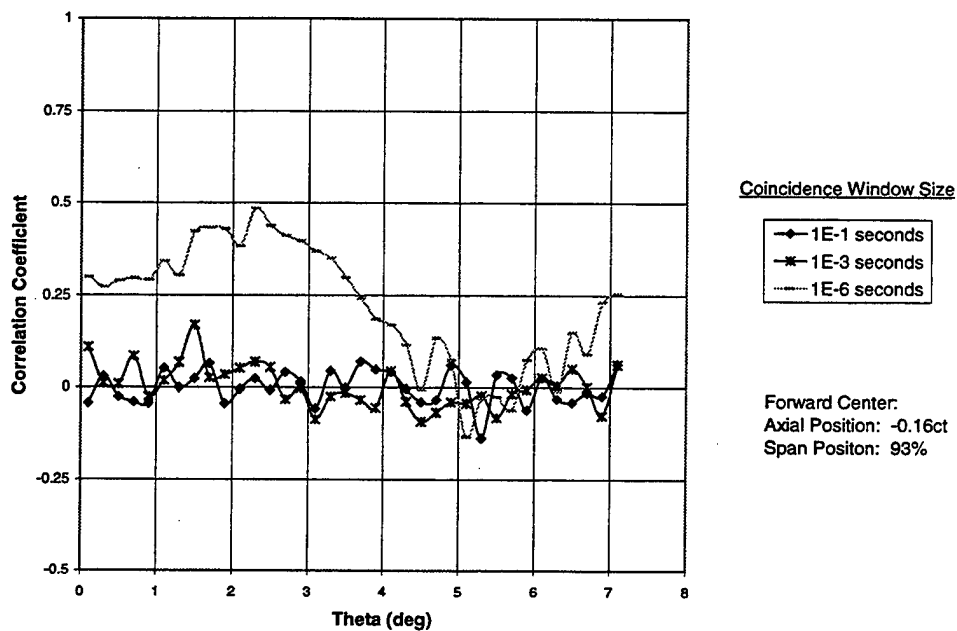
Figure 24. Effect of Concidence Window Size on Correlation Coefficient

In general, the larger the coincidence window, the less tangential variation appeared in the data. The larger correlation window increased the probability of incorrect matching of axial and tangential measurements. The data mismatch, in some cases, had the effect of smearing the data, causing the tangential flow variations to be lost.

A comparison (not shown) of data with those of Southward (0.1 second coincidence window size) revealed excellent agreement for velocity ratios and flow angle, both in magnitude and characteristic shape. The largest disagreement occurred in axial turbulence intensity (2.5% vs. 1.5%). Part of the difference could be attributed to the significantly larger tip gap used in the present work, 0.045 vice 0.02 inches, since the measurements were made in this proximity.

At 5,000 RPM, with a bin size of 0.1°, the probe volume traveled through a given bin in approximately 3.33 μsec. The shape of the probe volume was extremely elliptical, as shown in Figure 7, however, the diameter of the probe volume (88 μm), was approximately 40% of the bin width (225 μm). To minimize the effects of probe volume-bin overlap, the data runs were taken with the smallest coincidence window allowed by the equipment (1 μsec).

2. Measurements Upstream of the Rotor Blade (-0.16c_t)

Measurements were made at each of the three depths presented in Table 1 at the $-0.16c_t$ axial location, using the PHASE menu settings shown in APPENDIX E. For each data run, data rates were adequate to obtain the 20,000 specified data points. Window averaging was used during data reduction to obtain an average representative blade space with 400-800 data points per bin. Multiple runs were made at the center depth (93%) and resulted in excellent data repeatability (<5% scatter) as shown in Figure 29 to Figure 32. Calculations were made for velocity ratio (X_θ, X_z) flow angle(α), turbulence intensity (T_θ, T_z) and correlation coefficient ($c_{\theta z}$) using the equations given in the Section III.A.2, and the results are plotted in Figure 25 to Figure 36.

38
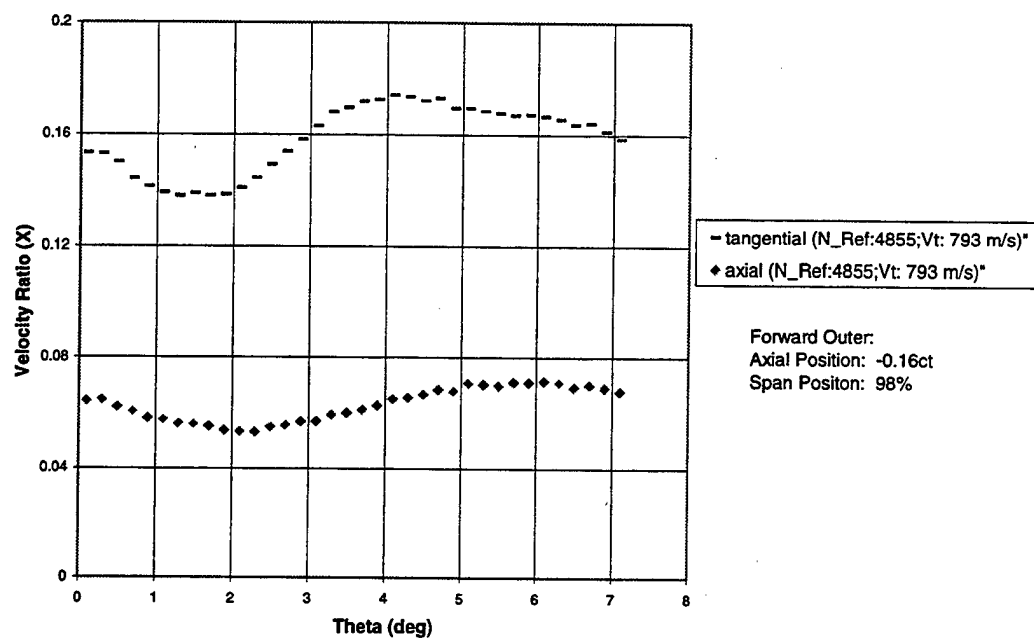
Figure 25. LDV Velocity Ratios for –0.16c$_t$ and 98% Span
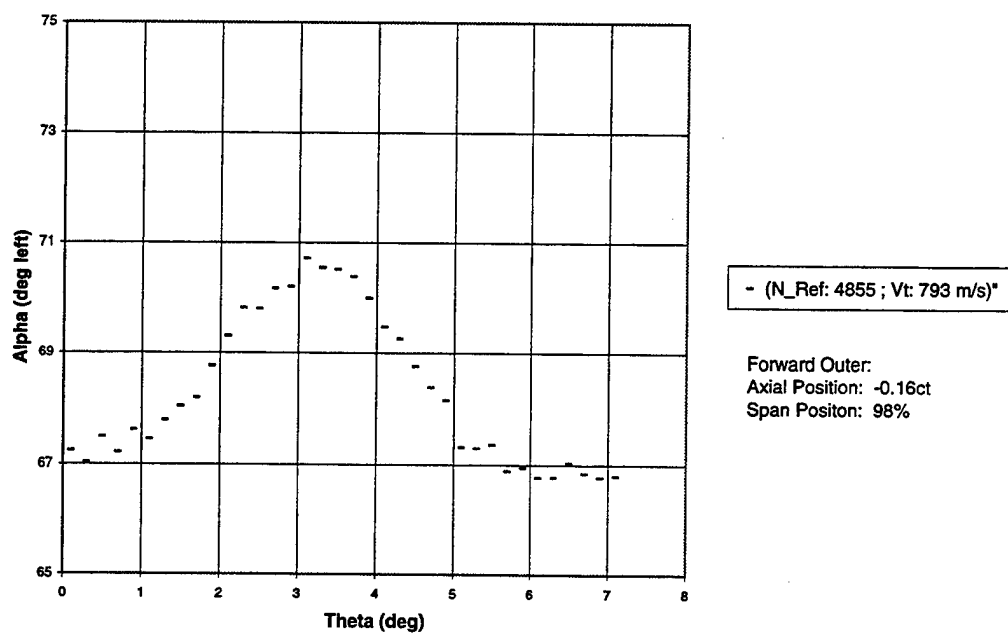
Figure 26. LDV Absolute Flow Angle for –0.16c$_t$ and 98% Span

39
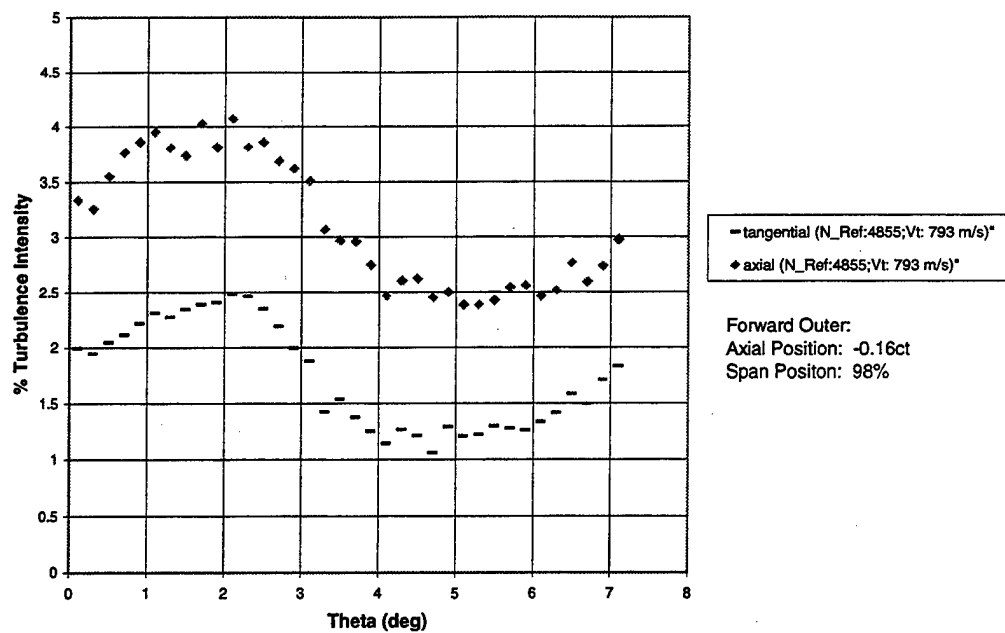
Figure 27. LDV Turbulence Intensity for –0.16c$_t$ and 98% Span
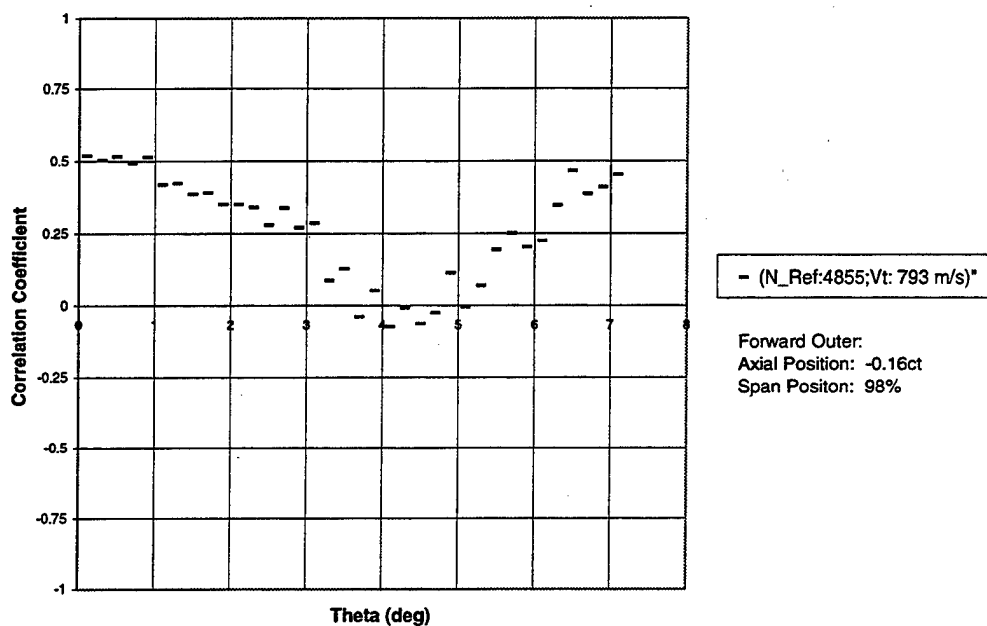
Figure 28. LDV Correlation Coefficient for –0.16c$_t$ and 98% Span

40
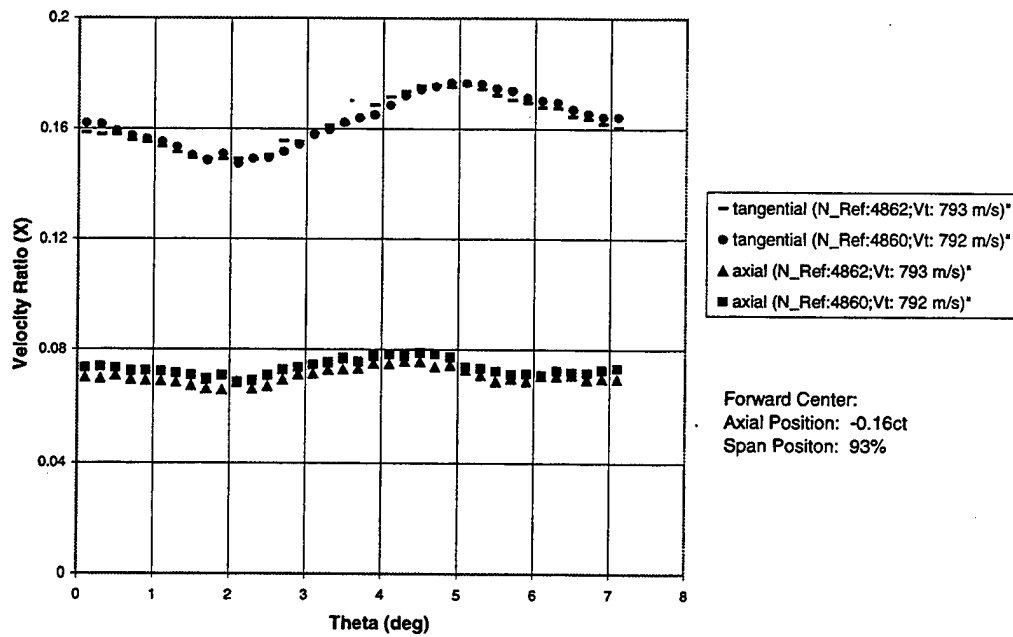
Figure 29. LDV Velocity Ratios for –0.16c$_t$ and 93% Span
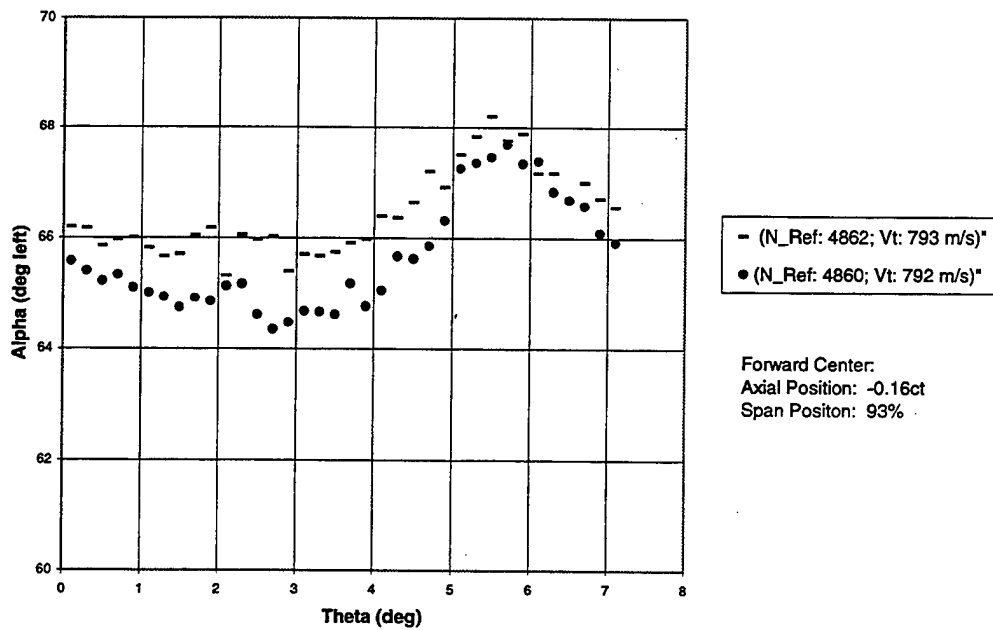
Figure 30. LDV Absolute Flow Angle for –0.16c$_t$ and 93% Span

41
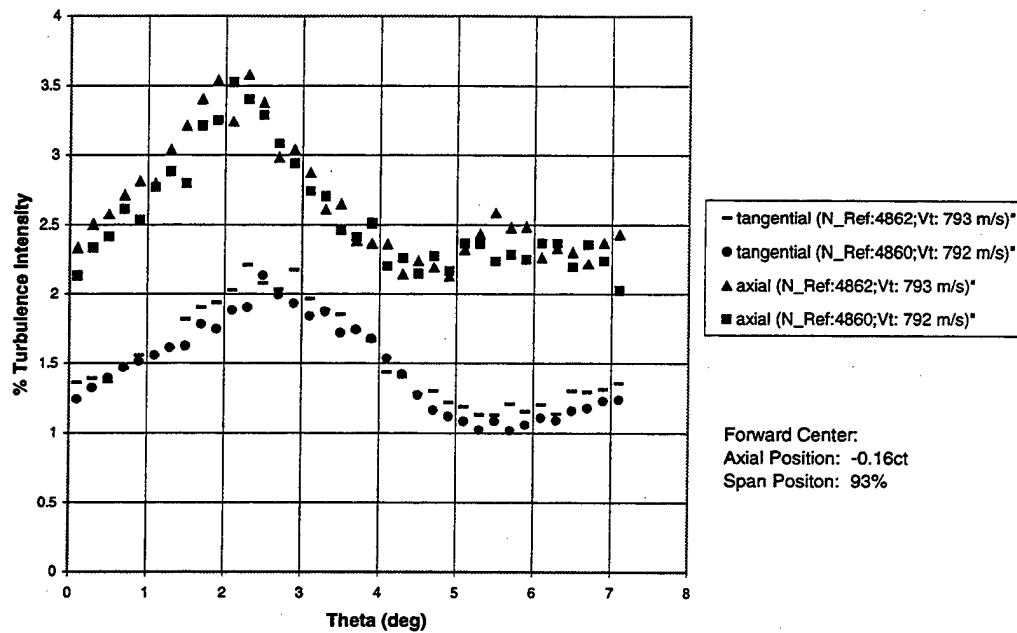
Figure 31. LDV Turbulence Intensity for –0.16c$_t$ and 93% Span
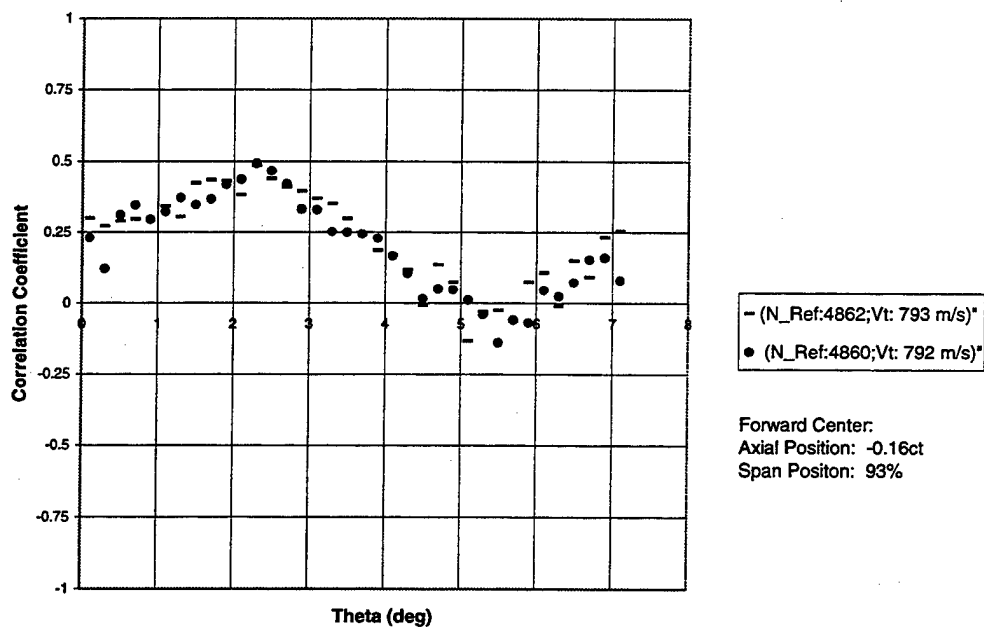
Figure 32. LDV Correlation Coefficient for –0.16c$_t$ and 93% Span
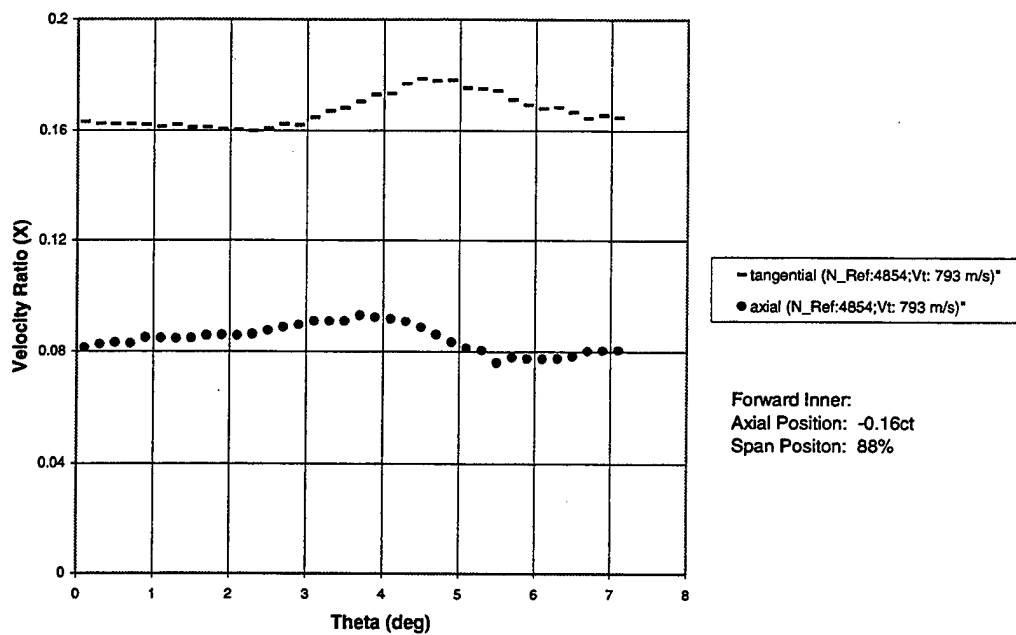
Figure 33. LDV Velocity Ratios for –0.16c_t and 88% Span
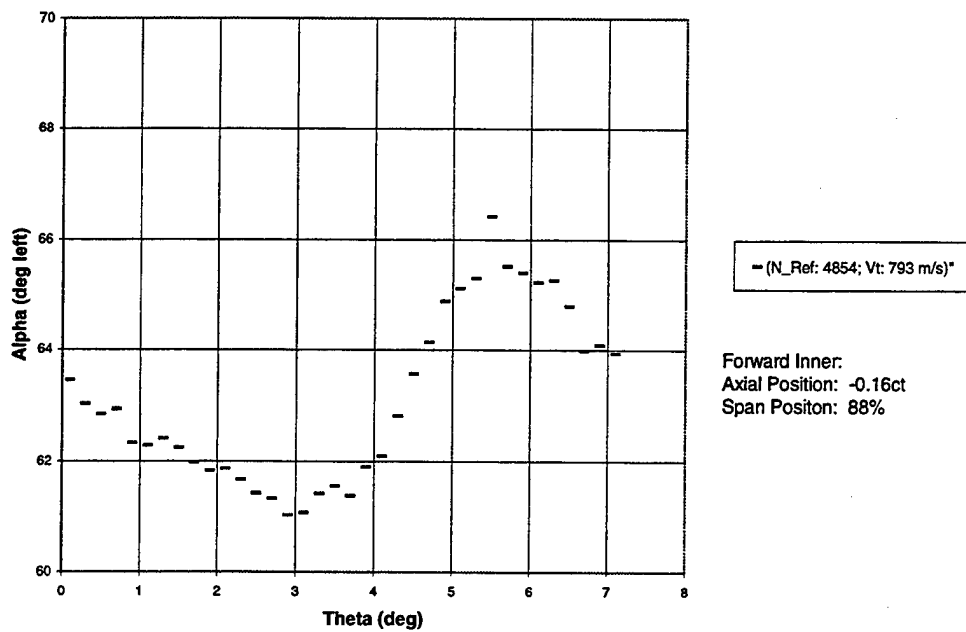
Figure 34. LDV Absolute Flow Angle for –0.16c_t and 88% Span

43
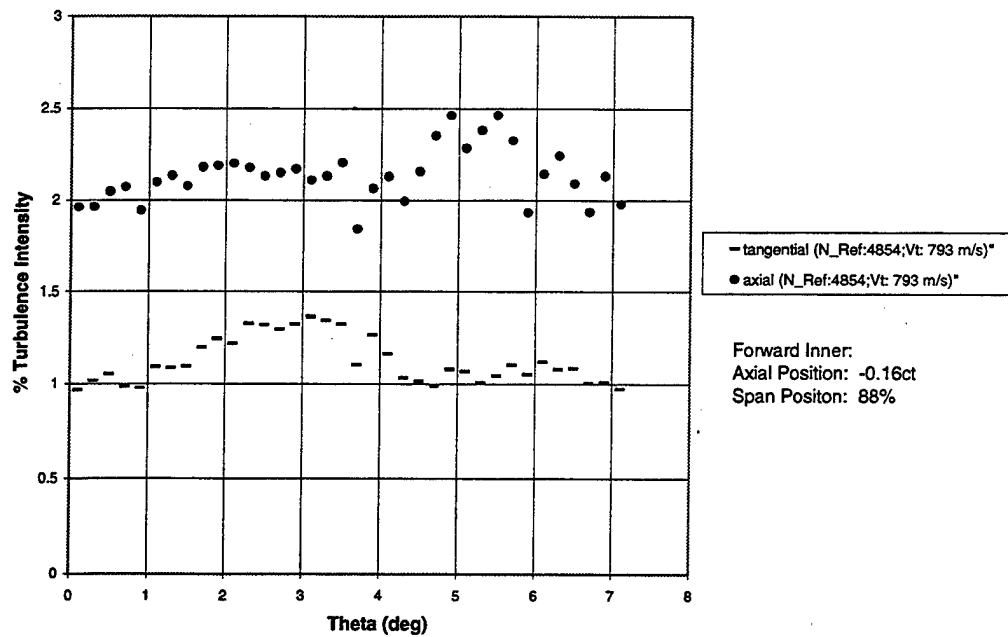
Figure 35. LDV Turbulence Intensity for –0.16c_t and 88% Span
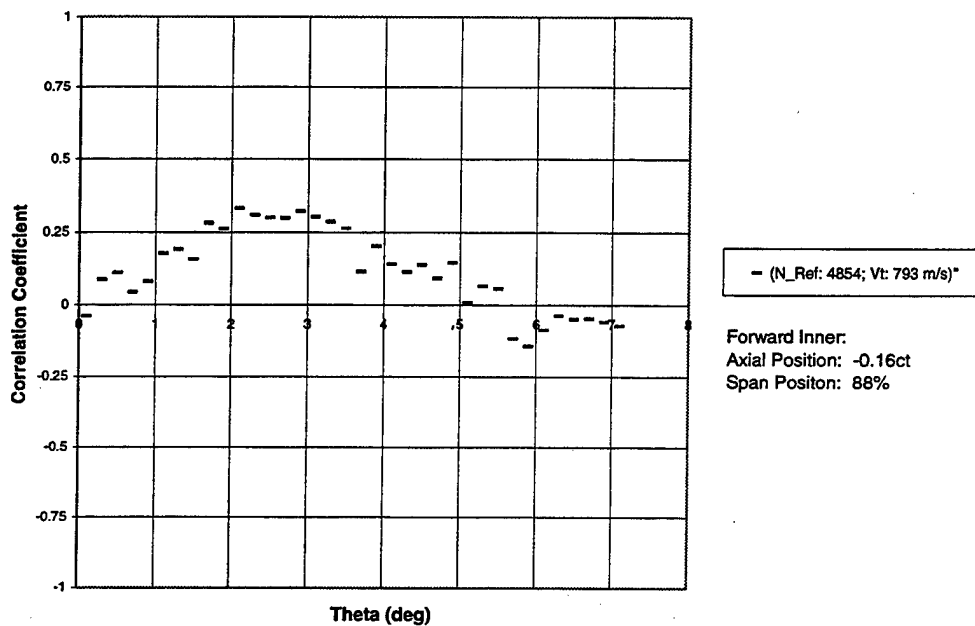
Figure 36. LDV Correlation Coefficient for –0.16c_t and 88% Span

44

a. Axial Velocity Distribution

Axial velocity was plotted for the outer, center and inner surveyed depths in Figure 25, Figure 29, and Figure 33, respectively. At the outer depth (98%), the data appeared as a sinusoid with a single, relatively sharp minimum (0.055 at 2° theta) and a single, relatively rounded maximum (0.070 at 6° theta), giving a "humped" appearance. The average axial velocity ratio value was 0.063. At the center depth (93%), the data developed a second local maximum giving the appearance of an uneven double hump. The absolute maximum (0.08) occurred at 4° theta and a local maximum (0.074) occurred at 0.5° theta. The average axial velocity ratio was 0.073. At the inner depth (88%), the data appeared as a skewed right single humped profile with minor perturbations on the shallow side slope. The axial velocity had an absolute maximum (0.095) at 4° theta, minimum (<0.08) at 6° theta, and an average value of 0.085.

The data clearly showed a decrease in average axial velocity ratio with increasing span (0.083 to 0.063), as well as blade-to-blade variation. The velocity decrease with increasing span is most likely due to penetration of the outer wall boundary layer. The tangential variation could be attributed to a combination of the stator wake deficit and the rotor blade 'bow wave', and their interaction.

b. Tangential Velocity Distribution

Tangential velocity was plotted for the outer, center and inner surveyed depths in Figure 25, Figure 29, and Figure 33, respectively. At the outer depth (98%), values varied from a relatively sharp minimum (0.14 at 2° theta), to a rounded maximum (0.175 at 4° theta), in a skewed left sinusoid, with an average value of approximately 0.155. At the center depth (93%), the well-defined maximum (0.175 at 5° theta) and minimum

45

(0.145 at 2° theta), with constant slopes between, had a nearly sawtooth shape with an average value of 0.16. At the inner depth (88%), the data appeared as a slightly left skewed Gaussian distribution, with a well-defined maximum (0.018 at 4.5° theta), and an average value of 0.17.

Similar to the axial velocity ratio, the data showed a decrease in average tangential velocity ratio with increasing span (0.17 to 0.155), as well as blade-to-blade periodicity. The velocity decrease with increasing span was most likely due to penetration of the outer wall boundary layer. The tangential variation could be attributed to flow turning as result of the rotor blade 'bow wave'. Based on the velocity data, the rotor blade leading edge stagnation streamlines most likely passed through the forward measurement volumes at a tangential position of approximately 2° theta, corresponding to the minimum flow velocity.

c.   Flow Angle

The flow angle (α) was computed from the ratio of the tangential and axial velocities and plotted for the outer, center and inner surveyed depths in Figure 26, Figure 30, and Figure 34, respectively. At the outer depth (98%), the data appeared as a sinusoid with a single minimum (67° at 6° theta), and maximum (70.5° at 3° theta), with an average value of 68.5°. At the center depth (93%), the data developed a second minor local maximum (65.5° at 2° theta) in the bucket of the sinusoid. The absolute maximum (68°) occurred at 5.5° theta and the absolute minimum (65°) occurred at 3° theta. The average flow angle was 66°. At the inner depth (88%), the data appeared as a slightly skewed left sinusoid with a single maximum (65.5° at 6° theta) and minimum (61° at 3° theta), with an average value of 63°.

The data clearly showed an increase in average flow angle with increasing span (63° to 68.5°) as well as blade-to-blade variation. In addition to the velocity ratio effects discussed above, the flow angle

46

increase with increasing span could be partially due to the upstream effects of the tip flow from the blade pressure side (PS) to the blade suction side (SS), in the rotor blade tip gap.

d.   Axial Turbulence Intensity

Axial turbulence intensity was plotted for the outer, center and inner surveyed depths in Figure 27, Figure 31, and Figure 35 respectively. At the outer depth (98%), the data appeared as a sinusoid with a single minimum (2.4% at 5° theta) and maximum (4.0% at 2° theta) and an average value of 3.3%. At the center depth (93%), the data developed a second minor local maximum (2.5% at 6° theta) in the bucket of the sinusoid. The absolute maximum (>3.5%) occurred at the 2° theta position and the absolute minimum (2.2%) occurred at 4.5° theta. The average axial turbulence intensity was 2.7%. At the inner depth (88%), the data appeared less organized, as a single large hump with several smaller humps. The absolute maximum (2.5%) occurred at 5° theta and the minimum (1.8%) occurred at 6° theta, with an average value of 2.2%.

The data clearly showed a significant increase in average axial turbulence intensity with increasing span (2.2% to 3.3%) as well as blade-to-blade variation, most likely due to the outer wall boundary layer viscous effects and vorticity approaching the tip gap region. The maximum value of the axial turbulence intensity correlated with the minimum value of the axial velocity component and vice versa, as would be expected from the definition given in Section III.A.2.

e.   Tangential Turbulence Intensity

Tangential turbulence intensity was plotted for the outer, center and inner surveyed depths in Figure 28, Figure 32, and Figure 36, respectively. At the outer depth (98%), the data appeared as a sinusoid with a single minimum (1.1% at 5° theta) and maximum (2.5% at 2°

theta), with an average value of 1.75%. At the center depth (93%), the data appeared as a sinusoid, with a single minimum (1.1% at 5.5° theta), and maximum (2.1% at 2.5° theta), and with an average value of 1.5%. At the inner depth (88%), the data became less organized, with a major and minor hump. The absolute maximum (1.4%) occurred at 3° theta and minimums (<1.0%) occurred at 5° and 7° theta, with an average value of 1.2%.

The data clearly showed a significant increase in average tangential turbulence intensity with increasing span (1.2% to 1.75%) as well as blade-to-blade variation. The maximum value of the tangential turbulence intensity correlated with the minimum value of the tangential velocity component and vice versa, as would be expected from the definition given in Section III.A.2.

f.   Correlation Coefficient

Correlation Coefficient was plotted for the outer, center and inner surveyed depths in Figure 27, Figure 31, and Figure 35 respectively. At the outer depth (98%), the data appeared as a sinusoid with a single minimum (-0.1 at 4° theta), and maximum (>0.5 at 2° theta), with an average value of 0.25. Most of the data was positive, indicating orbiting in the first and third quadrant of the cross-correlated velocity fluctuations. Slight negative, or near zero correlation, was measured between 4° and 5° theta. At the center depth (93%), the data appeared as a sinusoid with a single minimum (-0.2 at 5.5° theta), and maximum (0.5 at 2.5° theta), with an average value of 0.2. At the inner depth (88%), the data became slightly more scattered, but retained the sinusoid shape with a single maximum (0.3 at 2.5° theta), single minimum (-0.20 at 6° theta), and average value of 0.10.

The data clearly showed a significant increase in average correlation coefficient with increasing span (0.10 to 0.25), as well as

48

blade to blade variation. At the inner location, the values were approximately zero in the 5° to 7° tangential location, indicating near freestream turbulence and possibly the center of the blade to blade passage. This location would be consistent with the blade location analysis discussed above in the paragraph 2.a of the present Section IV.A.

3.   Measurements Within the Rotor Blade Passage

Measurements were made at each of the three depths presented in Table 1 at both the $0.35c_t$ and $0.84c_t$ axial locations. PHASE software was used to both delay and size the acquisition window per the settings of APPENDIX E, as discussed in Section III.A.1. Data rates were not adequate to obtain full 20K point data sets; raw data files ranged in size from 5% to 40% of a full raw data file. Even with window averaging, data point count varied considerably, and was as low as 4 points per bin. Data repeatability was assessed at the center depth as discussed below. Due to scatter between data sets, an average line is included for the $0.35c_t$ center depth (cc) plots. The data are presented as Figure 37 through Figure 61. A histogram of the number of data points for each measurement position is included following the data set for each axial location. Discussion of velocity components and flow angles is included following plots of each axial location. Although data are presented for turbulence intensity and correlation coefficient, the scatter as a result of the very low data rates preclude a meaningful analysis of the results.

49

a.   0.35 Rotor Blade Tip Chord Data Plots
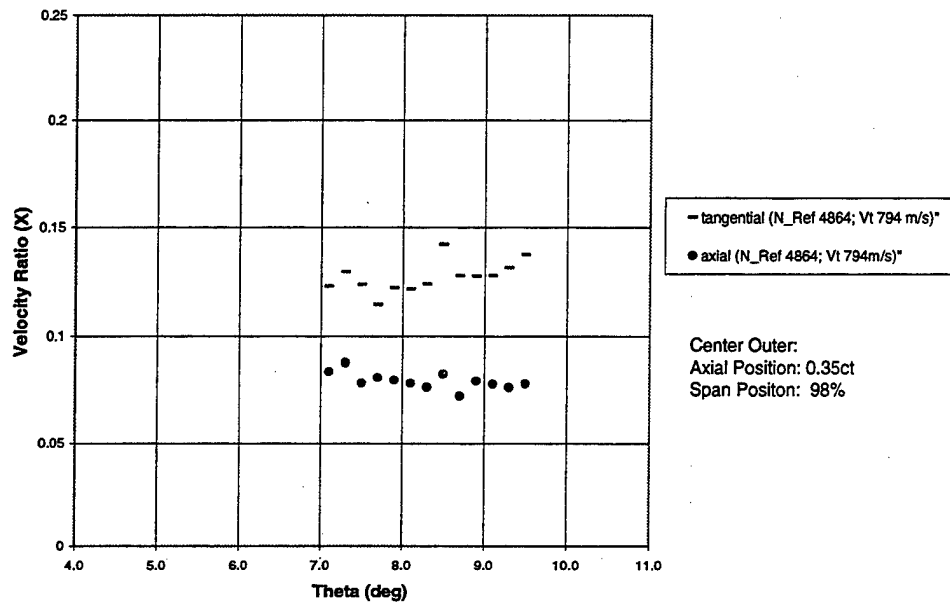
Figure 37. LDV Velocity Ratios for $0.35c_t$ and 98% Span
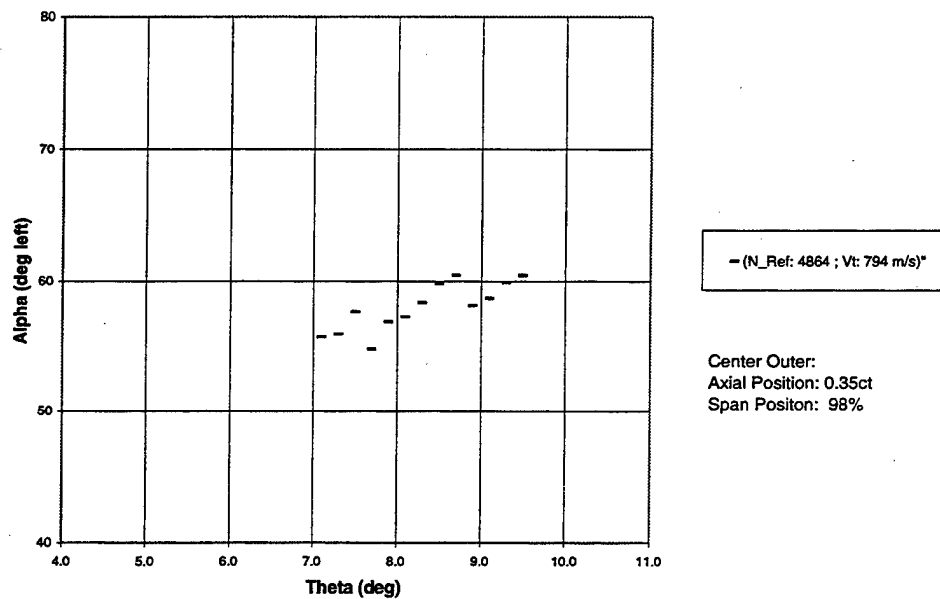
Figure 38. LDV Absolute Flow Angle for $0.35c_t$ and 98% Span

50
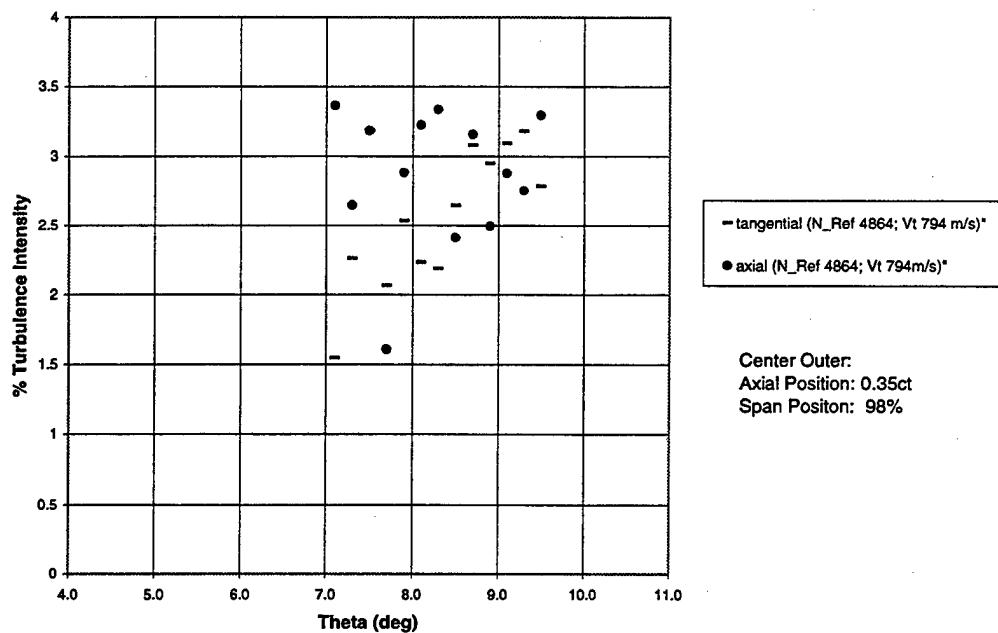
Figure 39. LDV Turbulence Intensity for $0.35c_t$ and 98% Span
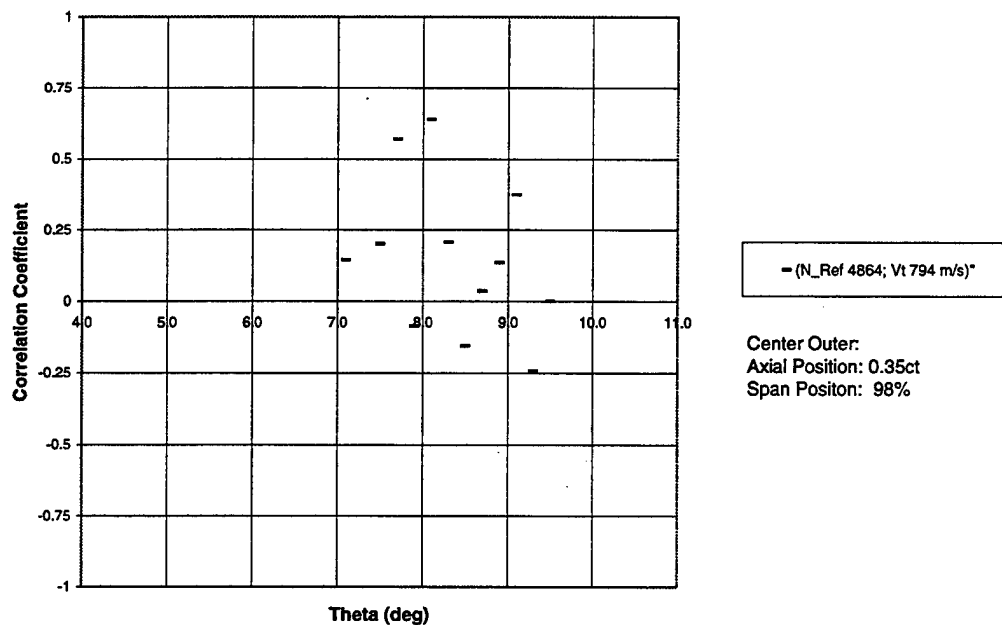
Figure 40. LDV Correlation Coefficient for $0.35c_t$ and 98%

51
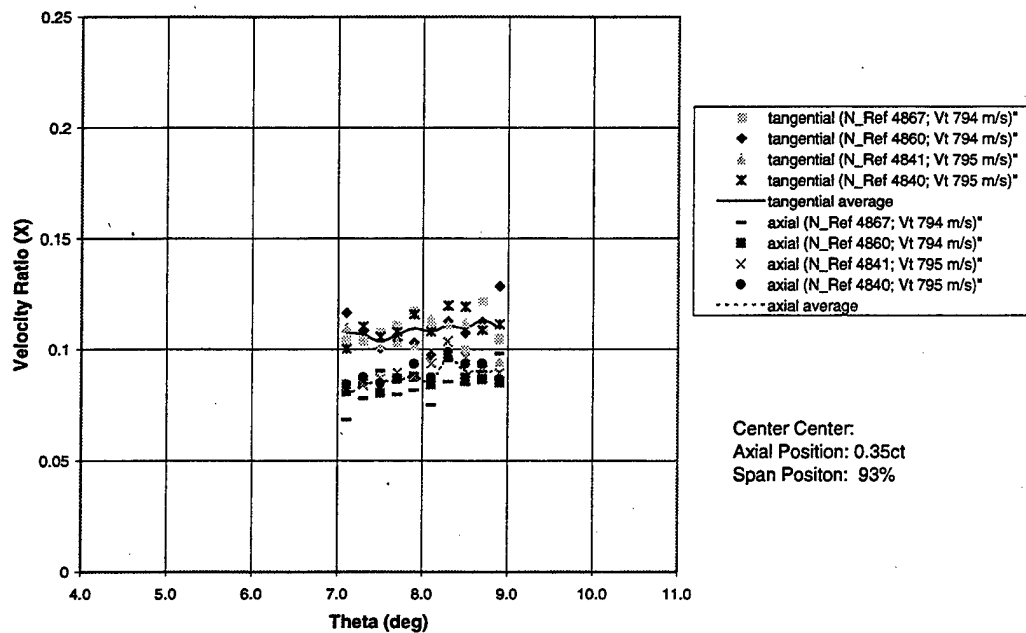
Figure 41. LDV Velocity Ratios for $0.35c_t$ and 93% Span
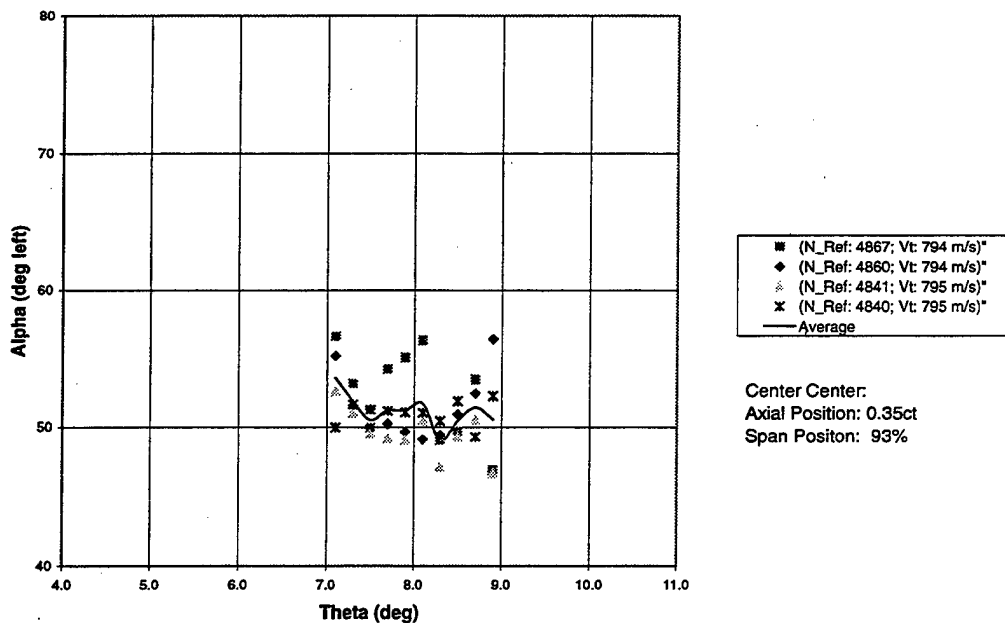
Figure 42. LDV Absolute Flow Angle for $0.35c_t$ and 93% Span

52
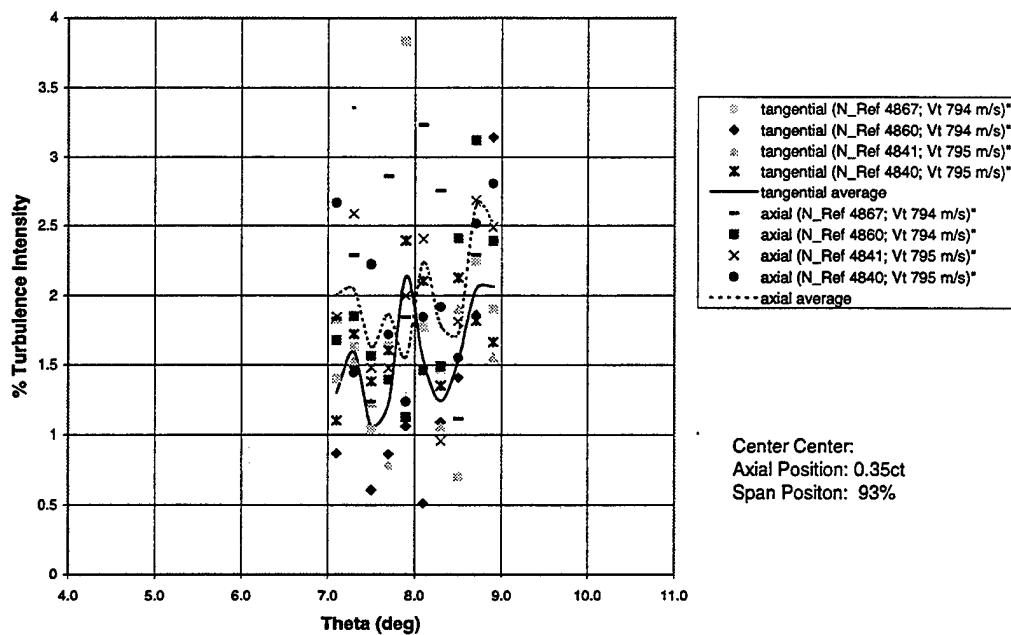
Figure 43. LDV Turbulence Intensity for $0.35c_t$ and 93% Span
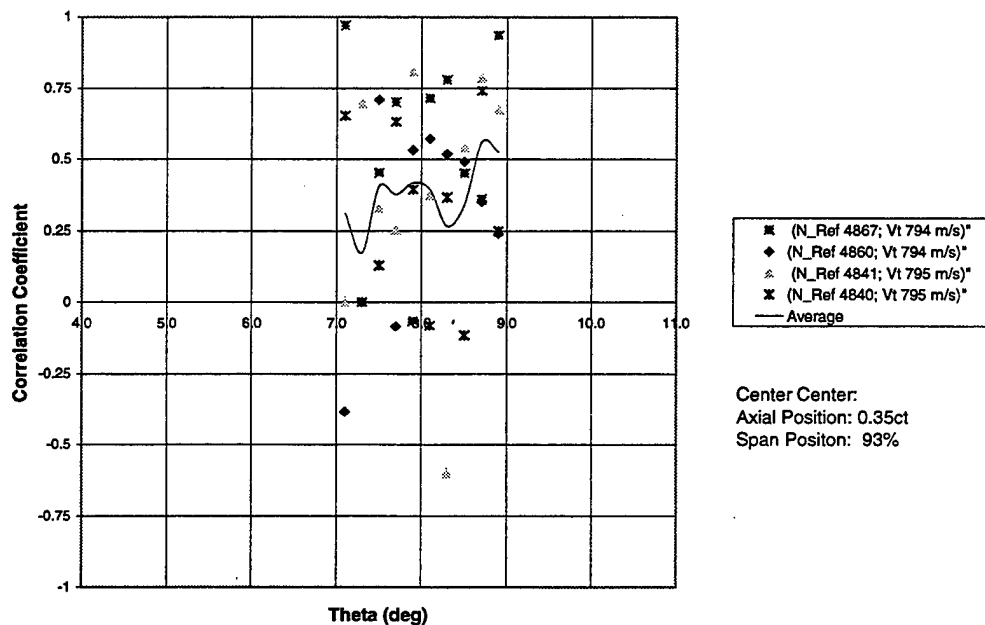
Figure 44. LDV Correlation Coefficient for $0.35c_t$ and 93%

53
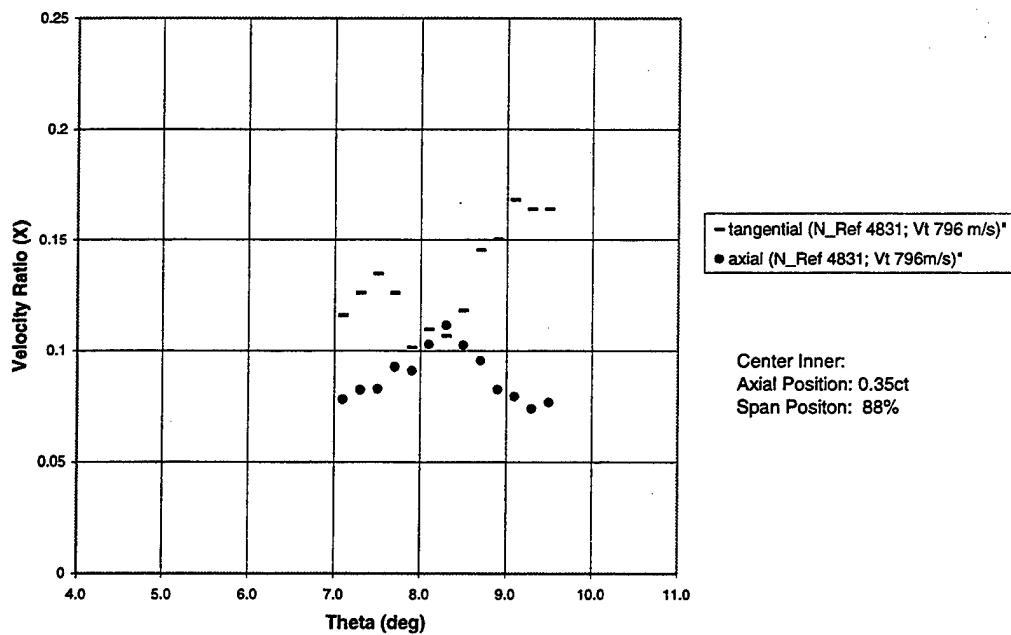
Figure 45. LDV Velocity Ratios for $0.35c_t$ and 88% Span
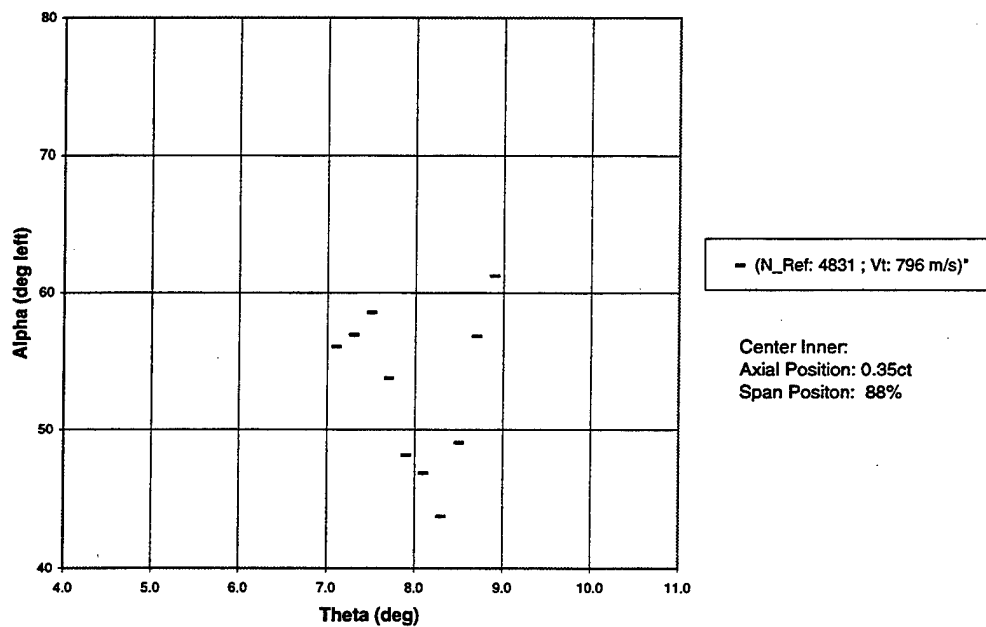
Figure 46. LDV Absolute Flow Angle for $0.35c_t$ and 88% Span

54
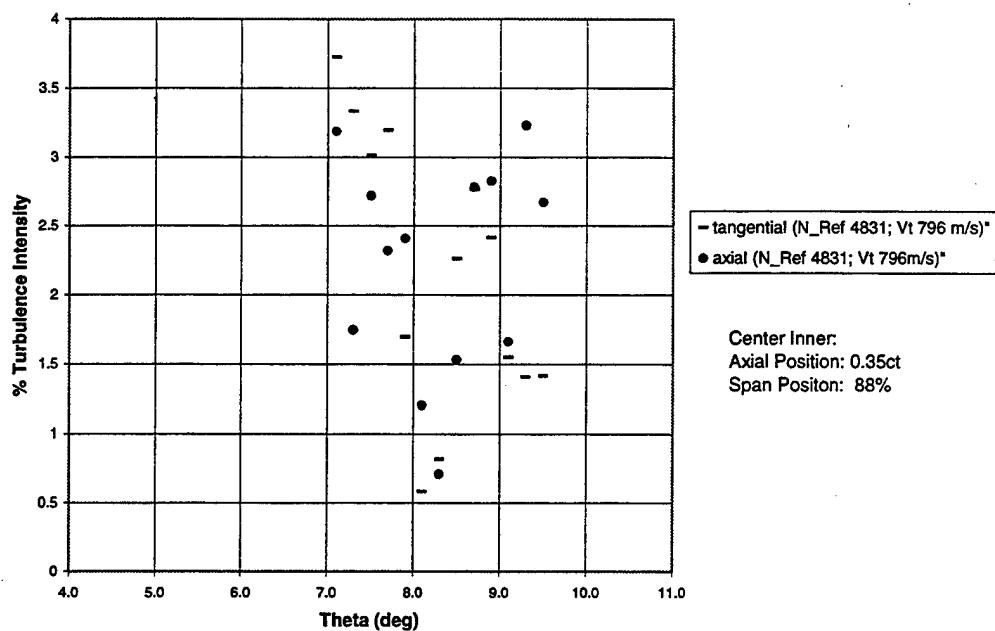
Figure 47. LDV Turbulence Intensity for 0.35c$_t$ and 88% Span
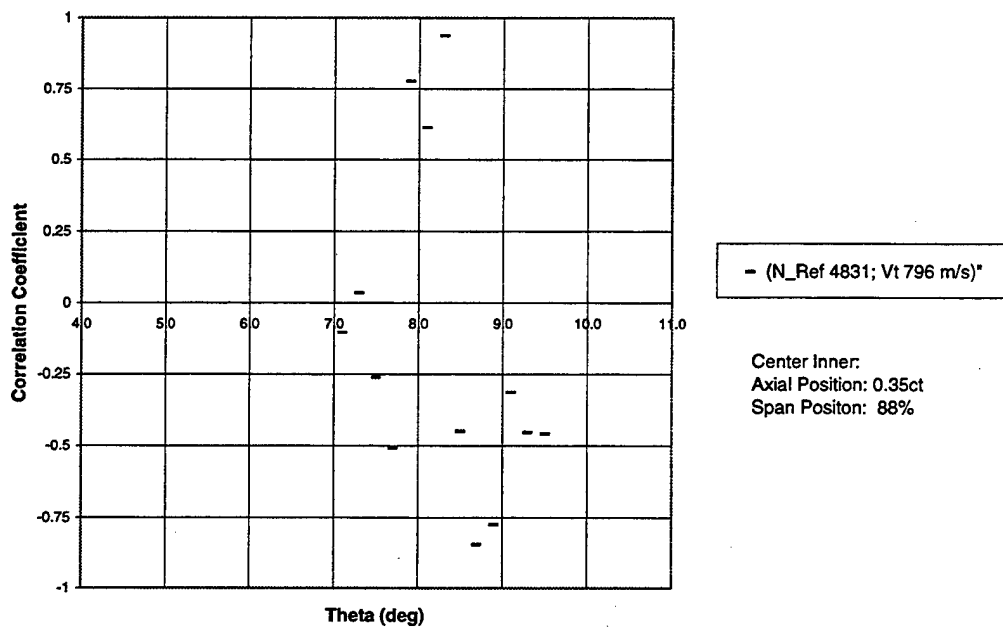
Figure 48. LDV Correlation Coefficient for 0.35c$_t$ and 88%

55
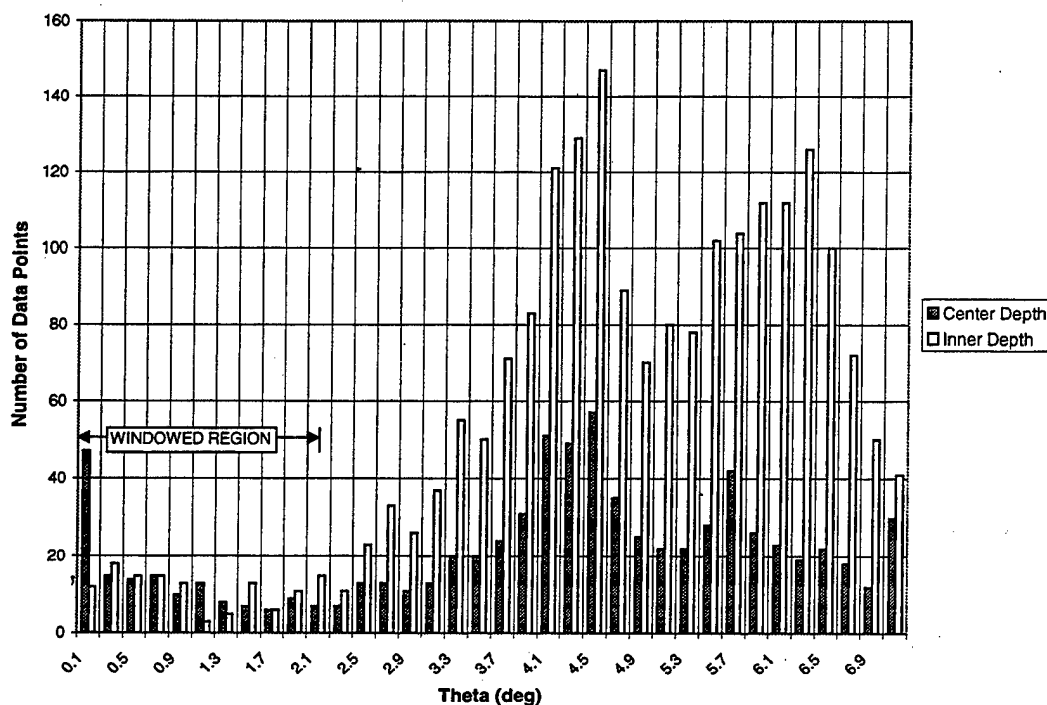
Figure 49. LDV Data Point Histogram for 0.35c$_t$

(1) **Blade Reflection**. Data were taken with and
without tangential windowing for the center and inner depths as described
in Section III.A.1. A histogram of number of data points for data runs
without windowing is shown as Figure 49. The figure also indicates the
theta region (approximately 0° to 2°) used to eliminate blade reflection.
This region corresponded closely to the area with the fewest data points.
The largest data point count occurred in the double peaked area from 4.3°
to 6.5° theta, which most likely represented both particle data and blade
reflection. At this axial location (0.35c$_t$) the tangential extent of the
blade was approximately 2.0° as shown in Figure 8, with two walls
separated by the hollow portion of the blade. The two data peaks most
likely correspond to reflection of the two blade walls and the sloped areas
either side of and between the peaks were due to circumferential blade
inconsistencies. Additional slope contribution could be due to an

56

accumulation of flow particles in close proximity to either the pressure side or suction side of the blades.

At the center depth measurement position (93%), the probe volume actually spanned from 90% to 96% (Figure 7). Therefore, the blade chopped approximately 80% of the probe volume; but this still permitted some flow particle measurements in the tip gap. For these reasons, the data shown outside the windowed region are considered to be dominated by blade reflection, but also to contain valid flow particle data for the outer and center depth measurement positions.

(2) Velocity Distributions. Velocity component distributions are shown in Figure 37, Figure 41 and Figure 45 for the outer, center and inner measurement depths, respectively.

The axial velocity profile at the inner depth (88%) had a well-defined maximum in the center of the plotted window (0.11 at 8.3° theta), and minimums of 0.075 at the window edges, for an average value of 0.09. At the center depth (93%), the maximum of the average plotted profile was barely noticeable (0.10 at 8.3° theta) with an average value of 0.085. The data scatter was approximately 0.015 (20%). At the outer depth (98%), the data were relatively constant, with a value of 0.08. The average value decreased slightly (0.09 to 0.08) with increasing span, however, the data variability shown at the center depth, Figure 41, exceeded the amount of any trend in the spanwise direction. The increased velocity shown toward the middle of the inner depth profile, indicates that a relatively higher speed occurred near the middle of the blade passage channel where the flow was less subject to both the blade and outer wall boundary layers.

The tangential velocity profile at the inner depth showed significant tangential variation with a single well-defined minimum (0.10 at 8.3° theta) and two maxima; the absolute maximum was 0.17 at 9.1° theta and the average was 0.13. The center depth showed a

57

relatively constant tangential average value of 0.11 and scatter of 0.02 (20%). The outer depth profile varied about an average of 0.125. The tangential velocity profiles were consistently greater than the axial values, but did not appear to present an organized trend in either the tangential or spanwise direction.

(3) **Flow Angle.** Flow Angle is shown in Figure 38, Figure 42, and Figure 46 for the outer, center and inner measurement depths, respectively.

The flow angle at the inner depth showed significant tangential variation, with a single well-defined minimum (44° at 8.3° theta), and two maxima; the absolute maximum was 61° at 8.9° theta and the average value was approximately 52°. The center depth profile varied about an average tangential value of 51°, with scatter of up to 9° (18%). The outer depth profile varied about an average value of 57°. The flow angle profiles did not appear to present an organized trend in the tangential direction, but a significant increase in flow angle occurred at the outer depth, indicating tip gap flow from the pressure side to the suction side.

b.   **0.84 Rotor Blade Tip Chord Data Plots**

Two data sets are plotted at each depth. At the outer depth, one set of data was tangentially windowed to eliminate blade reflection, while the second was left open for comparison. Data are presented in Figure 50 to Figure 62.
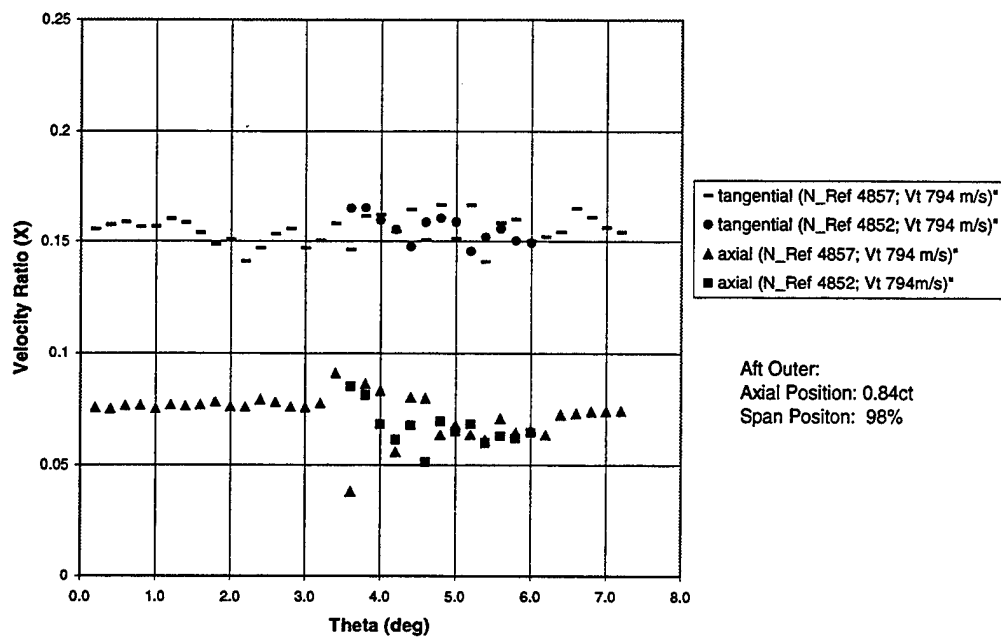
Figure 50. LDV Velocity Ratios for $0.84c_t$ and 98% Span
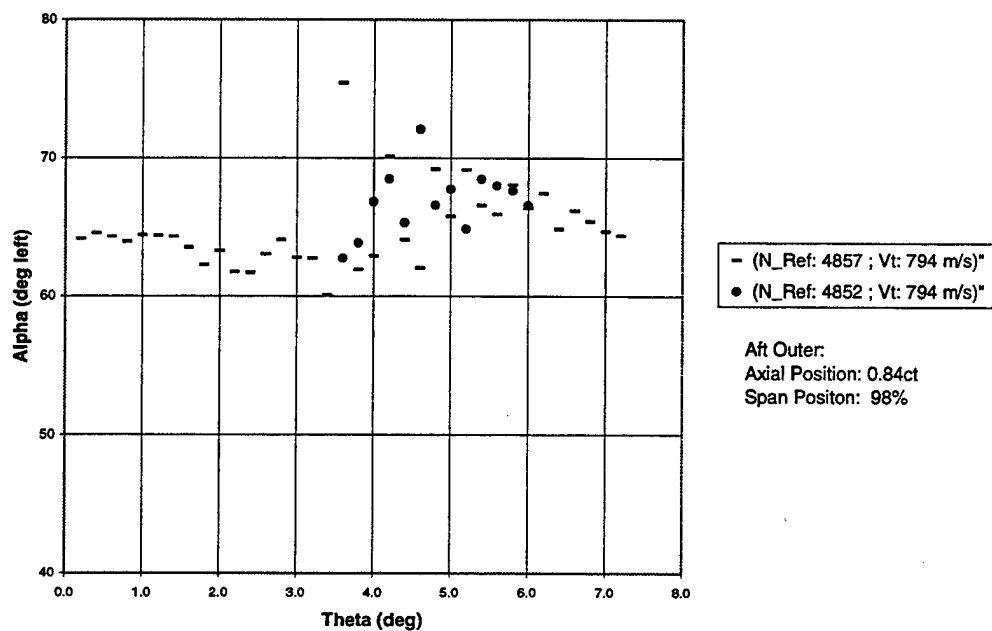
Figure 51. LDV Absolute Flow Angle for $0.84c_t$ and 98% Span

59
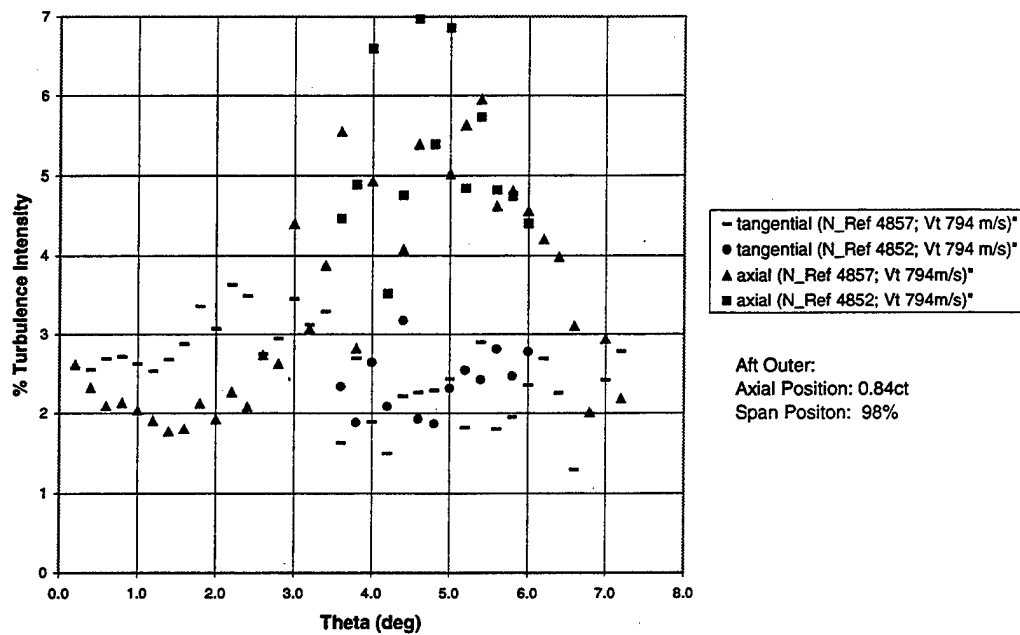
Figure 52. LDV Turbulence Intensity for 0.84c$_t$ and 98% Span
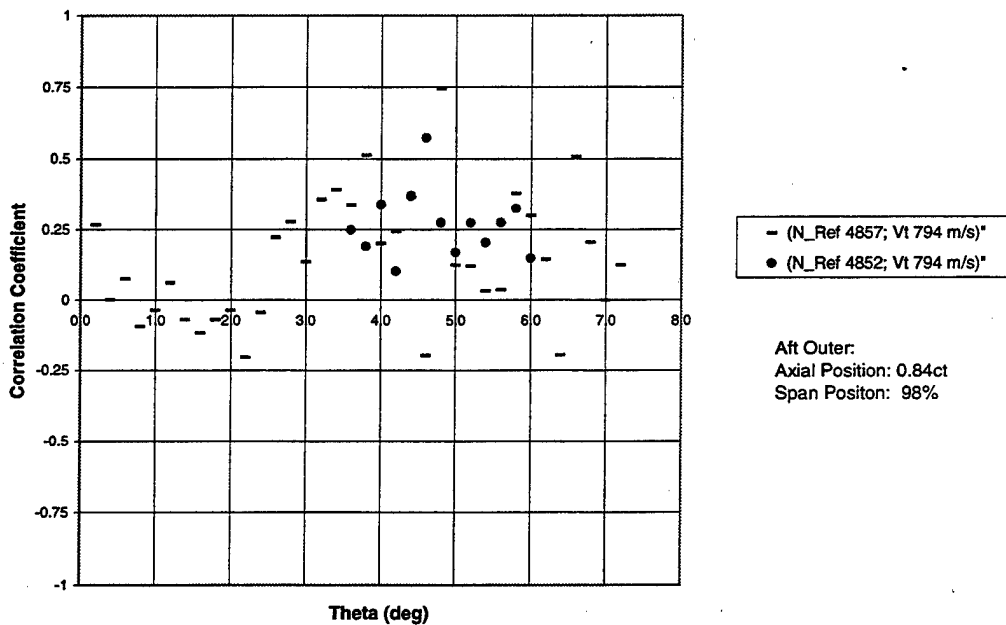
Figure 53. LDV Correlation Coefficient for 0.84c$_t$ and 98%
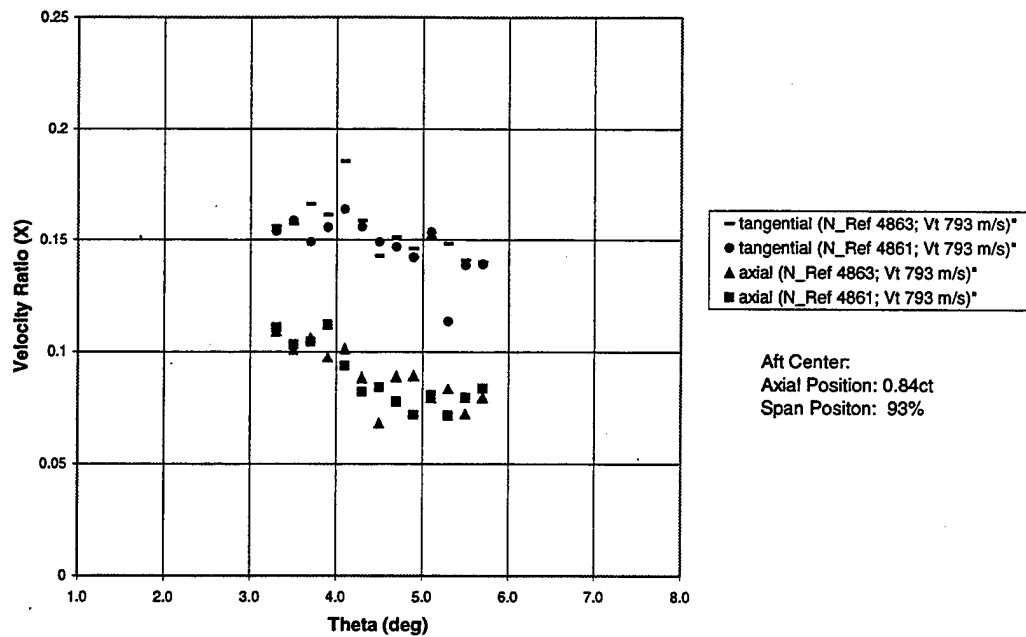
Figure 54. LDV Velocity Ratios for 0.84c_t and 93% Span
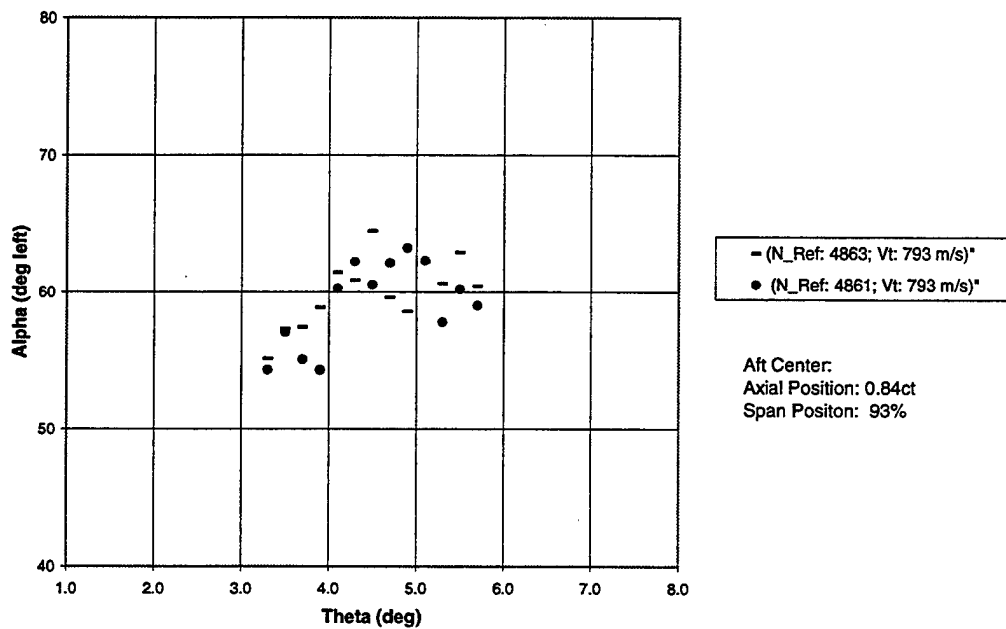
Figure 55. LDV Absolute Flow Angle for 0.84c_t and 93% Span

61
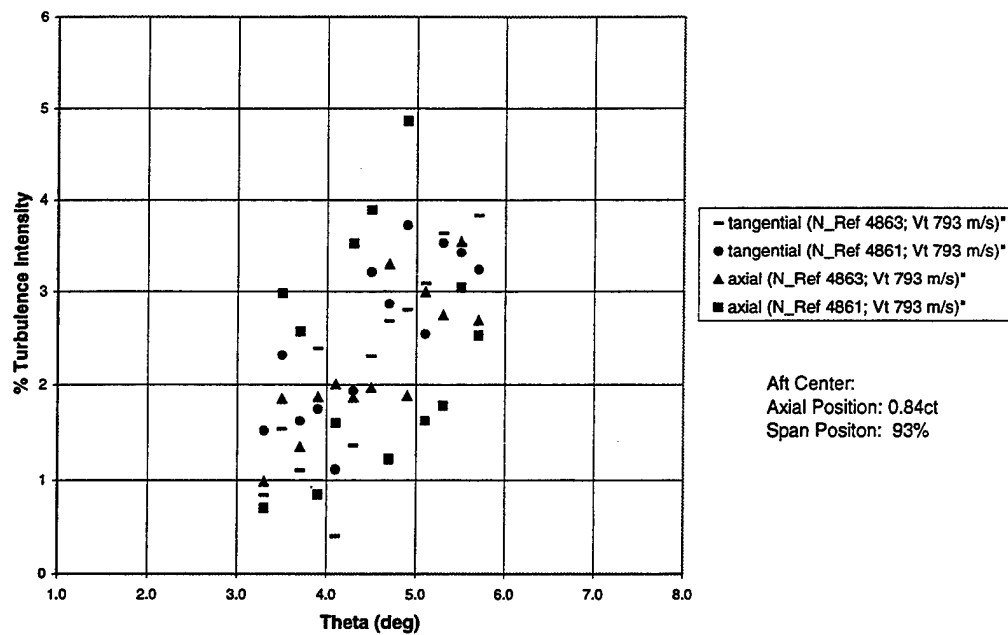
Figure 56. LDV Turbulence Intensity for 0.84c$_t$ and 93% Span
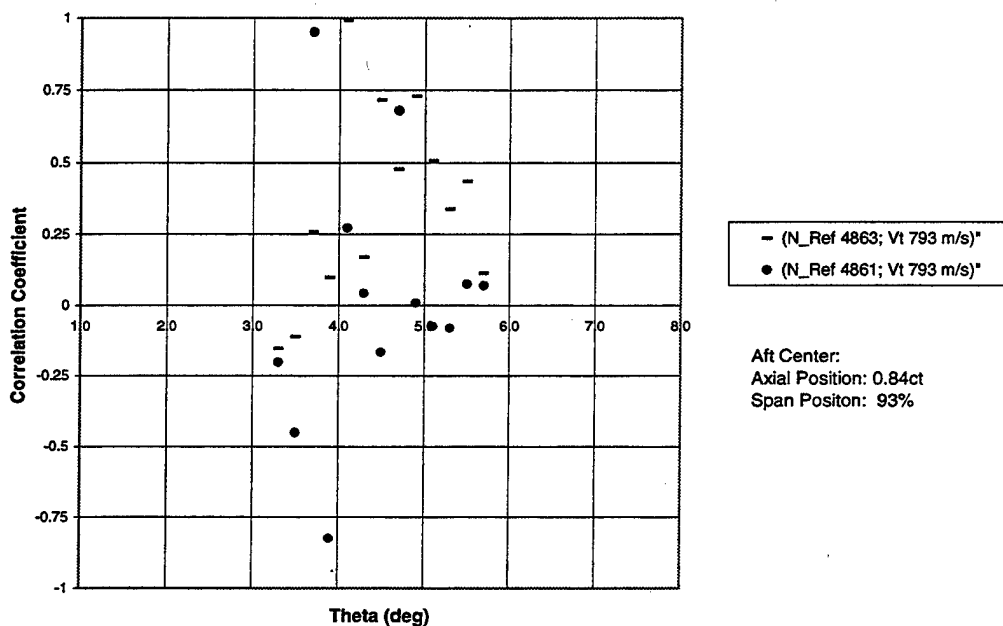
Figure 57. LDV Correlation Coefficient for 0.84c$_t$ and 93%
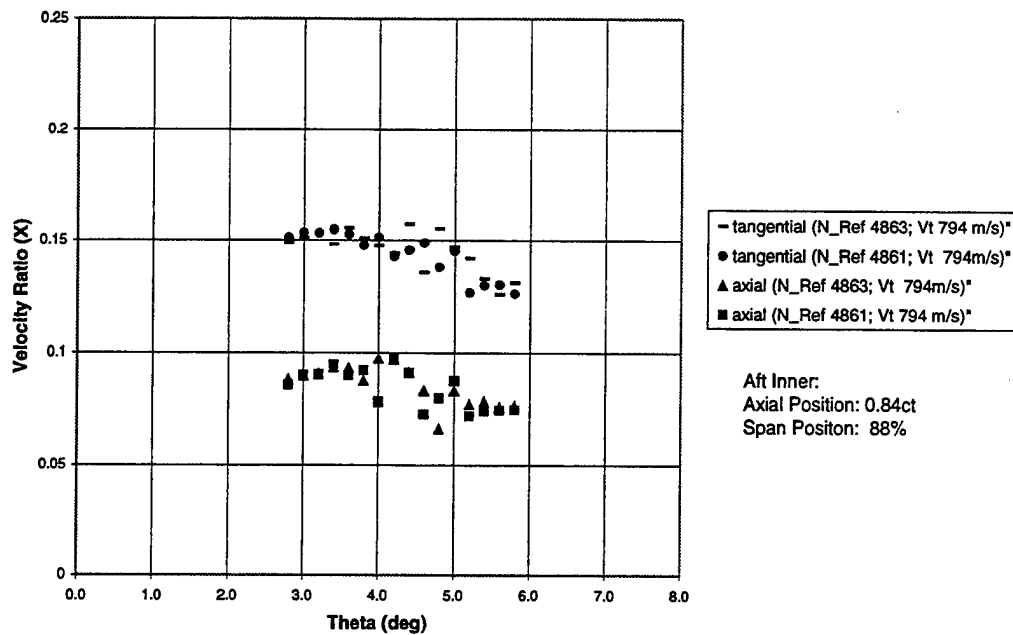
Figure 58. LDV Velocity Ratios for 0.84c$_t$ and 88% Span
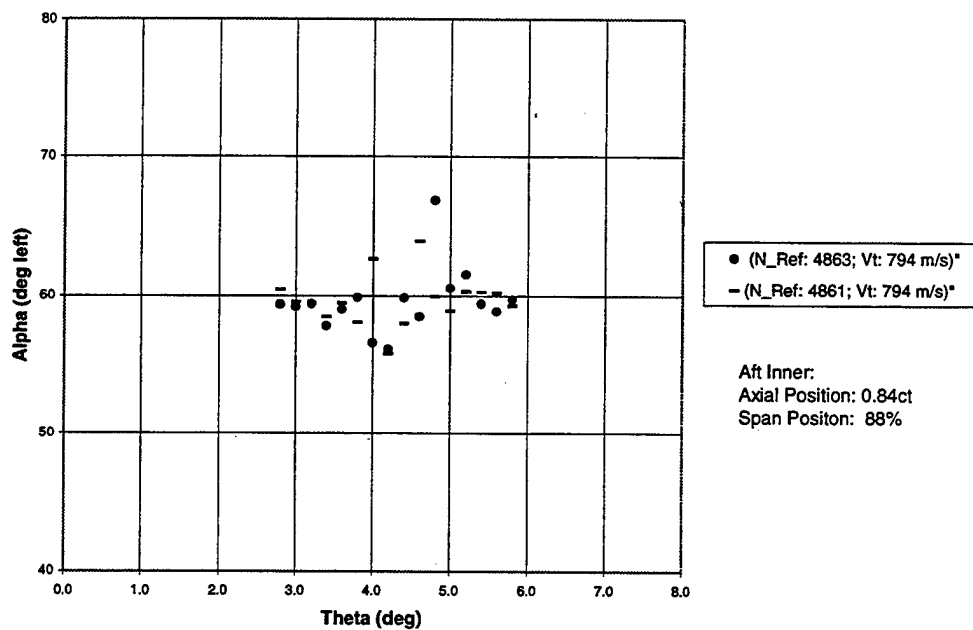
Figure 59. LDV Absolute Flow Angle for 0.84c$_t$ and 88% Span

63
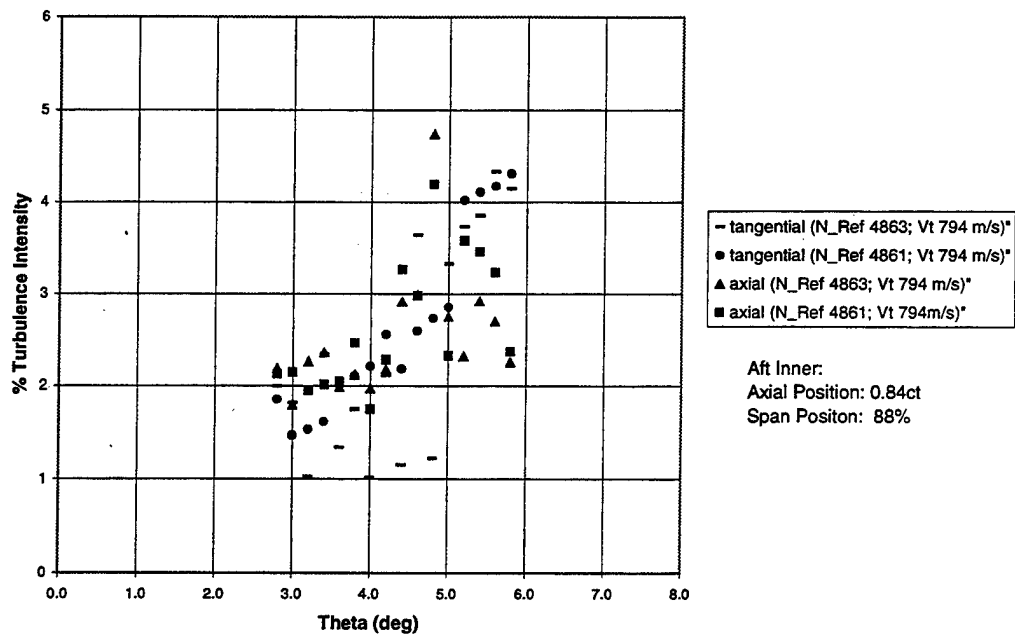
Figure 60. LDV Turbulence Intensity for $0.84c_t$ and 88% Span
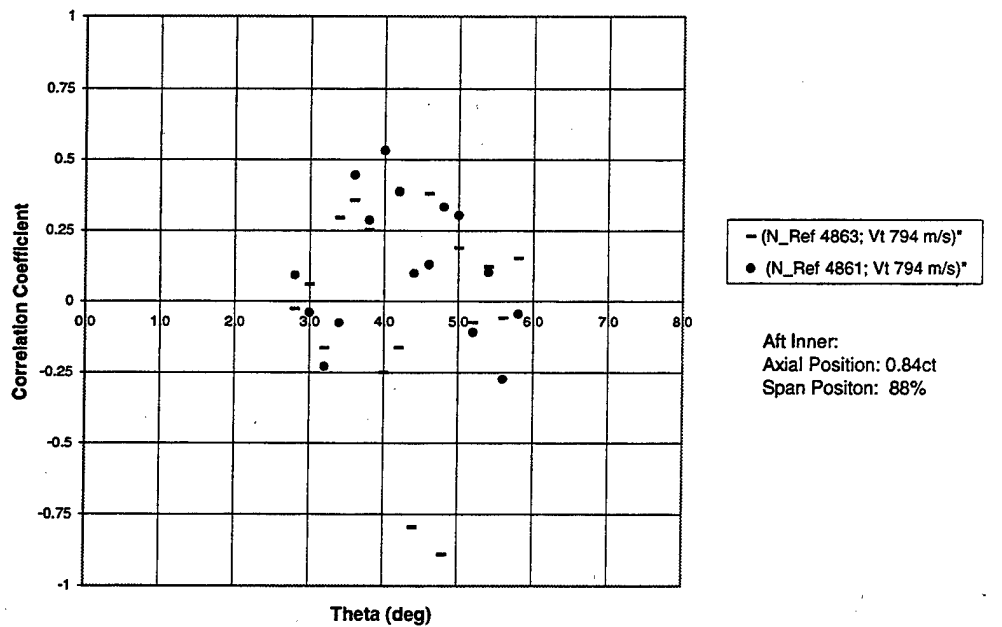
Figure 61. LDV Correlation Coefficient for $0.84c_t$ and 88%

64
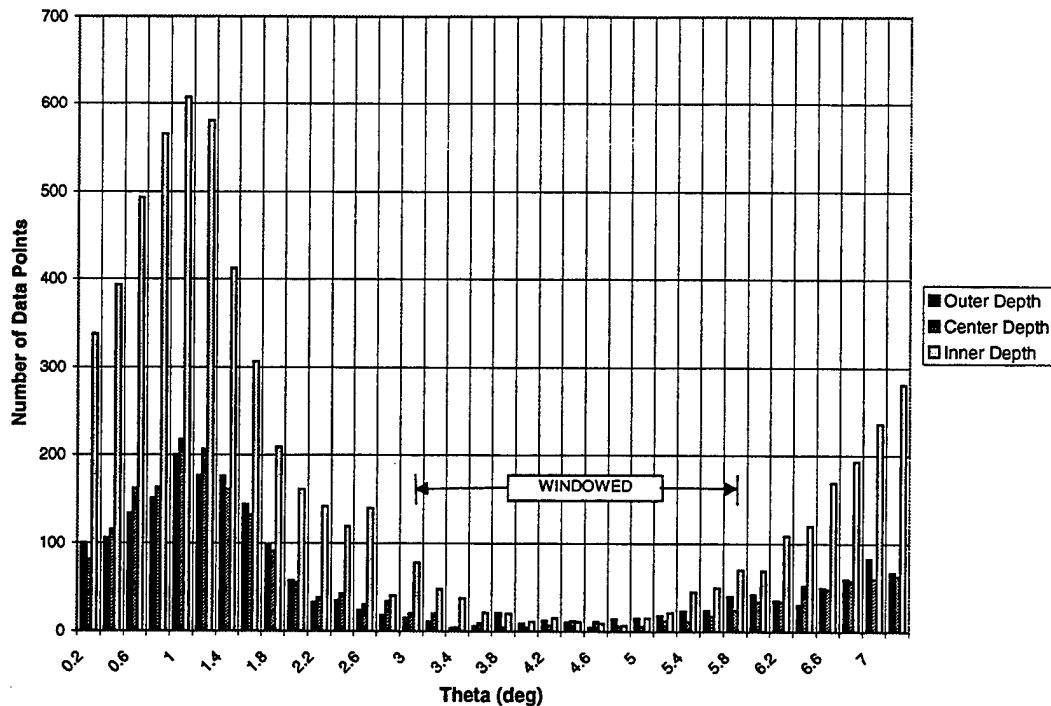
Figure 62. LDV Data Point Histogram for $0.84c_t$

(1)   **Blade Reflection**. Data were taken with and without tangential windowing as described in Section III.A.1. A histogram of data points for data runs at each depth is shown in Figure 62. The figure also indicates the theta region (approximately 3° to 6°) 'windowed' to eliminate blade reflection. This region corresponded to the area with the fewest data points. The peaked area, where the largest data point count occurred, most likely represented both particle data and blade reflection. At this axial location ($0.84c_t$) the tangential blade width was approximately 1.5°, as shown in Figure 8, which corresponded to approximately 7.5° to 9.0° theta. Geometric inconsistency, from variations in blade settings in the fir tree roots, could account for some of the slope in the data to either side of the peak. Additional slope contribution could be due to an accumulation of flow particles in close proximity to either the pressure side or suction side of the blades.

65

Since the outer depth measurement position (98%) spanned from 95% to 101% due to the probe volume size, blade tip clipping certainly occurred, as shown in Figure 7. For the center depth measurement position (90% to 96% span), the blade chopped the probe volume, but still permitted flow particle measurements in the tip gap. For these reasons, the data shown outside the windowed region should be considered to be contaminated by blade reflection, but also to contain flow particle data for the outer and center depth measurement positions.

(2) **Velocity Ratios**. Velocity ratios are shown in Figure 50, Figure 54, and Figure 58 for the outer, center and inner measurement depths, respectively.

The axial velocity profile at the inner depth (88%) varied slightly (0.01) about an average value of 0.085. At the center depth (93%), the trend was decreasing with increasing theta from a maximum of 0.11 to a minimum of 0.075, with an average value of 0.085. At the outer depth (98%), the data varied about an average axial velocity ratio of 0.075. The tangential variation was greatest within the windowed region (3.5° to 6.0°). Outside the windowed region, which included the tip gap as discussed above, the profile remained nearly constant. Although the blade reflection was minimized by using the procedure discussed above, it most likely still had a significant effect since the average number of data points per bin was more than quadrupled outside the tangential window. Overall, the average value decreased slightly (0.085 to 0.075) with increasing span.

The tangential velocity ratio at the inner depth decreased with increasing theta from 0.155 to 0.125, perhaps due to formation of the tip leakage vortex on the blade suction side. The average value was 0.14. At the center depth, the profile was similar to the inner depth, but the average value was increased to 0.15. The outer depth profile varied about an average value of 0.155, both within and outside

66

the windowed region. Overall, the tangential velocity profiles were consistently greater than the axial values and, on average, increased with increasing span.

(3) **Flow Angle**. Flow Angle is shown in Figure 51, Figure 55 and Figure 59 for the outer, center and inner measurement depths, respectively.

The flow angle at the inner depth was somewhat random, with an average value of approximately 59.5°. At the center depth, the profile increased with increasing theta from 55° to 62°. The outer depth profile varied from 62° to 71°, about an average value of 65°. The flow angle profiles did not appear to present an organized trend in the tangential direction, but a significant increase in flow angle occurred at the outer depth, indicating tip gap flow from the pressure side to the suction side.

B.   COMPUTATIONAL RESULTS

Computational solutions were carried out for both three-dimensional and quasi-three-dimensional blade passages using SWIFT and modified versions of RVCQ3D flow solvers, respectively.

1.   Three-Dimensional

SWIFT was used to solve the 3D flow using grids generated by TCGRID, as described in Section III.B.2. The grid initially generated by McKee [Ref. 6], referred to herein as the "coarse grid", was used to evaluate differences in turbulence models and boundary conditions on the flow solution. Based on comparisons of coarse grid exit plane computations with experimental measurements, a denser grid was determined to be necessary to improve the computational/experimental agreement. The denser grid, referred to herein as the "fine grid", was dimensioned and built as described in Section III.B.2.a.

67

a.   Convergence Results

The convergence histories for the coarse grid using the Baldwin-Lomax and k-ω turbulence models are shown in Figure 63.
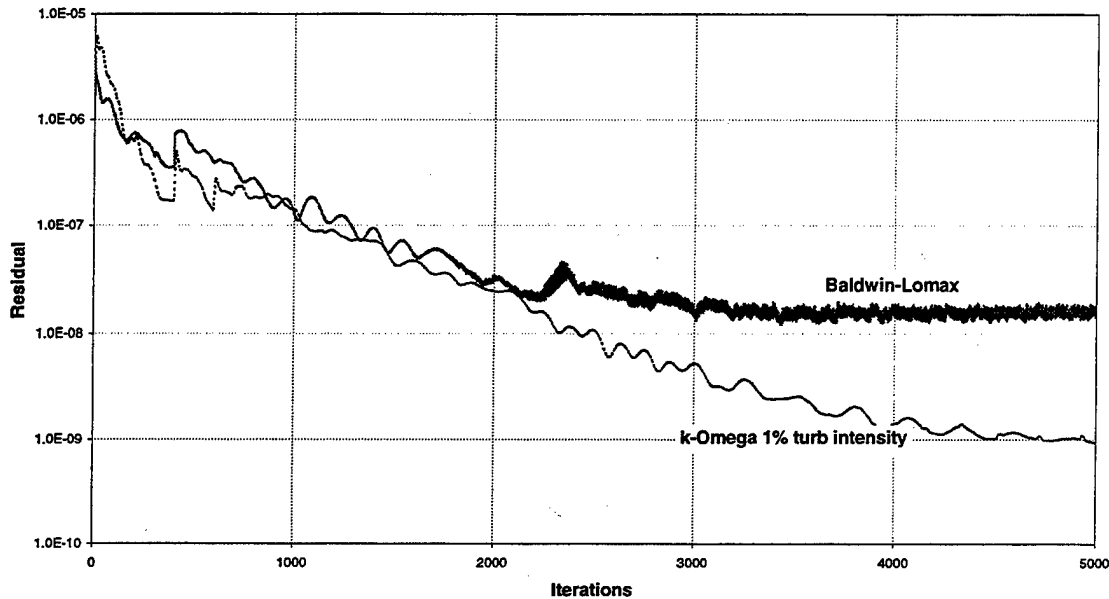
Figure 63. Coarse Grid Solution Residual History

The k-ω solution residuals converged approximately 3.5 orders of magnitude in 5000 iterations. The discontinuities apparent early in the convergence history corresponded to reductions of the first order viscosity used to stabilize the solution. The successfully converged solutions used the following boundary conditions:

- Inlet: P_0, T_0, and v_θ fixed at initial conditions. Riemann Invariant extrapolated from the interior.
- Between blade rows: Momentum averaging.
- Exit plane: Gile's characteristic boundary condition, with variable pressure blade-to-blade.

Restarts of the k-ω solution with 1% turbulence intensity were used to evaluate kinetic energy and fully-mixed-out blade row

68

averaging, as well as the low Re# k-ω turbulence model. Each of these restarts was run approximately 2000 additional iterations, and converged between one and two orders of magnitude.

For all the plotted solutions, the mass flow error was less than 1%, ranging from 0.5% for the k-ω solution with mixed out averaging, to 0.8% for the k-ω solution with energy averaging.

Although the fine grid was built to increase grid density, and numerous solutions were attempted, a steady-state solution was not obtained. Variations of 1st and 2nd order viscosity, turbulence modeling, boundary conditions, and Runge-Kutta solution schemes were attempted. Although many solution techniques were used, the nearest to success was when the solution was started with a high value of 1st order viscosity (0.5 to 1.0), and then halved on scheduled intervals between 400 and 800 iterations to reduce that value. The runs typically appeared to run well until the 1st order viscosity was reduced to near zero (0.008-0.031); then a steady increase in residual error eventually led to divergence.

b.   Exit Plane Flow Properties

The rotor exit plane property profiles were computed within SWIFT by tangential averaging across the blade passage at the k-plane spanwise locations, for each of the converged coarse grid solutions. Comparisons of between blade row averaging techniques, turbulence model types, and freestream turbulence intensities were made to determine parameter sensitivity. Mach number, swirl angle and total pressure profiles for the rotor exit plane are plotted in Figure 64, Figure 65 and Figure 66. The Mach number contours in the rotor exit plane, for k-ω with 2% turbulence intensity, are shown in Figure 67.
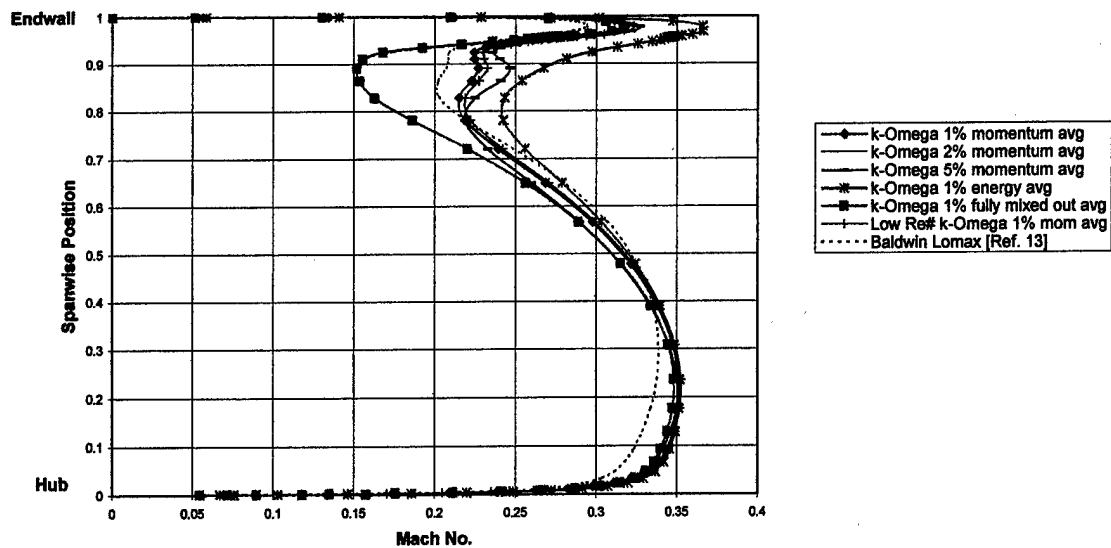
Figure 64. Rotor Exit Plane Mach Number Spanwise Profile
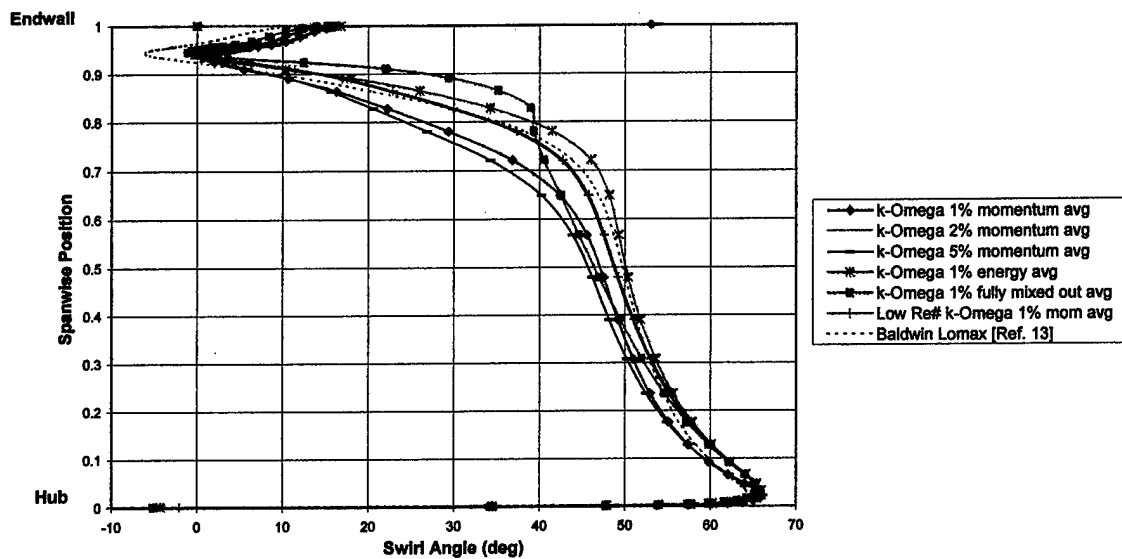
Figure 65. Rotor Exit Plane Swirl Angle Spanwise Profile

70
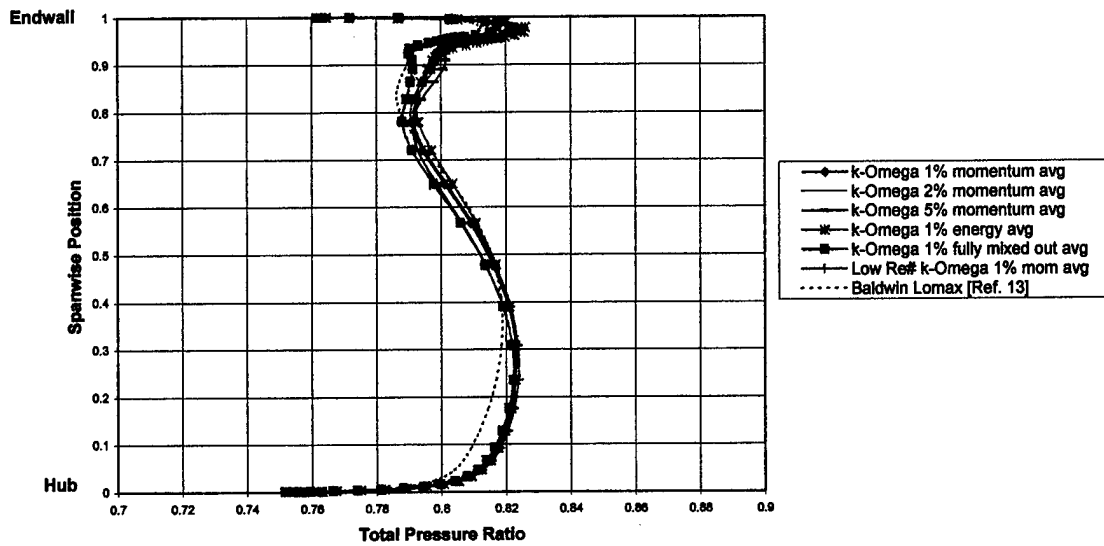
Figure 66. Rotor Exit Plane Total Pressure Ratio Spanwise Profile
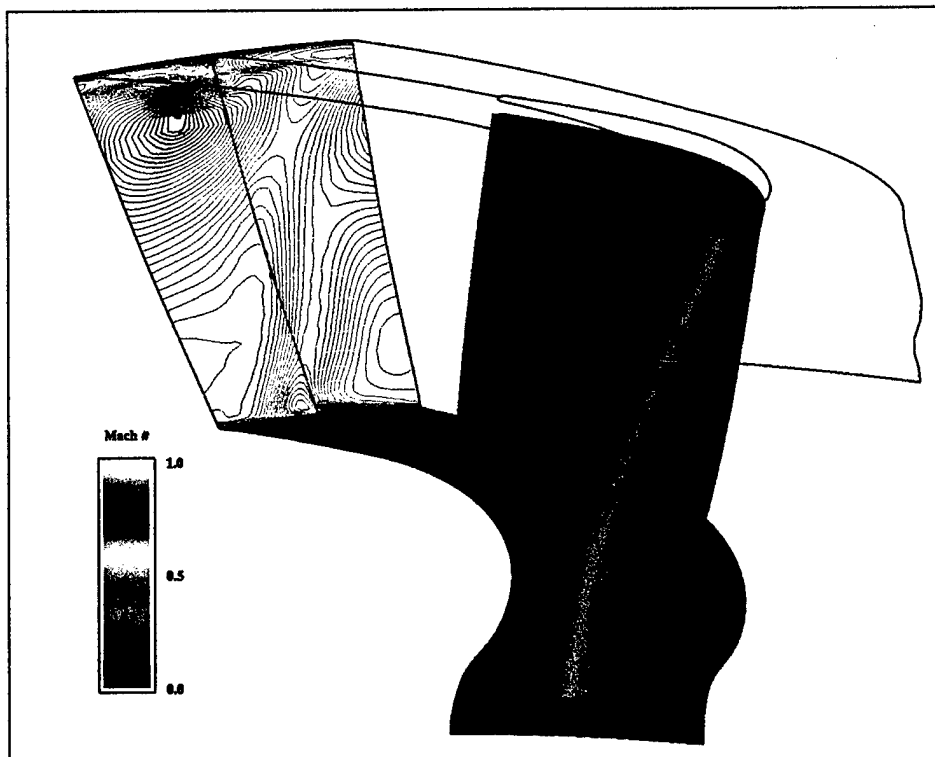
Figure 67. Rotor Exit Plane Mach Number Contours

71

The effect of blade row averaging method, or type, was evaluated by plotting solutions for energy, momentum and mixed out averaging. The type of blade row averaging appeared to significantly affect the exit profiles. In the endwall region of the Mach number profile, the Mach number varied by as much as 0.13 (80%). The fully-mixed-out averaging showed typically lower Mach number in this region, momentum averaging was higher, and energy averaging yielded the highest Mach number. The averaging type, likewise, resulted in changes on the swirl angle distribution. The total pressure results were relatively tightly grouped (within 1% to 2%) for all of the test conditions.

The effect of freestream turbulence intensity was evaluated by plotting 1%, 2% and 5% intensity solution profiles for the k-ω model. The profiles varied by a moderate amount. The most significant being swirl angle, where differences were as high as 10°.

The effect of turbulence model type was evaluated by plotting k-ω and low Re# k-ω models with 1% turbulence intensity, against Baldwin-Lomax. Turbulence model type had the least effect on the exit profiles of the evaluated parameters. Near the endwall, Mach number varied by approximately 0.02. Swirl angle varied by less than 10°; however, the B-L model predicted more negative swirl in the endwall region than the k-ω models.

For the k-ω solution with 2% turbulence intensity, the Mach number exit plane profile, (in Figure 64), increased through the endwall boundary layer to a sharply defined maximum (~0.33) at approximately 97% span, and then dropped to a minimum (~0.22) at approximately 90% span. The minimum in the profile corresponded to the dominant clockwise (CW) rotating tip leakage vortex, as can be seen in the Mach number contours in Figure 67. The high Mach number region near the outer wall is the downstream remainder of the high-speed, tip-gap flow. The Mach

number profiles, using momentum averaging between blade rows, consistently showed a local maximum at approximately 87% span. For the runs not providing a solution, this spanwise location was a point of divergence, with Mach number significantly "spiking". This may have been be due to the sharp flow turn and separation over the blade tip, which is discussed further in Section IV.D. Proceeding towards the hub, the Mach number profile gradually increased from the minimum at 80% span to a second maximum between 20% and 40% span, then rapidly decreased approaching the hub. The majority of the flow between 10% and 70% span could be described as the mid-passage freestream which was largely unaffected by the tip gap. Near the hub, the counter-clockwise vortex was due to the roll up of the hub boundary layer shearing with the accelerated turned flow from the suction side. The steep Mach number decreases at the hub and tip were due to the casing boundary layers.

The swirl angle, Figure 65, showed a well-defined minimum of approximately 0° at 95% span, and then increased throughout the span to a maximum of 65° near the hub. The minimum was due to the dominant tip-leakage flow, which gradually diminished away from the case wall.

The total pressure profile, Figure 66, shown as a fraction of the inlet total pressure, showed that the losses were highest in the vicinity of the tip-leakage vortex, as indicated by the Mach number and swirl angle profiles.

c. Constant Span Flow Properties

Flow Mach number contours and blade surface pressure distributions are shown at midspan in Figure 68 and Figure 69, respectively, using a k-ω turbulence model with 2% turbulence intensity. Mach number contours at 98% span (in the endwall region) are shown in Figure 70.
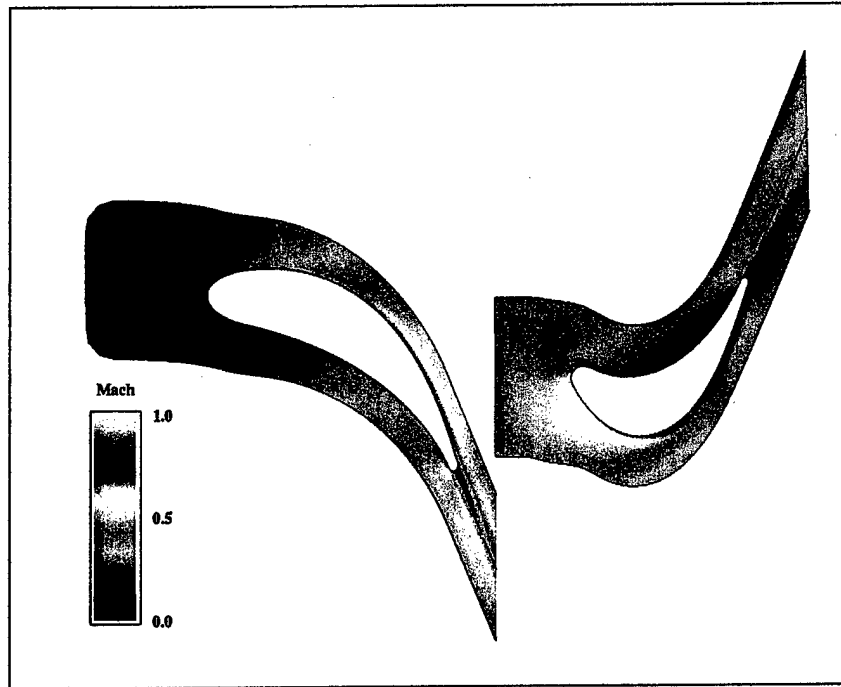
Figure 68. 3D Midspan Mach Number Distribution
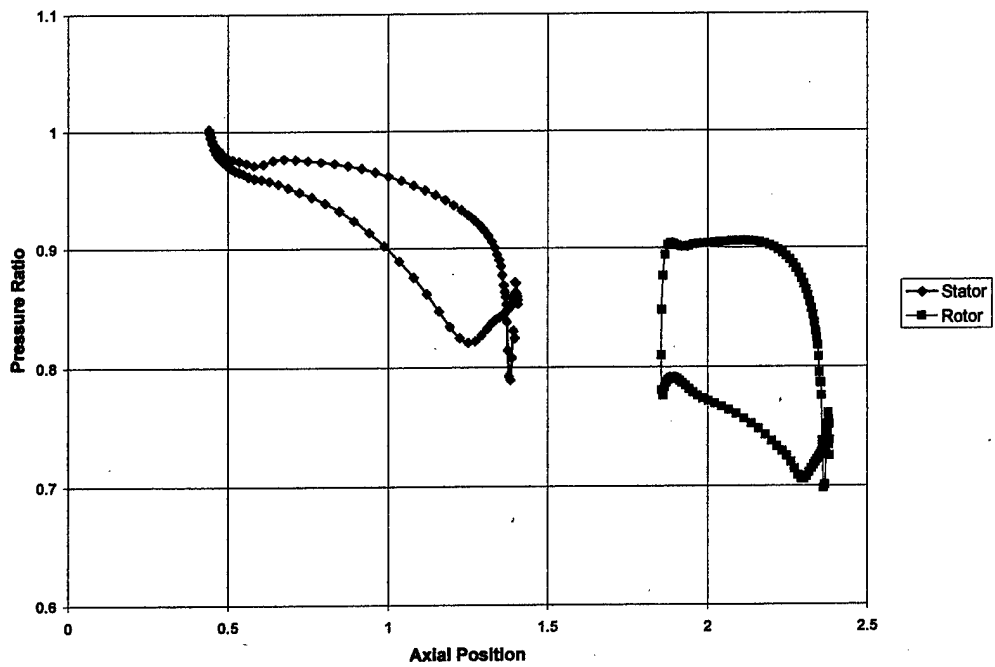
Figure 69. 3D Midspan Rotor and Stator Blade Surface Static Pressure Distributions

74
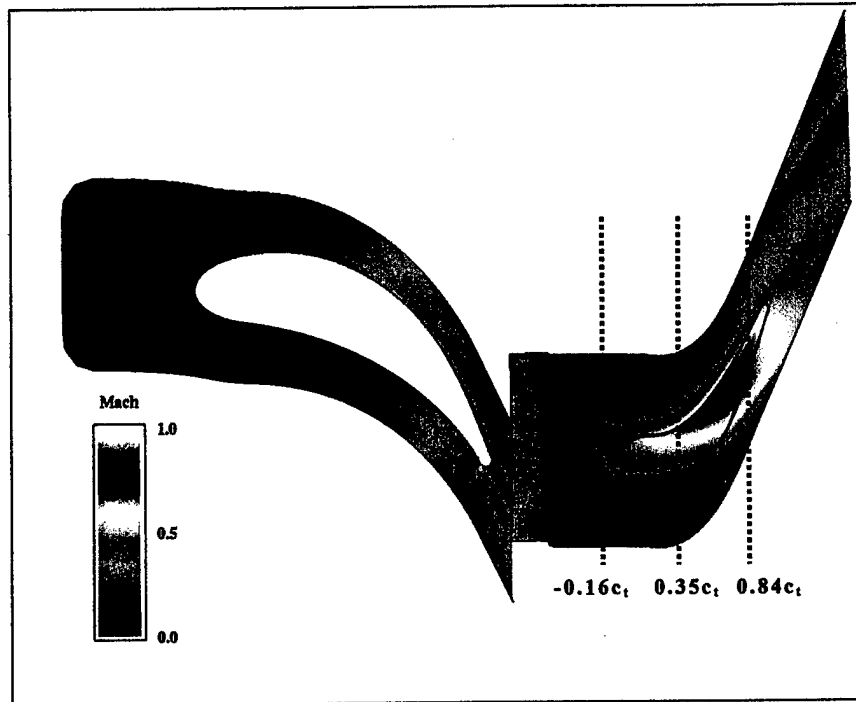
Figure 70. 3D Mach Distribution at 98% span

At midspan, Figure 68 showed the flow accelerating through the stator passage and clearly depicted the stator wake. The flow was circumferentially averaged between the grids, and transferred to the rotor grid. The flow over the rotor blade suction side accelerated with the region of highest Mach number forward of $0.25c_t$. The forward location of the rotor blade suction region was most likely due to the test corrected speed (5K RPM) being well below the turbine design corrected speed (~8K RPM), causing the rotor blade to operate off-design. The flow on the rotor blade pressure side decelerated to a stagnation region located at about 75% chord. The rotor wake was clearly evident, widening on the blade suction side. The midspan blade surface static pressure distribution, Figure 69, was calculated as a ratio with the inlet total pressure. The distributions show pressure changes, which correspond, to the discussed velocity changes.

In the endwall region, Figure 70, the rotor flow acceleration through the tip gap can be seen very clearly. Since the tip gap flow was in the same direction as the blade movement, this flow velocity was the highest in the flow field. More detail on the tip-gap flow acceleration is discussed in Section IV.D.

2.   Quasi-3D

The quasi-3D grid was generated and the flow solved as described in Section III.B. The flow solutions generated steady wakes, stationary with respect to the rotor blade. Work was in progress at the time of this report to complete an unsteady wake analysis.

a.   Quasi-3D Steady Wake Solutions

The solutions for wakes stationary relative to the rotor blade, as shown in Figure 15, were computed and the results are shown in Figure 71 and Figure 72 for the Wake 1 inlet profile.
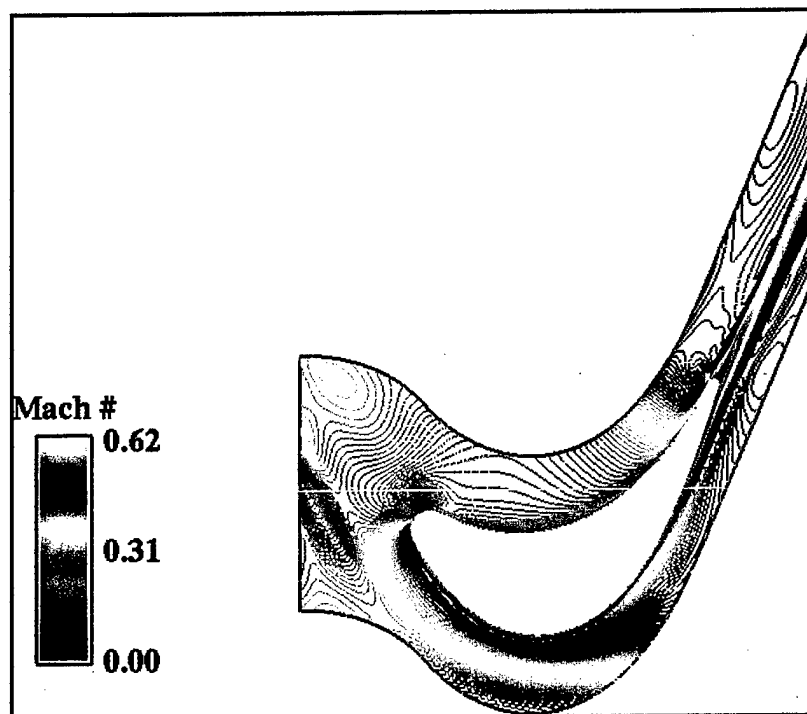
Figure 71. Quasi-3D Rotor Mach Number Contours with Stationary Wake (Relative Frame)
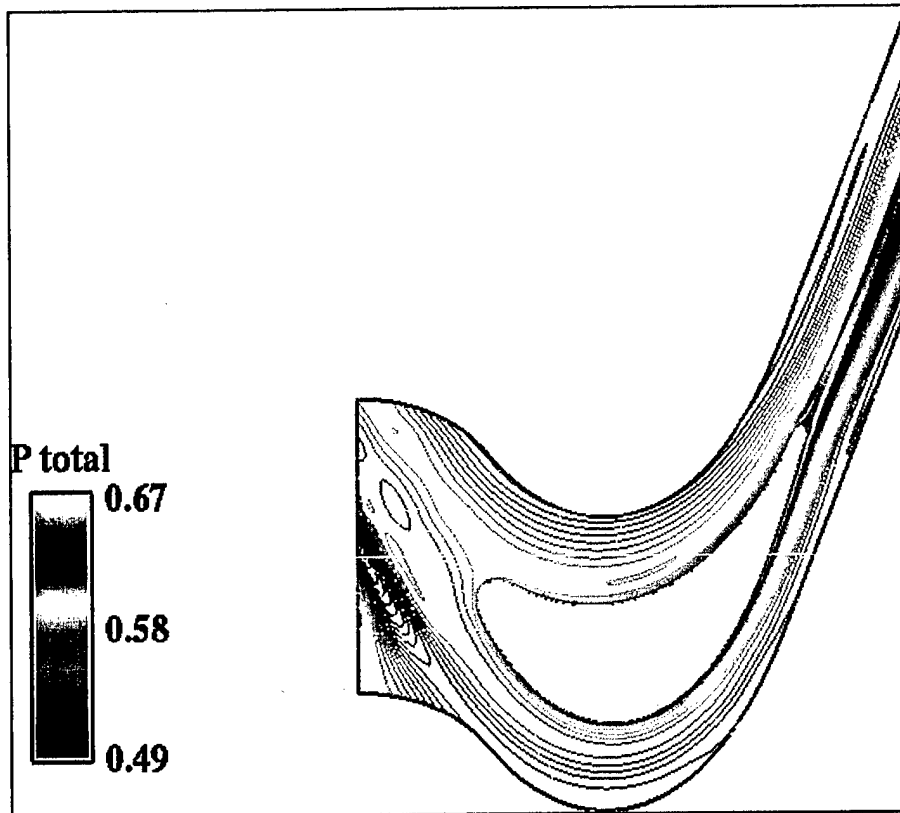
Figure 72. Quasi-3D Rotor Total Pressure with Stationary Wake (Relative Frame)

The figures clearly show the wake penetration at the rotor grid inlet, when compared to the constant inlet steady-state case shown in Figure 12. The most significant impact of the wake on the flow field appeared to be in the forward half of the rotor passage, for this case as well as the others. These flow field effects resulted in the variations of pressure distribution shown in Figure 73.
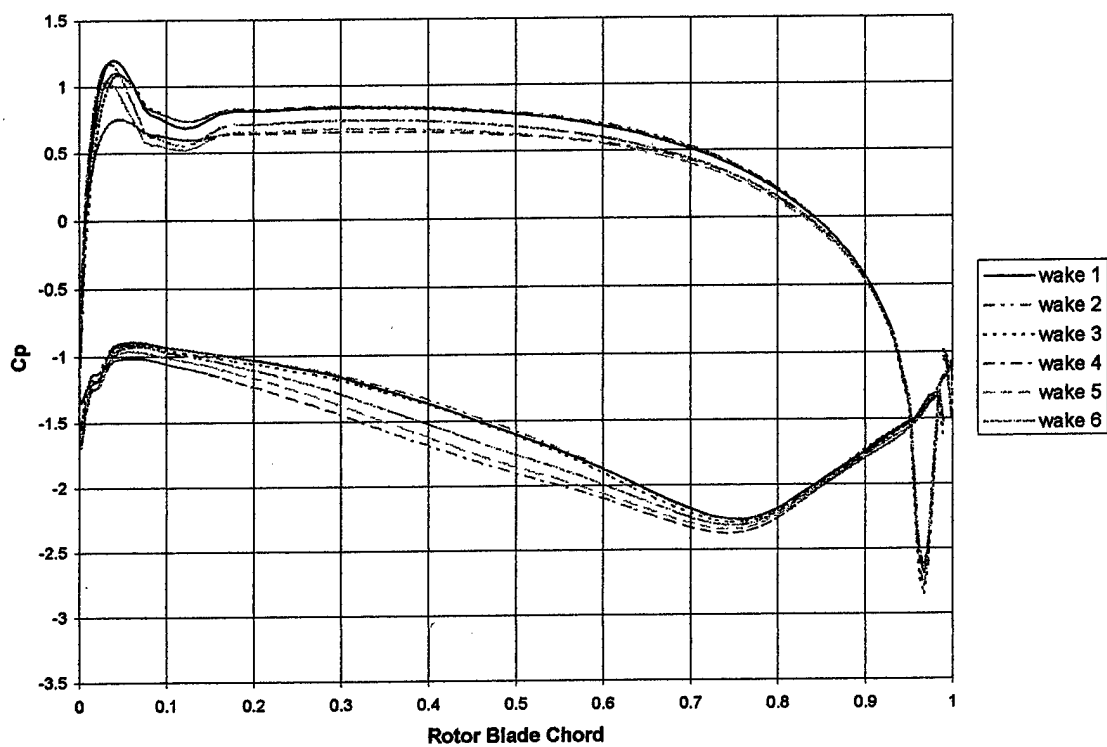
Figure 73. Quasi-3D Rotor Blade Surface Pressure Distributions - Steady Wake

Integrating the pressure distributions about the blade for each wake position resulted in the net bending force variation shown in Figure 74.
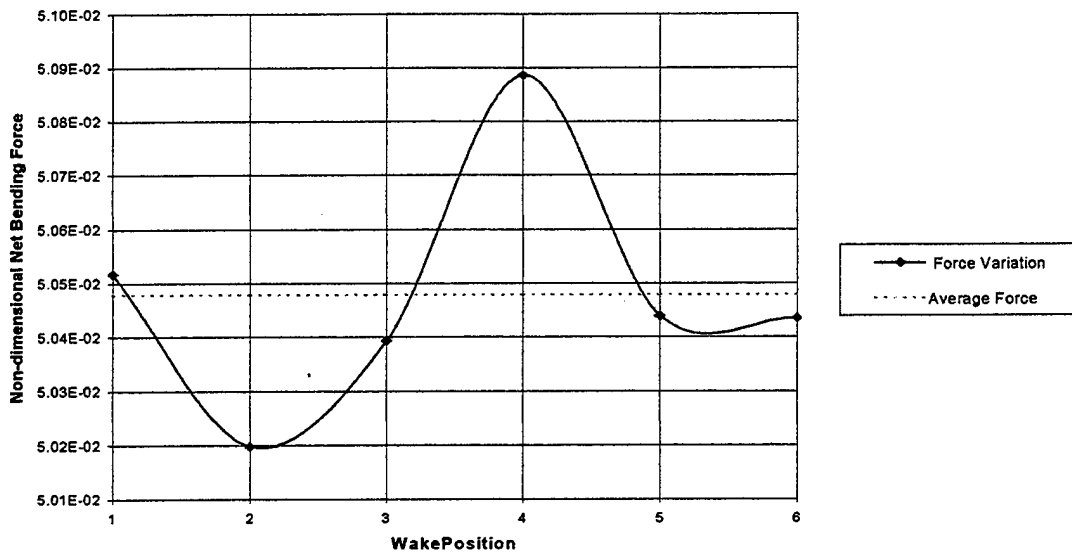
Figure 74. Quasi-3D Rotor Blade Bending Force Distribution

The figure clearly shows a nearly sinusoidal variation of force with wake position, with an amplitude of approximately 2%.

b.   Quasi-3D Unsteady Wake Solutions

Additional RVCQ3D modifications were being incorporated to permit the stator wake profile to transit across the rotor inlet during computation. Solutions using this modification had not been obtained at the time of this writing.

C. EXPERIMENTAL VERSUS COMPUTATIONAL RESULTS

1. Exit Plane Region

Three-dimensional computational results were compared with rotor exit plane cobra probe surveys conducted by McKee [Ref. 6]. Comparisons between the measured exit profiles and the computed exit profiles using the k-ω turbulence model with 2% turbulence intensity, and the Baldwin-Lomax model are shown in Figure 75, Figure 76 and Figure 77.
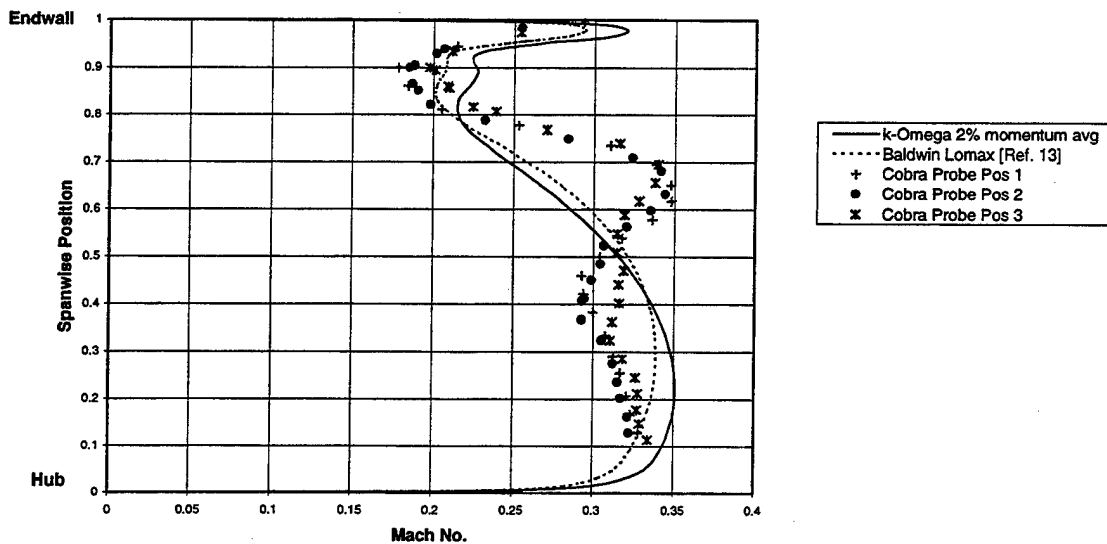
Figure 75. Comparison of Measured and Computed Exit Plane Mach No.

For the Mach number profile, Figure 75, the Baldwin-Lomax solution provided excellent agreement with cobra probe data from 80% span to the case wall. The k-ω solution was qualitatively similar, but consistently higher. Both solutions indicated the tip-gap flow and the resultant vortex was captured. At approximately 90% span, both computational solutions showed a local maximum that did not occur in the measured data. Between 10% and 70% span the computed exit profiles did

not match the measured profiles, however, the Baldwin-Lomax computation showed the better agreement. Maximum Mach number disagreement was 0.07 (20%) occurring at 70% span. Some of the disagreement in this spanwise range may have been due to sparse k-plane coverage. At 10% span, the cobra probe measurement closest to the hub, the computed solutions again agreed with the measured values.
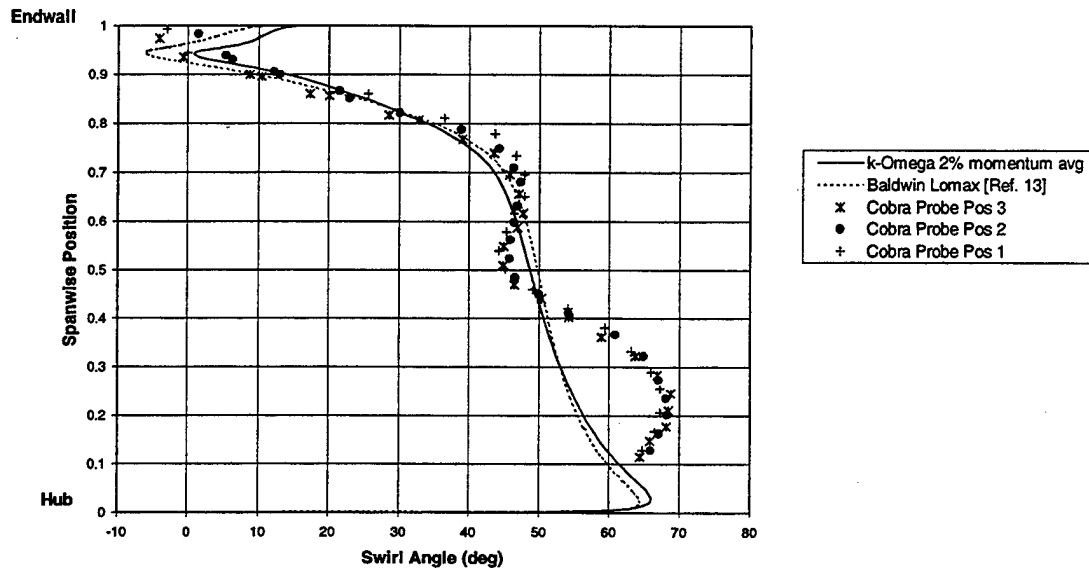
Figure 76. Comparison of Measured and Computed Exit Plane Swirl Angle

For the swirl angle profiles, Figure 76, both the k-ω and Baldwin-Lomax solutions showed excellent agreement with the cobra probe data from 60% span to the endwall. From 60% span to the hub, similar to the Mach number profile, the computed swirl angle profiles did not match the qualitative behavior of the measured data, which was again attributed to insufficient grid density.

81
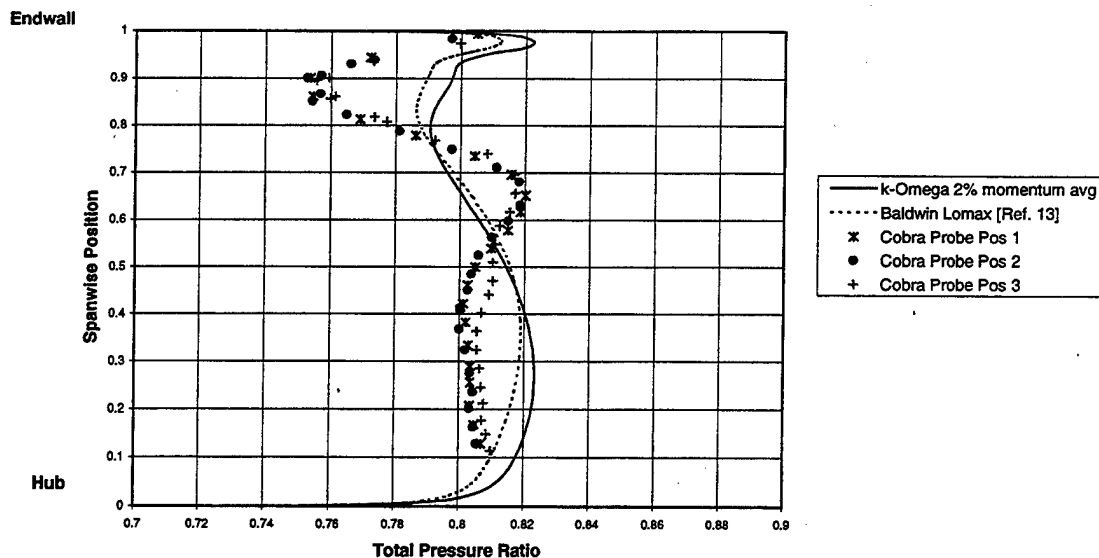
Figure 77. Comparison of Measured and Computed Exit Plane Total Pressure Ratio

For the total pressure profiles, Figure 77, neither the k-ω, nor the Baldwin-Lomax solutions matched the qualitative behavior of the measured data. The measured losses due to the tip vortex were approximately 4% higher than the computed values. The overall average of the profile loss, however, was nearly equal to the actual test data.

Overall, the Baldwin-Lomax solution provided the best agreement with the measured cobra probe data at the exit plane.

2. Endwall Region

Three-dimensional computational results were compared with LDV data for the variation of flow angle in both the tangential and radial directions. Comparisons of the LDV-measured and computed flow angle at the forward measurement axial location (-0.16c_t) are presented in Figure 78.
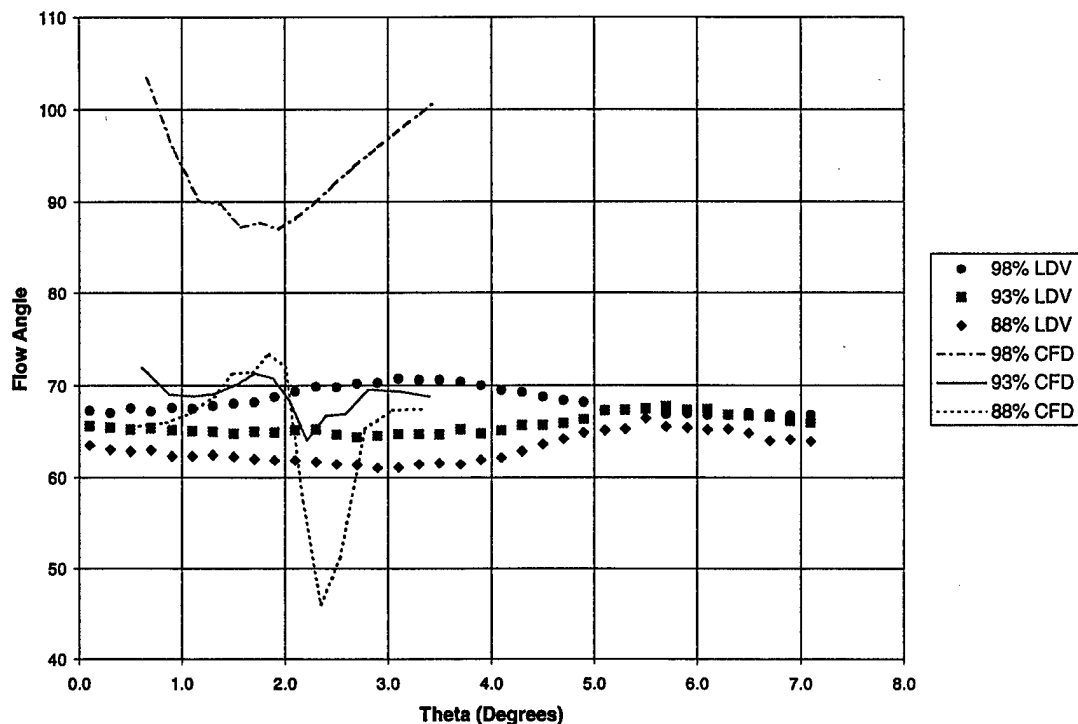
Figure 78. Comparison of LDV and CFD Flow Angle (-0.16c$_t$)

In general, the LDV data did not show nearly as much tangential variation in flow angle as did the CFD solution. For both the measured and computed data, the flow angle increased with increasing span. At the inner and center depths, the LDV and CFD data showed similar tangential trends, but significant quantitative differences. At the outer depth, the computed flow angle varied by as much as 35°. There were several probable sources that contributed to the disagreement:

- The measurement location was near the outer casing step, which significantly affected the flow. Flow separation/reversal due to the casing step, such as is shown in Figure 79, that varied even slightly between the actual and computed flow, would significantly effect the flow angles.
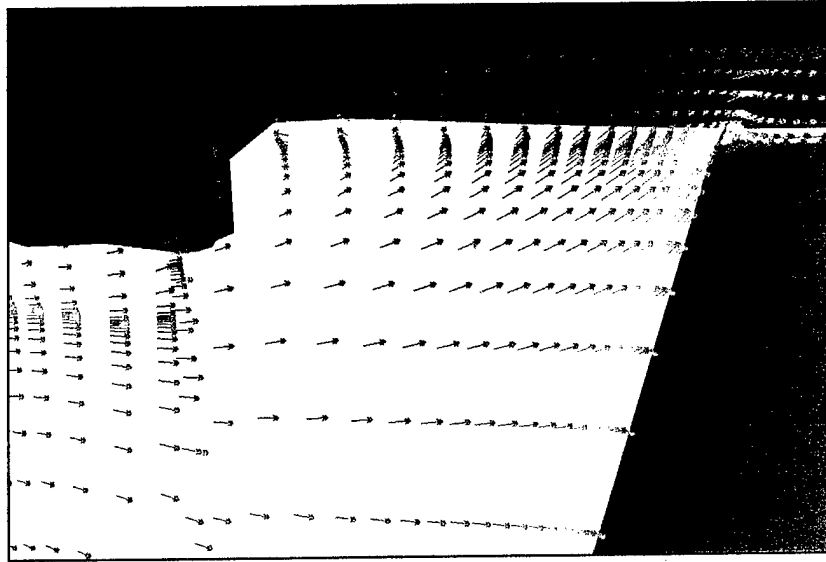
Figure 79. Outer Casing Step Velocity Vectors showing Flow Reversal (k-ω)

- The CFD solution at this axial location forward of the rotor blade may still be affected by the plane averaging which was applied between the rotor and stator.

- The LDV measurements were an "average" of the values within the probe volume, which covered approximately 6% of the blade span; thus, the 93% span position encompassed measurements between 90% to 96% span.

- The LDV measurements were made with a vented plug, allowing flow to escape the turbine casing through the measurement holes. The vented hole would most effect the flow nearest the endwall.

A qualitative assessment was made of the $0.35c_t$ and $0.84c_t$ axial positions by comparing the limited LDV data with CFD velocity vector distributions at corresponding spanwise planes (not shown). As expected, at the inner depth, the CFD flow fields showed that the primary flow turned, decreasing the flow angle, when proceeding aft in the rotor blade passage. The LDV data agreed, showing approximately 11 degrees of flow turning between the forward and center axial locations at each depth.

Proceeding to the aft ($0.84c_t$) axial location at the inner depth, the CFD solution showed significant tangential variation in flow angle, probably due to the tip-gap flow and subsequent vortex formation. The LDV data, likewise, showed a significant decrease in the tangential velocity ratio, Figure 58, and corresponding increase in turbulence intensity, Figure 60 in the measured region. These variations were most likely due to the tip gap vortex clearly shown on the blade suction surface ($0.84c_t$ measurement position) in Figure 70.

D.   SUMMARY OF FLOW FIELD CHARACTERISTICS

The flow field measured and calculated during the present work was subsonic throughout the turbine stage. The flow turned through both the stationary nozzle passages and through the rotating blade rows, causing endwall boundary layers and secondary flows to develop. The net effect was an extremely complex flow field, with numerous secondary flows as depicted in Figure 80.
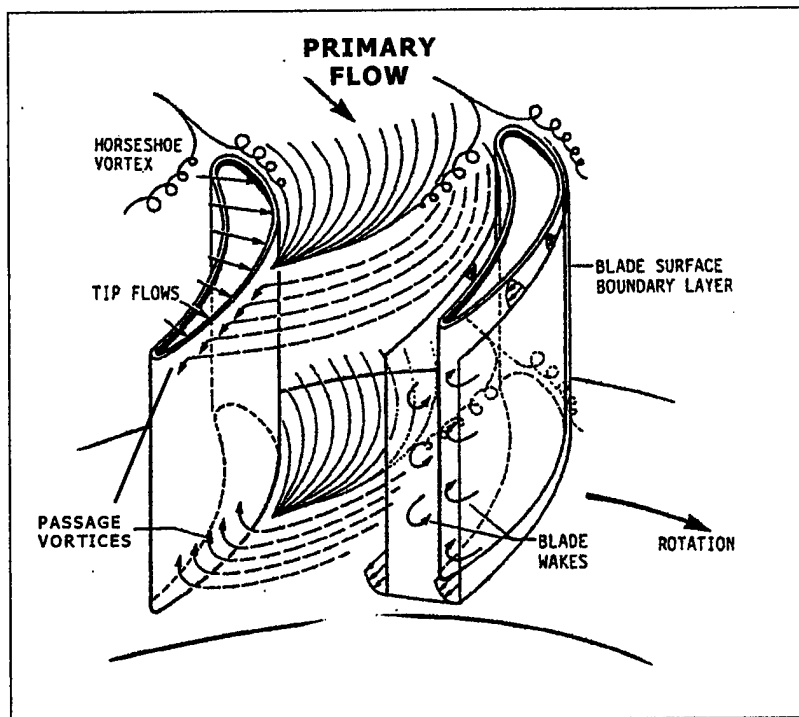
Figure 80. Turbine Rotor Blade Passage Flow Characteristics

85

The rotor blade passage exit plane secondary flow velocity vectors, mid-span Mach number distribution, and blade and hub surface pressures are shown in Figure 81. It is important to note that the colors of the secondary flow vectors indicate the flow Mach number at the corresponding grid location, consistent with Figure 67.
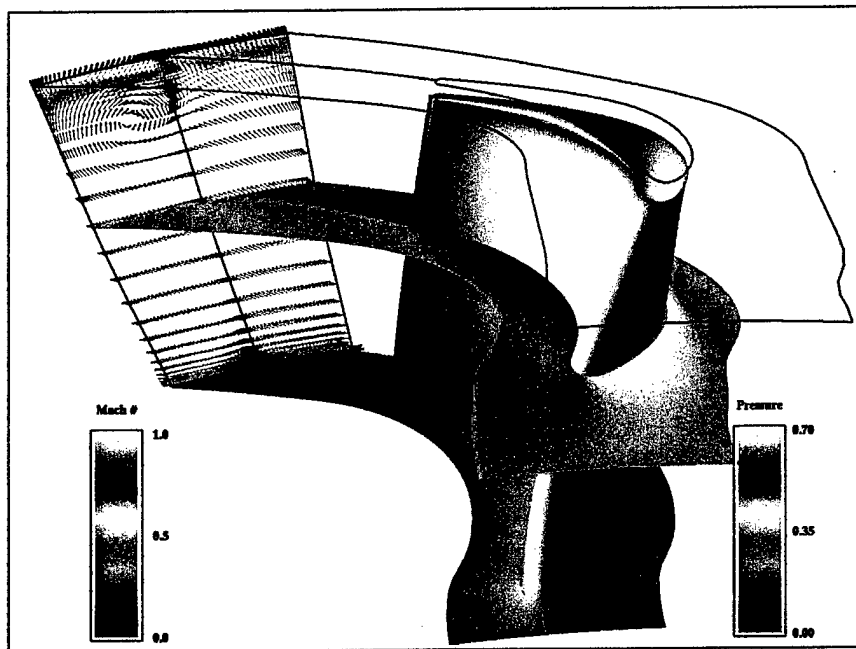
Figure 81. Rotor Blade Passage CFD Flow Characteristics (k-ω)

1.   Rotor Tip Gap Flow

The flow through the tip gap was prominent in the CFD solution. In the tip gap, flow accelerated from the pressure side (PS) to the suction side (SS) of the blade. The secondary flow direction was the same as the rotor blade movement, resulting in the region of highest flow field velocities. The flow was accelerated through the tip-gap due to the reduction in area resulting from an immediate separation from the rotor blade tip pressure side. The secondary flow field velocity vectors relative to the rotor blade, in a cross-passage grid plane near $0.75c_t$, as viewed from the rotor blade trailing edge, are depicted in Figure 82.

86
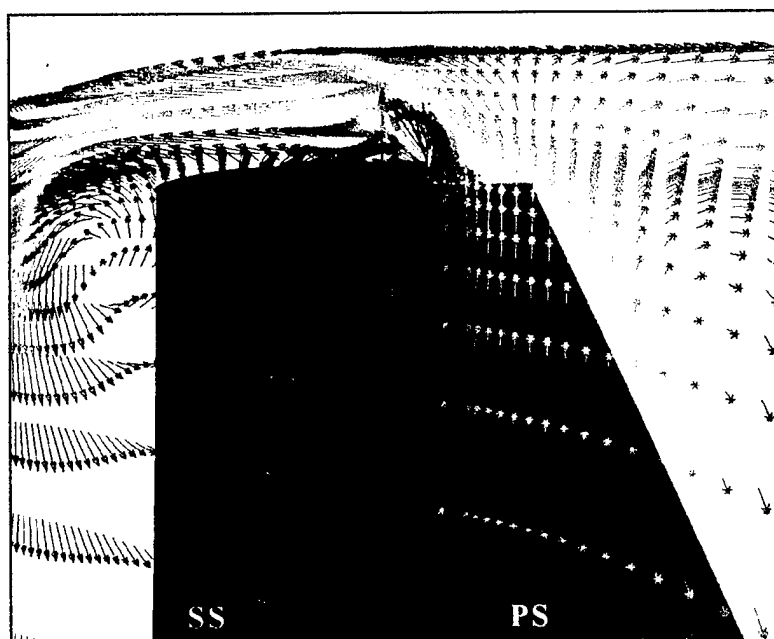
Figure 82. 3D Relative Secondary Flow Velocity Vectors Showing the Tip Gap Flow
Over the Blade
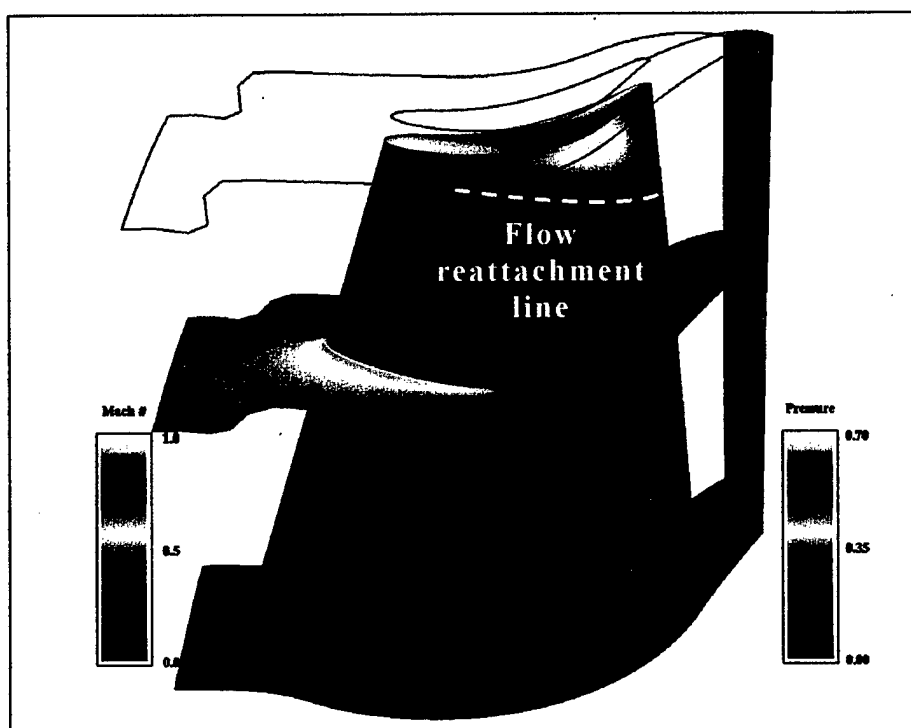
Figure 83. Rotor Blade Suction-Side Surface Pressure Distribution

As shown in Figure 82, the predominant secondary flow was towards the tip on the blade pressure side, and towards the hub on the blade suction side. The acceleration over the tip is clearly evident. The sharp turning of the high velocity flow however, caused regions of separated and reversed flow on the blade tip, as well as on the blade suction surface. The flow on the suction side is shown reattaching near the bottom of the figure (approximately 80% span). The suction side blade surface pressure distribution, in Figure 83, shows the region of relatively higher pressure where the reattachment occurred. Particle traces shown in Figure 84 clearly show the tip gap vortex forming, creating the separated flow region, on the blade suction side, and progressing downstream to the rotor exit plane.
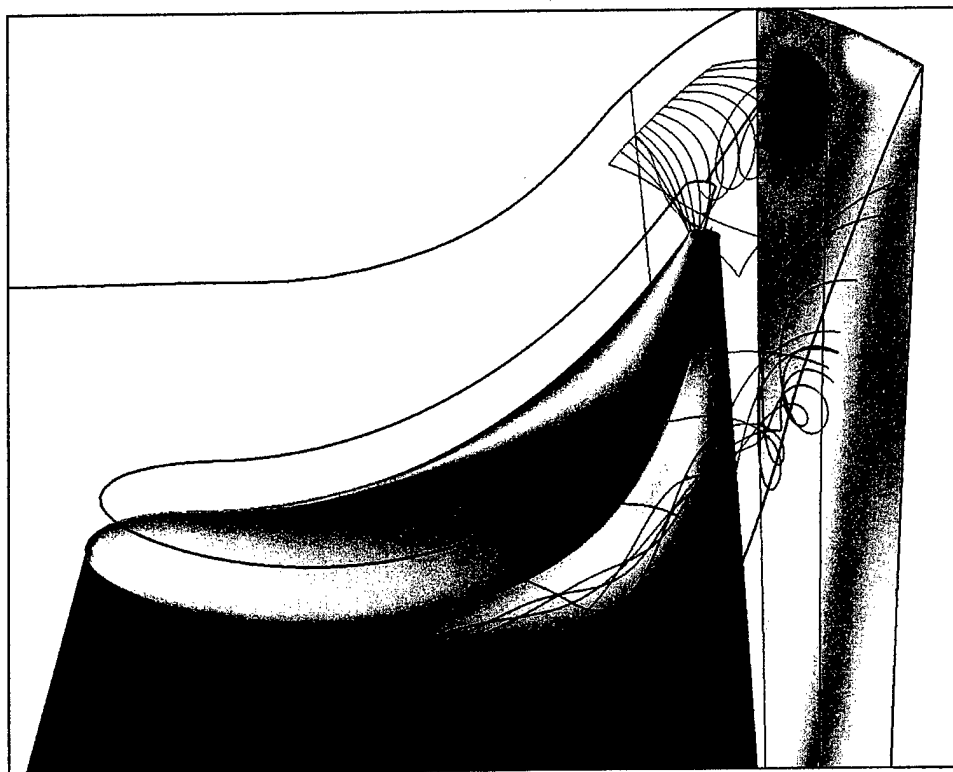
Figure 84. Tip Gap Flow Particle Traces

While not measured, physical evidence of the tip flow separation and reattachment was observed in the experiment and is shown in Figure 85.

Figure 85. Test Turbine Rotor Blade Suction Side

The dark regions near the blade tips, at approximately 80%-85% span, are most likely due to seeding particles in the separated tip flow reattaching as discussed above. The tip flow was most accelerated towards the aft portion of the blade. The LDV flow angle measurements at the outer depth were consistent with this behavior, increasing from an average of 57° to 65° at $0.35c_t$ and $0.84c_t$, respectively.

The downstream effects of the tip flow are seen clearly in the rotor exit plane velocity vector field, shown in Figure 81. A vortex is evident which extends across half the blade space, and occurs where the flow Mach number is a minimum. This behavior was consistent with the cobra probe exit profiles presented earlier, Figure 75, particularly with the minimum Mach number region measured at approximately 85% span.

2.   Casing Boundary Layers

The case wall boundary layer influence was apparent in the LDV data as well as in the CFD solutions. At each of the measured axial locations, the axial flow velocity decreased with increasing span. At the forward measured location, the tangential velocity component also decreased when proceeding towards the case wall. At the outer depths of both the center and aft axial locations, the tip-gap acceleration dominated the flow field, resulting in an increase in measured tangential (absolute) velocities approaching the case wall.

The hub boundary layer, although not measured, is seen in the calculated exit plane Mach number contours, in Figure 67, and in the secondary flow velocity vectors, in Figure 81. The rollup of the hub-wall boundary layer flow resulted in a corner vortex.

3.   Passage Vortex

When fluid is turned within an enclosed annular channel such as the stator passage, a secondary flow must develop as a result of non-uniform spanwise inertia forces associated with non-uniform spanwise flow velocity distribution. The resulting secondary flow, referred to as the "passage vortex", should be composed of twin counter-rotating vortices stacked within the passage. The vortices should spin such that the outer half of each sends flow towards the inner radius of curvature, and where the vortices meet within the passage, the flow should be towards the outer radius of curvature. The vorticity contours are plotted for the rotor exit plane in Figure 86.
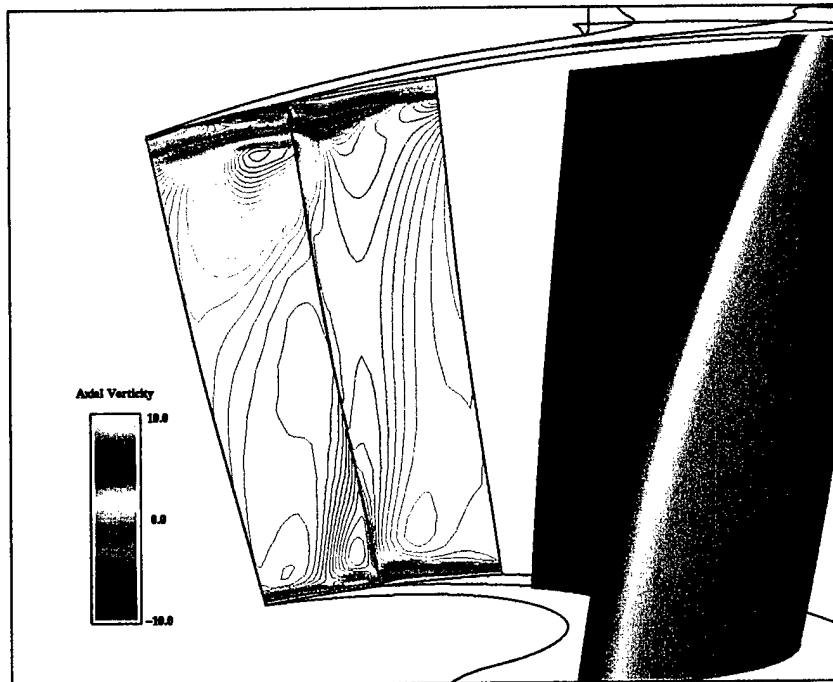
Figure 86. Rotor Exit Plane Vorticity Contours

From the figure, it can be seen that the tip-gap vortex dominated the passage secondary flow characteristics. The upper passage vortex appeared to be absorbed into the tip-gap vortex. The lower passage vortex appeared as the weaker of the vortices near the hub. The dominant hub vortex was due to the rollup of hub boundary layer interacting with the rotor blade wake.

4.   Stator and Rotor Wakes

The experimental measurement techniques and locations did not capture the effects of the stator or rotor wake profiles. The CFD solutions clearly showed both the stator and rotor blade wakes. However, the plane-averaging technique used by SWIFT eliminated the stator wake, preventing downstream effects to be analyzed. The rotor wake was shown intact to the exit plane in the CFD k-plane Mach number distribution shown in Figure 68. Since the CFD exit plane profiles, and cobra probe

91

measurement data were blade-to-blade averaged, the wake effects were
not resolved.

V. CONCLUSIONS

Overall, both experimental Laser Doppler Velocimetry (LDV) measurements and Computational Fluid Dynamics (CFD) solutions were successfully obtained to describe the axial turbine flow field. The LDV measurements were taken in the endwall region, upstream of the rotor blades, between the rotor blades, and within the rotor blade tip gap. The LDV data for velocity ratios and flow angles were repeatable, and showed definite trends. The exit-plane cobra probe data and CFD solutions were compared quantitatively for Mach number, swirl angle, and total pressure ratio, with good agreement. Several CFD parameters were varied to obtain the closest match with the experimental data, revealing that the Baldwin-Lomax turbulence model provided the best agreement within the scope of the investigation. The CFD solutions also showed consistency with the LDV data in the tip-gap region.

A. LASER DOPPLER VELOCIMETRY

LDV measurements were successfully taken in the endwall region and within the rotor blade tip gap of the test turbine. When measuring forward of the blade, the data rates were sufficient to complete sampling of a maximum of 20K data points around the rotor. Between the blades, the data rates were extremely low, permitting only a qualitative comparison of trends. The most significant problems associated with the LDV measurements are outlined as follows:

- Relatively Large Measurement Volume: The measurement volume was elliptical, with an aspect ratio of nearly twenty. The length of the probe volume (~0.064 in) was larger than the tip gap itself, causing the measurements to be spanwise averages of the flow through the tip gap. The large measurement volume

also caused both blade clipping and measurements from within the LDV access hole.

- Blade Reflection: Between-blade measurements were contaminated by blade reflections. Despite procedures and equipment set up to minimize blade reflections, the blade return was still significant due to a combination of highly reflective blade surfaces, as well as equipment limitations.

- Insufficient Data Rates: All the measurements between the blades had data rates below the real-time measurable threshold. Post-test analysis revealed data files as small as 5-10% of the maximum 20K data set size. The low data rates were attributed to non-optimum seeding and blade reflections. The data acquisition test time was limited to 999 seconds by the PHASE software.

- Effects of Vented Plug: All LDV measurements were taken with a plug which freely vented turbine flow to the test cell. Flow seeding passed through the measurement holes (which were 0.05 inches in diameter), as evidenced by the frequent cleanings required during testing. Since the LDV measurements were being completed in the endwall region, the venting may have had a significant effect on the measurements.

B.   COMPUTATIONAL FLUID DYNAMICS

1.   Three-Dimensional

CFD solutions were obtained for several turbulence models and intensities, as well as for the available methods of plane averaging, using the SWIFT computational software. All of the successful data runs were completed using a coarse grid composed of approximately 700K grid points. The grid provided sufficient density in the blade tip region to resolve the flow adequately for comparison with experimental data.

94

However, the grid density was insufficient to resolve the character of the midspan flow, as demonstrated by the profiles of properties at the exit.

A fine grid was successfully generated to increase grid density, and was composed of approximately two million points. A flow solution using the fine grid, however, was not successfully completed. Numerous runs using different combinations of turbulence modeling, boundary conditions, and between-grid averaging techniques, were attempted.

The CFD flow solution using the coarse grid provided excellent flow visualization. The extremely complex rotor flow features were successfully computed and helped considerably in explaining the significance of both the LDV and cobra probe experimental data.

2. Quasi-3D

Quasi-3D CFD solutions were successfully obtained for the rotor grid using a modified version of RVCQ3D software. The software modification permitted the rotor inlet flow to include a computed stator wake profile, held stationary relative to the rotor blade. The solution was obtained for the stator wake located at six tangential positions. Integration of the rotor blade surface pressure for each of the wake profiles revealed a net force variation of approximately 2%.

Additional modifications to RVCQ3D were initiated to permit the stator wake profile to move relative to the rotor blade, more realistically simulating the dynamic stator wake rotor flow field interaction.

VI. RECOMMENDATIONS

The following recommendations should be incorporated to address the deficiencies described in Section V.

A. LASER DOPPLER VELOCIMETRY

- Reduce the Measurement Volume: Modify the LDV system by incorporating a different optics assembly, which has a larger beam half angle (e.g.-450 mm focal length lens). With the ability of the traverse table system to move the laser breadboard, minimal effort would be required to incorporate a different optics setup within a wide range of focal lengths.

- Reduce Blade Reflection: The inherent reflectivity of the blades themselves could be reduced by finishing them with a non-reflective coating. This modification would be a significant modification to the TTR and should be incorporated concurrent with other major maintenance/modifications requiring disassembly. A second method for reducing blade reflection would be to pulse the laser such that the laser emissions are controlled to avoid blade reflection when performing between-blade measurements.

- Increase Between-Blade Data: Modification and movement of the seeding wand should be attempted in order to optimize the wand spray pattern for between-blade measurements. With a swirl angle of greater than 60 degrees in the endwall region, the tangential location of the seeding wand is critical, and it can only be optimized for one axial measurement location at a time. Additionally, LDV data acquisition software should be upgraded

from PHASE to PACE to eliminate the 999 seconds and 20K data point acquisition limitations.

- Repeat LDV Measurements with an Unvented Plug: Prior to changing the optics assembly, repeat the forward-hole measurements at each depth to quantify the impact of flow venting.

B. COMPUTATIONAL FLUID DYNAMICS

1. Three-dimensional

If a closer match with the exit plane profiles in the blade mid-span regions are desired, the CFD solutions should be repeated using a grid with increased mid-span density. Modeling of the hub leakage flow between the stator and the rotor should be attempted, in order to better predict the hub and midspan region flows.

2. Quasi-3D

Complete modification of the RVCQ3D code to permit the stator wake to transit relative to the rotor blade. Perform unsteady computations of the flowfield using a global time-stepping procedure, which needs to be determined by trial and error.

APPENDIX A.   3D GRID GENERATION FILES

A.   TCGRID INPUT FILE FOR STATOR

```
&nam1 merid=0 im=218 jm=45 km=84 itl=30 icap=12 igclt=0
    kmt=20 jmt=20 &end
&nam2 nle=19 nte=16 dsle=0.010 dste=0.0050 dswte=0.005
    dswex=0.01 dsmin=0.0001 dsmax=0.002 dshub=0.0001
    dstip=0.0001 dsthr=1.0 rcorn=.098 cltip=.045 dsclt=.0001 &end
&nam3 iterm=150 idbg=0 0 0 0 0 0 0 0 aabb=1.0 &end
&nam4 zbc=0.0000 0.0000 1.5000 0.0000 0.0000 1.5000
    rbc=4.0788 4.0788 4.0788 5.1480 5.1480 5.02425 &end
&nam5 iswift=1 dslap=.002 &end
'new data style with z,th,r format SSME HPFTP ** COARSE GRID **'
58 58
```

-0.9334116	-0.8467470	-0.7600824	-0.6734079	-0.5867434
-0.5000787	-0.4134042	-0.3267396	-0.2400750	-0.1534005
-0.066735901	0.019928699	0.1066032	0.1932678	0.2799324
0.3666069	0.4532715	0.5399361	0.6266007	0.6927030
0.7100379	0.7360452	0.7577163	0.7837138	0.8097210
0.8313921	0.8530533	0.8790606	0.9007317	0.9267291
0.9527364	0.9787437	1.004741	1.035075	1.061082
1.082743	1.193148	1.216443	1.239866	1.263398
1.287020	1.310730	1.334510	1.358349	1.382228
1.406137	1.430055	1.578555	1.617592	1.620448
1.622869	1.624487	1.625055	1.625623	1.627241
1.629662	1.632517	1.750000	2.650000	

3.790294	3.815232	3.838923	3.861406	3.882691
3.902798	3.921746	3.939557	3.956248	3.971821
3.986304	3.999689	4.012004	4.023261	4.033448
4.042595	4.050704	4.057773	4.063811	4.067732
4.068662	4.069979	4.070999	4.072147	4.073206
4.074018	4.074761	4.075573	4.076187	4.076830
4.077384	4.077850	4.078216	4.078533	4.078711
4.078780	4.078800	4.078800	4.078800	4.078800
4.078800	4.078800	4.078800	4.078800	4.078800
4.078800	4.078800	4.078800	4.078800	4.078800
4.078800	4.078800	4.078800	4.078800	4.078880
4.078800	4.078800	4.078800	4.078800	

-0.9334116	-0.8467470	-0.7600824	-0.6734079	-0.5867434
-0.5000787	-0.4134042	-0.3267396	-0.2400750	-0.1534005
-0.066735901	0.019928699	0.1066032	0.1932678	0.2799324
0.3666069	0.4532715	0.5399361	0.6266007	0.6875550
0.7114734	0.7353819	0.7592607	0.7830999	0.8068797
0.8305902	0.8542116	0.8777439	0.9011673	0.9244521
0.9513306	0.9781992	1.005068	1.031936	1.058805
1.085674	1.193148	1.216443	1.239866	1.263398
1.287020	1.310730	1.334510	1.358349	1.382228
1.406137	1.430055	1.578555	1.610000	1.626920
1.636248	1.645576	1.654905	1.664233	1.673561
1.682889	1.700000	1.750000	2.650000	

5.148000	5.148000	5.148000	5.148000	5.148000
5.148000	5.148000	5.148000	5.148000	5.148000
5.148000	5.148000	5.148000	5.148000	5.148000
5.148000	5.148000	5.148000	5.148000	5.148000
5.147713	5.146842	5.145396	5.143377	5.140783
5.137615	5.133873	5.129556	5.124685	5.119240
5.112617	5.105697	5.099371	5.092748	5.086125
5.079502	5.053010	5.047565	5.042694	5.038377
5.034636	5.031467	5.028873	5.026854	5.025408
5.024538	5.024250	5.024250	5.024250	5.033578
5.042906	5.052234	5.061563	5.070891	5.080219
5.089546	5.098875	5.098875	5.098875	

6 105 52

1.253538	1.245321	1.237104	1.228887	1.220670
1.212453	1.204236	1.196019	1.187802	1.179585
1.159042	1.138500	1.117958	1.097415	1.076872
1.056330	1.035787	1.015245	0.994703	0.974160
0.953618	0.933075	0.912533	0.891990	0.871448
0.850905	0.830362	0.809820	0.789277	0.768735
0.748192	0.727650	0.707107	0.686565	0.666022
0.645480	0.624937	0.604395	0.583853	0.563310
0.542768	0.522225	0.514008	0.505791	0.497574
0.489357	0.481140	0.472923	0.464706	0.456489
0.448272	0.440055	0.448272	0.456489	0.464706
0.472923	0.481140	0.489357	0.497574	0.505791
0.514008	0.522225	0.542768	0.563310	0.583853
0.604395	0.624937	0.645480	0.666022	0.686565
0.707107	0.727650	0.748192	0.768735	0.789277
0.809820	0.830362	0.850905	0.871448	0.891990
0.912533	0.933075	0.953618	0.974160	0.994703
1.015245	1.035787	1.056330	1.076872	1.097415
1.117958	1.138500	1.159042	1.179585	1.187802
1.196019	1.204236	1.212453	1.220670	1.228887
1.237104	1.245321	1.253538	1.261755	1.253538

-0.091840	-0.092470	-0.092070	-0.090110	-0.086510
-0.083090	-0.079820	-0.076700	-0.073720	-0.070860
-0.064230	-0.058240	-0.052800	-0.047850	-0.043320
-0.039170	-0.035340	-0.031820	-0.028560	-0.025530
-0.022730	-0.020120	-0.017690	-0.015430	-0.013320
-0.011340	-0.009500	-0.007770	-0.006150	-0.004630
-0.003200	-0.001860	-0.000610	0.000580	0.001680
0.002730	0.003710	0.004630	0.005490	0.006310
0.007360	0.008800	0.009500	0.010300	0.011190
0.012200	0.013360	0.014700	0.016280	0.018230
0.020880	0.027530	0.034180	0.036830	0.038780
0.040360	0.041700	0.042850	0.043870	0.044760
0.045550	0.046260	0.047700	0.048750	0.049580
0.050210	0.050640	0.050880	0.050910	0.050720
0.050320	0.049700	0.048850	0.047760	0.046430
0.044850	0.043010	0.040910	0.038520	0.035850
0.032870	0.029580	0.025960	0.022000	0.017680
0.012970	0.007860	0.002330	-0.003670	-0.010140
-0.017150	-0.024720	-0.032930	-0.041850	-0.045640
-0.049570	-0.053650	-0.057880	-0.062290	-0.066880
-0.071670	-0.076690	-0.081950	-0.088230	-0.091840

4.078800	4.078800	4.078800	4.078800	4.078800
4.078800	4.078800	4.078800	4.078800	4.078800
4.078800	4.078800	4.078800	4.078800	4.078800
4.078800	4.078800	4.078800	4.078800	4.078800
4.078800	4.078800	4.078800	4.078800	4.078800
4.078800	4.078800	4.078800	4.078800	4.078800
4.078800	4.078800	4.078800	4.078800	4.078800
4.078800	4.078800	4.078800	4.078800	4.078800
4.078800	4.078800	4.078800	4.078800	4.078800

4.078800	4.078800	4.078800	4.078800	4.078800
4.078800	4.078800	4.078800	4.078800	4.078800
4.078800	4.078800	4.078800	4.078800	4.078800
4.078800	4.078800	4.078800	4.078000	4.078800
4.078800	4.078800	4.078800	4.078800	4.078800
4.078800	4.078800	4.078800	4.078800	4.078800
4.078800	4.078800	4.078800	4.078800	4.078800
4.078800	4.078800	4.078800	4.078800	4.078800
4.078800	4.078800	4.078800	4.078800	4.078800
4.078800	4.078800	4.078800	4.078800	4.078800
4.078800	4.078800	4.078800	4.078800	4.078800
4.078800	4.078800	4.078800	4.078800	4.078800

1.295187	1.286555	1.277912	1.269279	1.260636
1.252004	1.243361	1.234728	1.226085	1.217453
1.195861	1.174259	1.152667	1.131075	1.109483
1.087881	1.066289	1.044698	1.023106	1.001504
0.979912	0.958320	·0.936728	0.915126	0.893534
0.871943	0.850351	0.828749	0.807157	0.785565
0.763973	0.742371	0.720779	0.699188	0.677596
0.655994	0.634402	0.612810	0.591218	0.569616
0.548024	0.526433	0.517790	0.509157	0.500514
0.491881	0.483239	0.474606	0.465963	0.457330
0.448698	0.440055	0.448698	0.457330	0.465963
0.474606	0.483239	0.491881	0.500514	0.509157
0.517790	0.526433	0.548024	0.569616	0.591218
0.612810	0.634402	0.655994	0.677596	0.699188
0.720779	0.742371	0.763973	0.785565	0.807157
0.828749	0.850351	0.871943	0.893534	0.915126
0.936728	0.958320	0.979912	1.001504	1.023106
1.044698	1.066289	1.087881	1.109483	1.131075
1.152667	1.174259	1.195861	1.217453	1.226085
1.234728	1.243361	1.252004	1.260636	1.269279
1.277912	1.286555	1.295187	1.303830	1.295187

-0.105940	-0.106470	-0.105920	-0.103260	-0.098990
-0.095010	-0.091270	-0.087750	-0.084410	-0.081230
-0.073920	-0.067340	-0.061380	-0.055920	-0.050880
-0.046230	-0.041900	-0.037860	-0.034080	-0.030540
-0.027210	-0.024070	-0.021100	-0.018310	-0.015660
-0.013150	-0.010770	-0.008510	-0.006360	-0.004320
-0.002380	0.000540	0.001220	0.002890	0.004490
0.006000	0.007450	0.008830	0.010140	0.011390
0.012740	0.014470	0.015300	0.016210	0.017230
0.018360	0.019630	0.021090	0.022790	0.024860
0.027620	0.034270	0.040910	0.043430	0.045270
0.046730	0.047940	0.048980	0.049870	0.050650
0.051320	0.051900	0.053040	0.053790	0.054280
0.054610	0.054770	0.054770	0.054580	0.054210
0.053650	0.052880	0.051910	0.050730	0.049310
0.047660	0.045750	0.043590	0.041160	0.038430
0.035390	0.032040	0.028330	0.024260	0.019790
0.014900	0.009560	0.003710	-0.002670	-0.009650
-0.017280	-0.025660	-0.034900	-0.045140	-0.049570
-0.054210	-0.059080	-0.064200	-0.069610	-0.075320
-0.081370	-0.087790	-0.094640	-0.102480	-0.105940

4.315162	4.315162	4.315162	4.315162	4.315162
4.315162	4.315162	4.315162	4.315162	4.315162
4.315162	4.315162	4.315162	4.315162	4.315162
4.315152	4.315162	4.315162	4.315162	4.315162
4.315162	4.315162	4.315162	4.315162	4.315162
4.315162	4.315162	4.315162	4.315162	4.315162
4.315162	4.315162	4.315162	4.315162	4.315162
4.315162	4.315162	4.315162	4.315162	4.315162
4.315162	4.315162	4.315162	4.315162	4.315162
4.315162	4.315162	4.315162	4.315162	4.315162

4.315162	4.315162	4.315162	4.315162	4.315162
4.315162	4.315162	4.315162	4.315162	4.315162
4.315162	4.315162	4.315162	4.315162	4.315162
4.315162	4.315162	4.315162	4.315162	4.315162
4.315162	4.315162	4.315162	4.315162	4.315162
4.315162	4.315162	4.315162	4.315162	4.315162
4.315162	4.315162	4.315162	4.315162	4.315162
4.315162	4.315162	4.315162	4.315162	4.315162
4.315162	4.315162	4.315162	4.315162	4.315162
4.315162	4.315162	4.315162	4.315162	4.315162
4.315162	4.315162	4.315162	4.315162	4.315162

1.336847	1.327788	1.318730	1.309671	1.300613
1.291554	1.282495	1.273437	1.264379	1.255320
1.232669	1.210027	1.187376	1.164735	1.142084
1.119442	1.096791	1.074150	1.051499	1.028857
1.006206	0.983565	0.960914	0.938272	0.915621
0.892980	0.870329	0.847687	0.825036	0.802395
0.779744	0.757102	0.734451	0.711810	0.689159
0.666517	0.643866	0.621225	0.598574	0.575933
0.553281	0.530640	0.521581	0.512523	0.503465
0.494406	0.485348	0.476289	0.467230	0.458172
0.449113	0.440055	0.449113	0.458172	0.467230
0.476289	0.485348	0.494406	0.503465	0.512523
0.521581	0.530640	0.553281	0.575933	0.598574
0.621225	0.643866	0.666517	0.689159	0.711810
0.734451	0.757102	0.779744	0.802395	0.825036
0.847687	0.870329	0.892980	0.915621	0.938272
0.960914	0.983565	1.006206	1.028857	1.051499
1.074150	1.096791	1.119442	1.142084	1.164735
1.187376	1.210027	1.232669	1.255320	1.264379
1.273437	1.282495	1.291554	1.300613	1.309671
1.318730	1.327788	1.336847	1.345905	1.336847

-0.103300	-0.103750	-0.103080	-0.099950	-0.095630
-0.091630	-0.087900	-0.084380	-0.081070	-0.077920
-0.070680	-0.064170	-0.058250	-0.052820	-0.047790
-0.043120	-0.038760	-0.034670	-0.030830	-0.027210
-0.023790	-0.020550	-0.017490	-0.014580	-0.011820
-0.009190	-0.006690	-0.004310	-0.002050	0.000110
0.002160	0.004120	0.005990	0.007770	0.009460
0.011070	0.012600	0.014060	0.015450	0.016770
0.018160	0.019950	0.020790	0.021720	0.022750
0.023900	0.025190	0.026660	0.028370	0.030460
0.033230	0.039850	0.046460	0.048960	0.050770
0.052200	0.053390	0.054410	0.055270	0.056030
0.056680	0.057240	0.058330	0.059030	0.059460
0.059730	0.059850	0.059800	0.059580	0.059180
0.058600	0.057830	0.056850	0.055680	0.054280
0.052660	0.050800	0.048690	0.046320	0.043670
0.040710	0.037440	0.033840	0.029860	0.025490
0.020690	0.015430	0.009650	0.003290	-0.003710
-0.011430	-0.019990	-0.029510	-0.040160	-0.044780
-0.049630	-0.054730	-0.060100	-0.065750	-0.071730
-0.078050	-0.084750	-0.091880	-0.099950	-0.103300

4.551525	4.551525	4.551525	4.551525	4.551525
4.551525	4.551525	4.551525	4.551525	4.551525
4.551525	4.551525	4.551525	4.551525	4.551525
4.551525	4.551525	4.551525	4.551525	4.551525
4.551525	4.551525	4.551525	4.551525	4.551525
4.551525	4.551525	4.551525	4.551525	4.551525
4.551525	4.551525	4.551525	4.551525	4.551525
4.551525	4.551525	4.551525	4.551525	4.551525
4.551525	4.551525	4.551525	4.551525	4.551525
4.551525	4.551525	4.551525	4.551525	4.551525
4.551525	4.551525	4.551525	4.551525	4.551525

4.551525	4.551525	4.551525	4.551525	4.551525
4.551525	4.551525	4.551525	4.551525	4.551525
4.551525	4.551525	4.551525	4.551525	4.551525
4.551525	4.551525	4.551525	4.551525	4.551525
4.551525	4.551525	4.551525	4.551525	4.551525
4.551525	4.551525	4.551525	4.551525	4.551525
4.551525	4.551525	4.551525	4.551525	4.551525
4.551525	4.551525	4.551525	4.551525	4.551525
4.551525	4.551525	4.551525	4.551525	4.551525
4.551525	4.551525	4.551525	4.551525	4.551525

1.378496	1.369022	1.359537	1.350063	1.340579
1.331105	1.321620	1.312146	1.302662	1.293187
1.269487	1.245786	1.222096	1.198395	1.174694
1.150994	1.127303	1.103603	1.079902	1.056201
1.032511	1.008810	0.985109	0.961409	0.937718
0.914017	0.890317	0.866616	0.842926	0.819225
0.795524	0.771824	0.748133	0.724433	0.700732
0.677031	0.653341	0.629640	0.605939	0.582239
0.558548	0.534847	0.525363	0.515889	0.506405
0.496931	0.487446	0.477972	0.468498	0.459013
0.449529	0.440055	0.449529	0.459013	0.468498
0.477972	0.487446	0.496931	0.506405	0.515889
0.525363	0.534847	0.558548	0.582239	0.605939
0.629640	0.653341	0.677031	0.700732	0.724433
0.748133	0.771824	0.795524	0.819225	0.842926
0.866616	0.890317	0.914017	0.937718	0.961409
0.985109	1.008810	1.032511	1.056201	1.079902
1.103603	1.127303	1.150994	1.174694	1.198395
1.222096	1.245786	1.269487	1.293187	1.302662
1.312146	1.321620	1.331105	1.340579	1.350063
1.359537	1.369022	1.378496	1.387980	1.378496

-0.087840	-0.088230	-0.087430	-0.084110	-0.080240
-0.076630	-0.073260	-0.070070	-0.067060	-0.064200
-0.057610	-0.051660	-0.046240	-0.041240	-0.036610
-0.032300	-0.028270	-0.024480	-0.020920	-0.017570
-0.014400	-0.011400	-0.008550	-0.005860	-0.003310
-0.000880	0.001420	0.003600	0.005680	0.007640
0.009510	0.011280	0.012950	0.014540	0.016040
0.017450	0.018780	0.020040	0.021210	0.022320
0.023570	0.025200	0.025990	0.026860	0.027820
0.028910	0.030130	0.031540	0.033190	0.035200
0.037910	0.044480	0.051060	0.053600	0.055450
0.056940	0.058180	0.059240	0.060160	0.060970
0.061670	0.062290	0.063520	0.064360	0.064940
0.065350	0.065590	0.065650	0.065530	0.065230
0.064740	0.064060	0.063170	0.062100	0.060800
0.059290	0.057560	0.055580	0.053360	0.050870
0.048110	0.045050	0.041670	0.037950	0.033860
0.029370	0.024420	0.018980	0.012980	0.006330
-0.001070	-0.009340	-0.018580	-0.028930	-0.033400
-0.038080	-0.042970	-0.048080	-0.053420	-0.059010
-0.064850	-0.070960	-0.077370	-0.084600	-0.087840

4.787888	4.787888	4.787888	4.787888	4.787888
4.787888	4.787888	4.787888	4.787888	4.787888
4.787888	4.787888	4.787888	4.787888	4.787888
4.787888	4.787888	4.787888	4.787888	4.787888
4.787888	4.787888	4.787888	4.787888	4.787888
4.787888	4.787888	4.787888	4.787888	4.787888
4.787888	4.787888	4.787888	4.787888	4.787888
4.787888	4.787888	4.787888	4.787888	4.787888
4.787888	4.787888	4.787888	4.787888	4.787888
4.787888	4.787888	4.787888	4.787888	4.787888
4.787888	4.787888	4.787888	4.787888	4.787888
4.787888	4.787888	4.787888	4.787888	4.787888

4.787888	4.787888	4.787888	4.787888	4.787888
4.787888	4.787888	4.787888	4.787888	4.787888
4.787888	4.787888	4.787888	4.787888	4.787888
4.787888	4.787888	4.787888	4.787888	4.787888
4.787888	4.787888	4.787888	4.787888	4.787888
4.787888	4.787888	4.787888	4.787888	4.787888
4.787888	4.787888	4.787888	4.787888	4.787888
4.787888	4.787888	4.787888	4.787888	4.787888
4.787888	4.787888	4.787888	4.787888	4.787888

1.420155	1.410255	1.400355	1.390455	1.380555
1.370655	1.360755	1.350855	1.340955	1.331055
1.306305	1.281555	1.256805	1.232055	1.207305
1.182555	1.157805	1.133055	1.108305	1.083555
1.058805	1.034055	1.009305	0.984555	0.959805
0.935055	0.910305	0.885555	0.860805	0.836055
0.811305	0.786555	0.761805	0.737055	0.712305
0.687555	0.662805	0.638055	0.613305	0.588555
0.563805	0.539055	0.529155	0.519255	0.509355
0.499455	0.489555	0.479655	0.469755	0.459855
0.449955	0.440055	0.449955	0.459855	0.469755
0.479655	0.489555	0.499455	0.509355	0.519255
0.529155	0.539055	0.563805	0.588555	0.613305
0.638055	0.662805	0.687555	0.712305	0.737055
0.761805	0.786555	0.811305	0.836055	0.860805
0.885555	0.910305	0.935055	0.959805	0.984555
1.009305	1.034055	1.058805	1.083555	1.108305
1.133055	1.157805	1.182555	1.207305	1.232055
1.256805	1.281555	1.306305	1.331055	1.340955
1.350855	1.360755	1.370655	1.380555	1.390455
1.400355	1.410255	1.420155	1.430055	1.420155

-0.068700	-0.069000	-0.068000	-0.064730	-0.061430
-0.058340	-0.055440	-0.052690	-0.050070	-0.047570
-0.041790	-0.036550	-0.031740	-0.027310	-0.023190
-0.019350	-0.015750	-0.012380	-0.009210	-0.006220
-0.003410	-0.000750	0.001770	0.004140	0.006380
0.008500	0.010500	0.012390	0.014180	0.015860
0.017430	0.018920	0.020310	0.021610	0.022820
0.023940	0.024980	0.025940	0.026820	0.027630
0.028670	0.030100	0.030790	0.031580	0.032460
0.033460	0.034600	0.035910	0.037470	0.039390
0.041990	0.048530	0.055060	0.057670	0.059590
0.061140	0.062460	0.063600	0.064600	0.065480
0.066260	0.066960	0.068390	0.069430	0.070240
0.070840	0.071250	0.071470	0.071490	0.071320
0.070950	0.070390	0.069630	0.068670	0.067510
0.066130	0.064540	0.062720	0.060670	0.058380
0.055830	0.053010	0.049900	0.046470	0.042710
0.038580	0.034030	0.029010	0.023450	0.017250
0.010300	0.002480	-0.006300	-0.016110	-0.020330
-0.024700	-0.029240	-0.033930	-0.038780	-0.043760
-0.048880	-0.054130	-0.059510	-0.065580	-0.068700

5.024250	5.024250	5.024250	5.024250	5.024250
5.024250	5.024250	5.024250	5.024250	5.024250
5.024250	5.024250	5.024250	5.024250	5.024250
5.024250	5.024250	5.024250	5.024250	5.024250
5.024250	5.024250	5.024250	5.024250	5.024250
5.024250	5.024250	5.024250	5.024250	5.024250
5.024250	5.024250	5.024250	5.024250	5.024250
5.024250	5.024250	5.024250	5.024250	5.024250
5.024250	5.024250	5.024250	5.024250	5.024250
5.024250	5.024250	5.024250	5.024250	5.024250
5.024250	5.024250	5.024250	5.024250	5.024250
5.024250	5.024250	5.024250	5.024250	5.024250
5.024250	5.024250	5.024250	5.024250	5.024250

5.024250	5.024250	5.024250	5.024250	5.024250
5.024250	5.024250	5.024250	5.024250	5.024250
5.024250	5.024250	5.024250	5.024250	5.024250
5.024250	5.024250	5.024250	5.024250	5.024250
5.024250	5.024250	5.024250	5.024250	5.024250
5.024250	5.024250	5.024250	5.024250	5.024250
5.024250	5.024250	5.024250	5.024250	5.024250
5.024250	5.024250	5.024250	5.024250	5.024250

1.441965	1.431837	1.421719	1.411601	1.401484
1.391366	1.381238	1.371120	1.361003	1.350885
1.325580	1.300276	1.274981	1.249677	1.224373
1.199078	1.173774	1.148479	1.123175	1.097870
1.072576	1.047271	1.021967	0.996673	0.971368
0.946074	0.920769	0.895465	0.870170	0.844866
0.819562	0.794267	0.768963	0.743658	0.718364
0.693059	0.667765	0.642461	0.617156	0.591862
0.566557	0.541253	0.531135	0.521017	0.510899
0.500782	0.490654	0.480536	0.470418	0.460301
0.450173	0.440055	0.450173	0.460301	0.470418
0.480536	0.490654	0.500782	0.510899	0.521017
0.531135	0.541253	0.566557	0.591862	0.617156
0.642461	0.667765	0.693059	0.718364	0.743658
0.768963	0.794267	0.819562	0.844866	0.870170
0.895465	0.920769	0.946074	0.971368	0.996673
1.021967	1.047271	1.072576	1.097870	1.123175
1.148479	1.173774	1.199078	1.224373	1.249677
1.274981	1.300276	1.325580	1.350885	1.361003
1.371120	1.381238	1.391366	1.401484	1.411601
1.421719	1.431837	1.441965	1.452083	1.441965

-0.059560	-0.059790	-0.058630	-0.055470	-0.052450
-0.049610	-0.046930	-0.044380	-0.041950	-0.039630
-0.034240	-0.029330	-0.024820	-0.020650	-0.016770
-0.013160	-0.009770	-0.006590	-0.003610	-0.000800
0.001850	0.004350	0.006710	0.008930	0.011030
0.013000	0.014870	0.016620	0.018260	0.019810
0.021250	0.022600	0.023850	0.025010	0.026090
0.027070	0.027980	0.028800	0.029530	0.030200
0.031150	0.032470	0.033130	0.033880	0.034720
0.035670	0.036770	0.038040	0.039560	0.041440
0.043990	0.050510	0.057020	0.059650	0.061610
0.063200	0.064550	0.065720	0.066760	0.067670
0.068490	0.069230	0.070750	0.071890	0.072800
0.073500	0.073990	0.074280	0.074370	0.074270
0.073960	0.073460	0.072750	0.071850	0.070740
0.069430	0.067910	0.066170	0.064200	0.062000
0.059550	0.056850	0.053860	0.050580	0.046980
0.043010	0.038650	0.033830	0.028480	0.022500
0.015770	0.008160	-0.000410	-0.009970	-0.014060
-0.018300	-0.022670	-0.027170	-0.031770	-0.036480
-0.041260	-0.046100	-0.050980	-0.056520	-0.059560

5.148000	5.148000	5.148000	5.148000	5.148000
5.148000	5.148000	5.148000	5.148000	5.148000
5.148000	5.148000	5.148000	5.148000	5.148000
5.148000	5.148000	5.148000	5.148000	5.148000
5.148000	5.148000	5.148000	5.148000	5.148000
5.148000	5.148000	5.148000	5.148000	5.148000
5.148000	5.148000	5.148000	5.148000	5.148000
5.148000	5.148000	5.148000	5.148000	5.148000
5.148000	5.148000	5.148000	5.148000	5.148000
5.148000	5.148000	5.148000	5.148000	5.148000
5.148000	5.148000	5.148000	5.148000	5.148000
5.148000	5.148000	5.148000	5.148000	5.148000
5.148000	5.148000	5.148000	5.148000	5.148000
5.148000	5.148000	5.148000	5.148000	5.148000

```
5.148000     5.148000     5.148000     5.148000     5.148000
5.148000     5.148000     5.148000     5.148000     5.148000
5.148000     5.148000     5.148000     5.148000     5.148000
5.148000     5.148000     5.148000     5.148000     5.148000
5.148000     5.148000     5.148000     5.148000     5.148000
5.148000     5.148000     5.148000     5.148000     5.148000
5.148000     5.148000     5.148000     5.148000     5.148000
```

B. TCGRID INPUT FILE FOR ROTOR AND TIP GAP

```
&nam1 merid=0 im=318 jm=45 km=84 itl=62 icap=12 igclt=1 kmt=20 jmt=20 &end
&nam2 nle=19 nte=24 dsle=.010 dste=.005 dshub=.0001
    dstip=.0001 dswte=.005 dswex=.01 dsthr=1.0 dsmin=.0001
    dsmax=.002 rcorn=0 cltip=.045 dsclt=.0001 &end
&nam3 iterm=100 idbg=0 0 0 0 0 0 0 0 aabb=1.0 &end
&nam4 zbc=1.5    1.5    2.65    1.5    1.5    2.65
    rbc=4.0788  4.0788  4.0788  5.02425  5.02425  5.098875  &end
&nam5 iswift=1 dslap=.002&end
'SSME HPFTP ADT FIRST STAGE ROTOR'
58  58
```

-0.9334116	-0.8467470	-0.7600824	-0.6734079	-0.5867434
-0.5000787	-0.4134042	-0.3267396	-0.2400750	-0.1534005
-0.066735901	0.019928699	0.1066032	0.1932678	0.2799324
0.3666069	0.4532715	0.5399361	0.6266007	0.6927030
0.7100379	0.7360452	0.7577163	0.7837138	0.8097210
0.8313921	0.8530533	0.8790606	0.9007317	0.9267291
0.9527364	0.9787437	1.004741	1.035075	1.061082
1.082743	1.193148	1.216443	1.239866	1.263398
1.287020	1.310730	1.334510	1.358349	1.382228
1.406137	1.430055	1.578555	1.617592	1.620448
1.622869	1.624487	1.625055	1.625623	1.627241
1.629662	1.632517	1.750000	2.650000	
3.790294	3.815232	3.838923	3.861406	3.882691
3.902798	3.921746	3.939557	3.956248	3.971821
3.986304	3.999689	4.012004	4.023261	4.033448
4.042595	4.050704	4.057773	4.063811	4.067732
4.068662	4.069979	4.070999	4.072147	4.073206
4.074018	4.074761	4.075573	4.076187	4.076830
4.077384	4.077850	4.078216	4.078533	4.078711
4.078780	4.078800	4.078800	4.078800	4.078800
4.078800	4.078800	4.078800	4.078800	4.078800
4.078800	4.078800	4.078800	4.078800	4.078800
4.078800	4.078800	4.078800	4.078800	4.078880
4.078800	4.078800	4.078800	4.078800	
-0.9334116	-0.8467470	-0.7600824	-0.6734079	-0.5867434
-0.5000787	-0.4134042	-0.3267396	-0.2400750	-0.1534005
-0.066735901	0.019928699	0.1066032	0.1932678	0.2799324
0.3666069	0.4532715	0.5399361	0.6266007	0.6875550
0.7114734	0.7353819	0.7592607	0.7830999	0.8068797
0.8305902	0.8542116	0.8777439	0.9011673	0.9244521
0.9513306	0.9781992	1.005068	1.031936	1.058805
1.085674	1.193148	1.216443	1.239866	1.263398
1.287020	1.310730	1.334510	1.358349	1.382228
1.406137	1.430055	1.578555	1.610000	1.626920
1.636248	1.645576	1.654905	1.664233	1.673561
1.682889	1.700000	1.750000	2.650000	
5.148000	5.148000	5.148000	5.148000	5.148000
5.148000	5.148000	5.148000	5.148000	5.148000
5.148000	5.148000	5.148000	5.148000	5.148000
5.148000	5.148000	5.148000	5.148000	5.148000
5.147713	5.146842	5.145396	5.143377	5.140783
5.137615	5.133873	5.129556	5.124685	5.119240
5.112617	5.105697	5.099371	5.092748	5.086125
5.079502	5.053010	5.047565	5.042694	5.038377
5.034636	5.031467	5.028873	5.026854	5.025408
5.024538	5.024250	5.024250	5.024250	5.033578
5.042906	5.052234	5.061563	5.070891	5.080219
5.089546	5.098875	5.098875	5.098875	

```
5 105 50
```

2.485395	2.494305	2.485395	2.476487	2.467575
2.458665	2.449755	2.440845	2.431935	2.423025

2.414115	2.405205	2.382930	2.360655	2.338380
2.316105	2.293830	2.271555	2.249280	2.227005
2.204730	2.182455	2.160180	2.137905	2.115630
2.093355	2.071080	2.048805	2.026530	2.004255
1.981980	1.959705	1.937430	1.915155	1.892880
1.870605	1.848330	1.826055	1.803780	1.781505
1.759230	1.736955	1.714680	1.692405	1.683495
1.674585	1.665675	1.656765	1.647855	1.638945
1.630035	1.621125	1.612215	1.603305	1.612215
1.621125	1.630035	1.638945	1.647855	1.656765
1.665675	1.674585	1.683495	1.692405	1.714680
1.736955	1.759230	1.781505	1.803780	1.826055
1.848330	1.870605	1.892880	1.915155	1.937430
1.959705	1.981980	2.004255	2.026530	2.048805
2.071080	2.093355	2.115630	2.137905	2.160180
2.182455	2.204730	2.227005	2.249280	2.271555
2.293830	2.316105	2.338380	2.360655	2.382930
2.405205	2.414115	2.423025	2.431935	2.440845
2.449755	2.458665	2.467575	2.476485	2.485395

0.071650	0.067930	0.060270	0.053470	0.046890
0.040570	0.034500	0.028680	0.023140	0.017860
0.012850	0.008110	-0.002630	-0.011890	-0.019840
-0.026690	-0.032640	-0.037830	-0.042360	-0.046320
-0.049760	-0.052740	-0.055290	-0.057440	-0.059210
-0.060610	-0.061680	-0.062410	-0.062820	-0.062910
-0.062690	-0.062170	-0.061330	-0.060190	-0.058740
-0.056970	-0.054880	-0.052460	-0.049700	-0.046580
-0.043080	-0.039180	-0.034860	-0.030070	-0.028020
-0.025880	-0.023650	-0.021330	-0.018920	-0.016400
-0.013760	-0.010740	-0.006920	0.000080	0.006670
0.008870	0.010160	0.010860	0.011120	0.011130
0.010950	0.010600	0.010120	0.009500	0.007660
0.005980	0.004500	0.003220	0.002130	0.001220
0.000480	-0.000080	-0.000470	-0.000680	-0.000740
-0.000620	-0.000330	0.000130	0.000750	0.001560
0.002540	0.003710	0.005070	0.006630	0.008390
0.010380	0.012600	0.015070	0.017810	0.020850
0.024220	0.027970	0.032150	0.036830	0.042130
0.048230	0.050940	0.053850	0.057000	0.060410
0.064180	0.068390	0.071500	0.072180	0.071650

4.078800	4.078800	4.078800	4.078800	4.078800
4.078800	4.078800	4.078800	4.078800	4.078800
4.078800	4.078800	4.078800	4.078800	4.078800
4.078800	4.078800	4.078800	4.078800	4.078800
4.078800	4.078800	4.078800	4.078800	4.078800
4.078800	4.078800	4.078800	4.078800	4.078800
4.078800	4.078800	4.078800	4.078800	4.078800
4.078800	4.078800	4.078800	4.078800	4.078800
4.078800	4.078800	4.078800	4.078800	4.078800
4.078800	4.078800	4.078800	4.078800	4.078800
4.078800	4.078800	4.078800	4.078800	4.078800
4.078800	4.078800	4.078800	4.078800	4.078800
4.078800	4.078800	4.078800	4.078800	4.078800
4.078800	4.078800	4.078800	4.078800	4.078800
4.078800	4.078800	4.078800	4.078800	4.078800
4.078800	4.078800	4.078800	4.078800	4.078800
4.078800	4.078800	4.078800	4.078800	4.078800
4.078800	4.078800	4.078800	4.078800	4.078800
4.078800	4.078800	4.078800	4.078800	4.078800
4.078800	4.078800	4.078800	4.078800	4.078800
4.078800	4.078800	4.078800	4.078800	4.078800
4.078800	4.078800	4.078800	4.078800	4.078800

2.459467	2.467387	2.459467	2.451547	2.443627
2.435707	2.427787	2.419867	2.411947	2.404027
2.396107	2.388187	2.368387	2.348587	2.328787
2.308987	2.289187	2.269387	2.249587	2.229787

2.209987	2.190187	2.170387	2.150587	2.130787
2.110987	2.091187	2.071387	2.051587	2.031787
2.011987	1.992187	1.972387	1.952587	1.932787
1.912987	1.893187	1.873387	1.853587	1.833787
1.813987	1.794187	1.774387	1.754587	1.746667
1.738747	1.730827	1.722907	1.714987	1.707067
1.699147	1.691227	1.683307	1.675387	1.683307
1.691227	1.699147	1.707067	1.714987	1.722907
1.730827	1.738747	1.746667	1.754587	1.774387
1.794187	1.813987	1.833787	1.853587	1.873387
1.893187	1.912987	1.932787	1.952587	1.972387
1.992187	2.011987	2.031787	2.051587	2.071387
2.091187	2.110987	2.130787	2.150587	2.170387
2.190187	2.209987	2.229787	2.249587	2.269387
2.289187	2.308987	2.328787	2.348587	2.368387
2.388187	2.396107	2.404027	2.411947	2.419867
2.427787	2.435707	2.443627	2.451547	2.459467

0.063210	0.060000	0.053520	0.047740	0.042100
0.036620	0.031290	0.026130	0.021140	0.016320
0.011680	0.007210	-0.003160	-0.012440	-0.020660
-0.027920	-0.034300	-0.039920	-0.044860	-0.049220
-0.053060	-0.056430	-0.059380	-0.061920	-0.064080
-0.065860	-0.067270	-0.068340	-0.069050	-0.069430
-0.069470	-0.069170	-0.068540	-0.067570	-0.066260
-0.064610	-0.062590	-0.060220	-0.057470	-0.054320
-0.050760	-0.046750	-0.042280	-0.037290	-0.035150
-0.032910	-0.030570	-0.028130	-0.025580	-0.022940
-0.020180	-0.017190	-0.013470	-0.006990	-0.000990
0.001090	0.002380	0.003180	0.003620	0.003730
0.003550	0.003210	0.002730	0.002130	0.000230
-0.001830	-0.003650	-0.005250	-0.006630	-0.007810
-0.008790	-0.009570	-0.010140	-0.010520	-0.010710
-0.010700	-0.010490	-0.010090	-0.009480	-0.008670
-0.007650	-0.006410	-0.004950	-0.003250	-0.001310
0.000870	0.003330	0.006070	0.009120	0.012490
0.016230	0.020360	0.024920	0.029980	0.035620
0.041940	0.044690	0.047590	0.050650	0.053900
0.057360	0.061090	0.063280	0.063730	0.063210

4.317637	4.317637	4.317637	4.317637	4.317637
4.317637	4.317637	4.317637	4.317637	4.317637
4.317637	4.317637	4.317637	4.317637	4.317637
4.317637	4.317637	4.317637	4.317637	4.317637
4.317637	4.317637	4.317637	4.317637	4.317637
4.317637	4.317637	4.317637	4.317637	4.317637
4.317637	4.317637	4.317637	4.317637	4.317637
4.317637	4.317637	4.317637	4.317637	4.317637
4.317637	4.317637	4.317637	4.317637	4.317637
4.317637	4.317637	4.317637	4.317637	4.317637
4.317637	4.317637	4.317637	4.317637	4.317637
4.317637	4.317637	4.317637	4.317637	4.317637
4.317637	4.317637	4.317637	4.317637	4.317637
4.317637	4.317637	4.317637	4.317637	4.317637
4.317637	4.317637	4.317637	4.317637	4.317637
4.317637	4.317637	4.317637	4.317637	4.317637
4.317637	4.317637	4.317637	4.317637	4.317637
4.317637	4.317637	4.317637	4.317637	4.317637
4.317637	4.317637	4.317637	4.317637	4.317637

2.430747	2.437677	2.430747	2.423817	2.416887
2.409957	2.403027	2.396097	2.389167	2.382237
2.375307	2.368377	2.351052	2.333727	2.316402
2.299077	2.281752	2.264427	2.247102	2.229777
2.212452	2.195127	2.177802	2.160477	2.143152
2.125827	2.108502	2.091177	2.073852	2.056527

2.039202	2.021877	2.004552	1.987227	1.969902
1.952577	1.935252	1.917927	1.900602	1.883277
1.865952	1.848627	1.831302	1.813977	1.807047
1.800117	1.793187	1.786257	1.779327	1.772397
1.765467	1.758537	1.751607	1.744677	1.751607
1.758537	1.765467	1.772397	1.779327	1.786257
1.793187	1.800117	1.807047	1.813977	1.831302
1.848627	1.865952	1.883277	1.900602	1.917927
1.935252	1.952577	1.969902	1.987227	2.004552
2.021877	2.039202	2.056527	2.073852	2.091177
2.108502	2.125827	2.143152	2.160477	2.177802
2.195127	2.212452	2.229777	2.247102	2.264427
2.281752	2.299077	2.316402	2.333727	2.351052
2.368377	2.375307	2.382237	2.389167	2.396097
2.403027	2.409957	2.416887	2.423817	2.430747
0.054680	0.051920	0.046510	0.041660	0.036910
0.032230	0.027660	0.023170	0.018800	0.014520
0.010360	0.006310	-0.003300	-0.012140	-0.020190
-0.027460	-0.033980	-0.039790	-0.044960	-0.049540
-0.053600	-0.057180	-0.060330	-0.063070	-0.065420
-0.067400	-0.069040	-0.070330	-0.071300	-0.071940
-0.072270	-0.072270	-0.071970	-0.071350	-0.070420
-0.069160	-0.067570	-0.065640	-0.063370	-0.060720
-0.057700	-0.054260	-0.050390	-0.046050	-0.044170
-0.042200	-0.040140	-0.037990	-0.035740	-0.033380
-0.030920	-0.028280	-0.025020	-0.019360	-0.014140
-0.012290	-0.011120	-0.010340	-0.009860	-0.009650
-0.009670	-0.009900	-0.010250	-0.010700	-0.012230
-0.014040	-0.015640	-0.017010	-0.018180	-0.019130
-0.019870	-0.020410	-0.020740	-0.020870	-0.020800
-0.020520	-0.020040	-0.019350	-0.018460	-0.017360
-0.016040	-0.014500	-0.012740	-0.010740	-0.008510
-0.006020	-0.003280	-0.000270	0.003040	0.006650
0.010580	0.014870	0.019540	0.024630	0.030190
0.036280	0.038880	0.041580	0.044400	0.047330
0.050380	0.053550	0.054910	0.055170	0.054680
4.556475	4.556475	4.556475	4.556475	4.556475
4.556475	4.556475	4.556475	4.556475	4.556475
4.556475	4.556475	4.556475	4.556475	4.556475
4.556475	4.556475	4.556475	4.556475	4.556475
4.556475	4.556475	4.556475	4.556475	4.556475
4.556475	4.556475	4.556475	4.556475	4.556475
4.556475	4.556475	4.556475	4.556475	4.556475
4.556475	4.556475	4.556475	4.556475	4.556475
4.556475	4.556475	4.556475	4.556475	4.556475
4.556475	4.556475	4.556475	4.556475	4.556475
4.556475	4.556475	4.556475	4.556475	4.556475
4.556475	4.556475	4.556475	4.556475	4.556475
4.556475	4.556475	4.556475	4.556475	4.556475
4.556475	4.556475	4.556475	4.556475	4.556475
4.556475	4.556475	4.556475	4.556475	4.556475
4.556475	4.556475	4.556475	4.556475	4.556475
4.556475	4.556475	4.556475	4.556475	4.556475
4.556475	4.556475	4.556475	4.556475	4.556475
4.556475	4.556475	4.556475	4.556475	4.556475
4.556475	4.556475	4.556475	4.556475	4.556475
2.399542	2.405482	2.399542	2.393602	2.387662
2.381722	2.375782	2.369842	2.363902	2.357962
2.352022	2.346082	2.331232	2.316382	2.301532
2.286682	2.271832	2.256982	2.242132	2.227282
2.212432	2.197582	2.182732	2.167882	2.153032
2.138182	2.123332	2.108482	2.093632	2.078782
2.063932	2.049082	2.034232	2.019382	2.004532
1.989682	1.974832	1.959982	1.945132	1.930282

110

1.915432	1.900582	1.885732	1.870882	1.864942
1.859002	1.853062	1.847122	1.841182	1.835242
1.829302	1.823362	1.817422	1.811482	1.817422
1.823362	1.829302	1.835242	1.841182	1.847122
1.853062	1.859002	1.864942	1.870882	1.885732
1.900582	1.915432	1.930282	1.945132	1.959982
1.974832	1.989682	2.004532	2.019382	2.034232
2.049082	2.063932	2.078782	2.093632	2.108482
2.123332	2.138182	2.153032	2.167882	2.182732
2.197582	2.212432	2.227282	2.242132	2.256982
2.271832	2.286682	2.301532	2.316382	2.331232
2.346082	2.352022	2.357962	2.363902	2.369842
2.375782	2.381722	2.387662	2.393602	2.399542

0.046150	0.043810	0.039360	0.035390	0.031450
0.027570	0.023730	0.019950	0.016220	0.012560
0.008950	0.005410	-0.003130	-0.011200	-0.018740
-0.025740	-0.032150	-0.037970	-0.043220	-0.047900
-0.052040	-0.055690	-0.058880	-0.061650	-0.064050
-0.066120	-0.067860	-0.069310	-0.070480	-0.071380
-0.072010	-0.072380	-0.072500	-0.072360	-0.071970
-0.071320	-0.070410	-0.069230	-0.067780	-0.066040
-0.064010	-0.061650	-0.058950	-0.055870	-0.054530
-0.053120	-0.051640	-0.050090	-0.048440	-0.046700
-0.044830	-0.042790	-0.040240	-0.035600	-0.031200
-0.029630	-0.028610	-0.027920	-0.027470	-0.027230
-0.027160	-0.027210	-0.027340	-0.027550	-0.028380
-0.029480	-0.030430	-0.031170	-0.031720	-0.032070
-0.032220	-0.032170	-0.031930	-0.031490	-0.030860
-0.030030	-0.029010	-0.027800	-0.026380	-0.024780
-0.022970	-0.020960	-0.018750	-0.016340	-0.013710
-0.010870	-0.007800	-0.004520	-0.001000	0.002770
0.006780	0.011060	0.015620	0.020470	0.025640
0.031160	0.033470	0.035840	0.038270	0.040780
0.043350	0.045700	0.046510	0.046630	0.046150

4.795312	4.795312	4.795312	4.795312	4.795312
4.795312	4.795312	4.795312	4.795312	4.795312
4.795312	4.795312	4.795312	4.795312	4.795312
4.795312	4.795312	4.795312	4.795312	4.795312
4.795312	4.795312	4.795312	4.795312	4.795312
4.795312	4.795312	4.795312	4.795312	4.795312
4.795312	4.795312	4.795312	4.795312	4.795312
4.795312	4.795312	4.795312	4.795312	4.795312
4.795312	4.795312	4.795312	4.795312	4.795312
4.795312	4.795312	4.795312	4.795312	4.795312
4.795312	4.795312	4.795312	4.795312	4.795312
4.795312	4.795312	4.795312	4.795312	4.795312
4.795312	4.795312	4.795312	4.795312	4.795312
4.795312	4.795312	4.795312	4.795312	4.795312
4.795312	4.795312	4.795312	4.795312	4.795312
4.795312	4.795312	4.795312	4.795312	4.795312
4.795312	4.795312	4.795312	4.795312	4.795312
4.795312	4.795312	4.795312	4.795312	4.795312
4.795312	4.795312	4.795312	4.795312	4.795312
4.795312	4.795312	4.795312	4.795312	4.795312
4.795312	4.795312	4.795312	4.795312	4.795312

2.367308	2.372258	2.367308	2.362358	2.357408
2.352458	2.347508	2.342558	2.337608	2.332658
2.327708	2.322758	2.310383	2.298008	2.285633
2.273258	2.260883	2.248508	2.236133	2.223758
2.211383	2.199008	2.186633	2.174258	2.161883
2.149508	2.137133	2.124758	2.112383	2.100008
2.087633	2.075258	2.062883	2.050508	2.038133
2.025758	2.013383	2.001008	1.988633	1.976258
1.963883	1.951508	1.939133	1.926758	1.921808
1.916858	1.911908	1.906958	1.902008	1.897058

1.892108	1.887158	1.882208	1.877258	1.882208
1.887158	1.892108	1.897058	1.902008	1.906958
1.911908	1.916858	1.921808	1.926758	1.939133
1.951508	1.963883	1.976258	1.988633	2.001008
2.013383	2.025758	2.038133	2.050508	2.062883
2.075258	2.087633	2.100008	2.112383	2.124758
2.137133	2.149508	2.161883	2.174258	2.186633
2.199008	2.211383	2.223758	2.236133	2.248508
2.260883	2.273258	2.285633	2.298008	2.310383
2.322758	2.327708	2.332658	2.337608	2.342558
2.347508	2.352458	2.357408	2.362358	2.367308
0.038110	0.036140	0.032570	0.029390	0.026220
0.023060	0.019930	0.016810	0.013710	0.010640
0.007590	0.004560	-0.002870	-0.010090	-0.017030
-0.023650	-0.029890	-0.035660	-0.040930	-0.045660
-0.049840	-0.053490	-0.056660	-0.059410	-0.061810
-0.063900	-0.065720	-0.067290	-0.068630	-0.069760
-0.070690	-0.071420	-0.071970	-0.072330	-0.072510
-0.072520	-0.072340	-0.071980	-0.071430	-0.070690
-0.069740	-0.068570	-0.067180	-0.065530	-0.064800
-0.064010	-0.063180	-0.062300	-0.061340	-0.060280
-0.059090	-0.057690	-0.055900	-0.052310	-0.048780
-0.047520	-0.046700	-0.046140	-0.045730	-0.045430
-0.045200	-0.045040	-0.044940	-0.044880	-0.044930
-0.045190	-0.045380	-0.045390	-0.045210	-0.044860
-0.044320	-0.043600	-0.042690	-0.041610	-0.040350
-0.038900	-0.037280	-0.035480	-0.033500	-0.031340
-0.029000	-0.026490	-0.023810	-0.020950	-0.017920
-0.014710	-0.011340	-0.007790	-0.004080	-0.000200
0.003850	0.008060	0.012430	0.016960	0.021660
0.026510	0.028500	0.030510	0.032540	0.034600
0.036690	0.038110	0.038550	0.038550	0.038110
5.034150	5.034150	5.034150	5.034150	5.034150
5.034150	5.034150	5.034150	5.034150	5.034150
5.034150	5.034150	5.034150	5.034150	5.034150
5.034150	5.034150	5.034150	5.034150	5.034150
5.034150	5.034150	5.034150	5.034150	5.034150
5.034150	5.034150	5.034150	5.034150	5.034150
5.034150	5.034150	5.034150	5.034150	5.034150
5.034150	5.034150	5.034150	5.034150	5.034150
5.034150	5.034150	5.034150	5.034150	5.034150
5.034150	5.034150	5.034150	5.034150	5.034150
5.034150	5.034150	5.034150	5.034150	5.034150
5.034150	5.034150	5.034150	5.034150	5.034150
5.034150	5.034150	5.034150	5.034150	5.034150
5.034150	5.034150	5.034150	5.034150	5.034150
5.034150	5.034150	5.034150	5.034150	5.034150
5.034150	5.034150	5.034150	5.034150	5.034150
5.034150	5.034150	5.034150	5.034150	5.034150
5.034150	5.034150	5.034150	5.034150	5.034150
5.034150	5.034150	5.034150	5.034150	5.034150
5.034150	5.034150	5.034150	5.034150	5.034150
5.034150	5.034150	5.034150	5.034150	5.034150
0.000000	0.000000	0.000000	0.000000	0.000000
0.000000	0.000000	0.000000	0.000000	0.000000
0.000000	0.000000	0.000000	0.000000	0.000000
0.000000	0.000000	0.000000	0.000000	0.000000
0.000000	0.000000	0.000000	0.000000	0.000000
0.000000	0.000000	0.000000	0.000000	0.000000
0.000000	0.000000	0.000000	0.000000	0.000000
0.000000	0.000000	0.000000	0.000000	0.000000
0.000000	0.000000	0.000000	0.000000	0.000000
0.000000	0.000000	0.000000	0.000000	0.000000
0.000000	0.000000	0.000000	0.000000	0.000000
0.000000	0.000000	0.000000	0.000000	0.000000

```
0.000000      0.000000      0.000000      0.000000      0.000000
0.000000      0.000000      0.000000      0.000000      0.000000
0.000000      0.000000      0.000000      0.000000      0.000000
0.000000      0.000000      0.000000      0.000000      0.000000
0.000000      0.000000      0.000000      0.000000      0.000000
0.000000      0.000000      0.000000      0.000000      0.000000
0.000000      0.000000      0.000000      0.000000      0.000000
0.000000      0.000000      0.000000      0.000000      0.000000
0.000000      0.000000      0.000000      0.000000      0.000000
```

APPENDIX B.   3D FLOW SOLVER FILES/PARAMETERS

A.   SWIFT BOUNDARY CONDITION PARAMETERS

Inlet	IBCIN=3: Annular blade row, subsonic inflow. P_0, T_0, and v_θ fixed at initial conditions. Riemann invariant extrapolated from interior.
Between Blade Rows (Mixing Plane Technique)	IQAV=0: Energy averaging
	IQAV=1: Momentum averaging
	IQAV=2: Fully mixed-out averaging
Exit	IBCEX=3: Radial equilibrium equation, constant pressure blade-to-blade
	IBCEX=4: Giles' characteristics, variable pressure blade-to-blade

Table 3. SWIFT Boundary Conditions

B.   SWIFT PARAMETER INPUT FILE FOR COMBINED GRID

```
'SSME HPFTP ADT FIRST STAGE STATOR AND ROTOR'
&nl2 nstg=4 cfl=4.0 avisc1=0.0 avisc2=2.0 avisc4=2.0
    eps=2.0 pck=0.15 itmax=400 ivdt=1 ndis=2
    refms=.2 ipc=0 &end
&nl3 ibcin=3 ibcex=4 ires=1 iresti=1
    kbcor=1 &end
&nl4 igeom=1 ga=1.4 om=-.03809 prat=0.75 expt=0.0 &end
&nl5 ilt=2 renr=564075.8 tw=0.0
    jedge=30 kedgh=30 kedgt=30
    dblh=0.005 dblt=0.005 hrough=4.0 tlength=0.00015
    tintens=.01 itur=2 &end
&nl6 oar=0.0 mioe=3 iqav=1 &end
 row    P0       Mx       Mtheta   Mr       T0
   0  1.0000   0.1700   0.0000   0.0000   1.0000
   1  0.9850   0.1980  -0.6720   0.0000   1.0000
   2  0.8000   0.1928   0.2298   0.0000   0.9600
```

C.   SWIFT 'FORT.10' INPUT FILE FOR COMBINED GRID

```
grid type im  jm km  i1  i2  i3 nin nex nhub ntip nlr row om omh omt
  1   2 218  46 84  30 104   0 999  -2   0    0   0   1 0.  0.  0.
  2   2 318  46 84  62 154  65  -1 999   0    3   0   2 1.  1.  0.
  3   3 196  20 20   0   0  65   0   0   0    2   0   2 1.  1.  0.
```

APPENDIX C.   QUASI-3D GRID GENERATION FILES

A.   GRAPE INPUT FOR STATOR MIDSPAN PLANE

```
&GRID1  JMAX=310, KMAX=50, NTETYP=3, NAIRF=5, JAIRF=105, NIBDST=6,
DSI=0.0001, JTEBOT=46, JTETOP=265, NORDA=0,3, NOBSHP=7, XLEFT=0, XRIGHT=1.5,
XLE=0.4401, XTE=1.3459, NOUT=4, RCORN=0.0, MAXITA=0,300
&END
&GRID2  PITCH=0.54996, NOBCAS=0, DSRA=0.45, DSLE=.0005, DSTE=.002, NLE=30,
NTE=16, YSCL=4.551525, WAKEP=1.5, DSOBI=.001,
OMEGA=1.3, OMEGP=0.3, OMEGQ=0.3, OMEGR=0.3, OMEGS=0.3,
AAAI=0.5, BBBI=0.5, CCCI=0.5, DDDI=0.5
&END
&GRID3
AIRFX=
    1.336847,     1.327788,     1.318730,     1.309671,     1.300613,
    1.291554,     1.282495,     1.273437,     1.264379,     1.255320,
    1.232669,     1.210027,     1.187376,     1.164735,     1.142084,
    1.119442,     1.096791,     1.074150,     1.051499,     1.028857,
    1.006206,     0.983565,     0.960914,     0.938272,     0.915621,
    0.892980,     0.870329,     0.847687,     0.825036,     0.802395,
    0.779744,     0.757102,     0.734451,     0.711810,     0.689159,
    0.666517,     0.643866,     0.621225,     0.598574,     0.575933,
    0.553281,     0.530640,     0.521581,     0.512523,     0.503465,
    0.494406,     0.485348,     0.476289,     0.467230,     0.458172,
    0.449113,     0.440055,     0.449113,     0.458172,     0.467230,
    0.476289,     0.485348,     0.494406,     0.503465,     0.512523,
    0.521581,     0.530640,     0.553281,     0.575933,     0.598574,
    0.621225,     0.643866,     0.666517,     0.689159,     0.711810,
    0.734451,     0.757102,     0.779744,     0.802395,     0.825036,
    0.847687,     0.870329,     0.892980,     0.915621,     0.938272,
    0.960914,     0.983565,     1.006206,     1.028857,     1.051499,
    1.074150,     1.096791,     1.119442,     1.142084,     1.164735,
    1.187376,     1.210027,     1.232669,     1.255320,     1.264379,
    1.273437,     1.282495,     1.291554,     1.300613,     1.309671,
    1.318730,     1.327788,     1.336847,     1.345905,     1.336847,
AIRFY=
   -0.103300,    -0.103750,    -0.103080,    -0.099950,    -0.095630,
   -0.091630,    -0.087900,    -0.084380,    -0.081070,    -0.077920,
   -0.070680,    -0.064170,    -0.058250,    -0.052820,    -0.047790,
   -0.043120,    -0.038760,    -0.034670,    -0.030830,    -0.027210,
   -0.023790,    -0.020550,    -0.017490,    -0.014580,    -0.011820,
   -0.009190,    -0.006690,    -0.004310,    -0.002050,     0.000110,
    0.002160,     0.004120,     0.005990,     0.007770,     0.009460,
    0.011070,     0.012600,     0.014060,     0.015450,     0.016770,
    0.018160,     0.019950,     0.020790,     0.021720,     0.022750,
    0.023900,     0.025190,     0.026660,     0.028370,     0.030460,
    0.033230,     0.039850,     0.046460,     0.048960,     0.050770,
    0.052200,     0.053390,     0.054410,     0.055270,     0.056030,
    0.056680,     0.057240,     0.058330,     0.059030,     0.059460,
    0.059730,     0.059850,     0.059800,     0.059580,     0.059180,
    0.058600,     0.057830,     0.056850,     0.055680,     0.054280,
    0.052660,     0.050800,     0.048690,     0.046320,     0.043670,
    0.040710,     0.037440,     0.033840,     0.029860,     0.025490,
    0.020690,     0.015430,     0.009650,     0.003290,    -0.003710,
   -0.011430,    -0.019990,    -0.029510,    -0.040160,    -0.044780,
   -0.049630,    -0.054730,    -0.060100,    -0.065750,    -0.071730,
   -0.078050,    -0.084750,    -0.091880,    -0.099950,    -0.103300
&END
```

B.   GRAPE INPUT FOR ROTOR MIDSPAN PLANE

```
&GRID1  JMAX=330, KMAX=50, NTETYP=3, NAIRF=5, JAIRF=105, NIBDST=6,
DSI=0.0001, JTEBOT=56, JTETOP=275, NORDA=0,3, NOBSHP=7, XLEFT=1.5, XRIGHT=2.65,
XLE=1.7447, XTE=2.4377, NOUT=4, RCORN=0.0, MAXITA=0,300
&END
&GRID2  PITCH=0.57258, NOBCAS=0, DSRA=0.58, DSLE=.0005, DSTE=.002, NLE=40,
NTE=22, YSCL=4.556475, XTFRAC=0.8, WAKEP=1.5, DSOBI=.001,
OMEGA=1.3, OMEGP=0.3, OMEGQ=0.3, OMEGR=0.3, OMEGS=0.3,
AAAI=0.5, BBBI=0.5, CCCI=0.5, DDDI=0.5
&END
&GRID3
AIRFX=
        2.430747,       2.437677,       2.430747,       2.423817,       2.416887,
        2.409957,       2.403027,       2.396097,       2.389167,       2.382237,
        2.375307,       2.368377,       2.351052,       2.333727,       2.316402,
        2.299077,       2.281752,       2.264427,       2.247102,       2.229777,
        2.212452,       2.195127,       2.177802,       2.160477,       2.143152,
        2.125827,       2.108502,       2.091177,       2.073852,       2.056527,
        2.039202,       2.021877,       2.004552,       1.987227,       1.969902,
        1.952577,       1.935252,       1.917927,       1.900602,       1.883277,
        1.865952,       1.848627,       1.831302,       1.813977,       1.807047,
        1.800117,       1.793187,       1.786257,       1.779327,       1.772397,
        1.765467,       1.758537,       1.751607,       1.744677,       1.751607,
        1.758537,       1.765467,       1.772397,       1.779327,       1.786257,
        1.793187,       1.800117,       1.807047,       1.813977,       1.831302,
        1.848627,       1.865952,.      1.883277,       1.900602,       1.917927,
        1.935252,       1.952577,       1.969902,       1.987227,       2.004552,
        2.021877,       2.039202,       2.056527,       2.073852,       2.091177,
        2.108502,       2.125827,       2.143152,       2.160477,       2.177802,
        2.195127,       2.212452,       2.229777,       2.247102,       2.264427,
        2.281752,       2.299077,       2.316402,       2.333727,       2.351052,
        2.368377,       2.375307,       2.382237,       2.389167,       2.396097,
        2.403027,       2.409957,       2.416887,       2.423817,       2.430747,
AIRFY=
        0.054680,       0.051920,       0.046510,       0.041660,       0.036910,
        0.032230,       0.027660,       0.023170,       0.018800,       0.014520,
        0.010360,       0.006310,      -0.003300,      -0.012140,      -0.020190,
       -0.027460,      -0.033980,      -0.039790,      -0.044960,      -0.049540,
       -0.053600,      -0.057180,      -0.060330,      -0.063070,      -0.065420,
       -0.067400,      -0.069040,      -0.070330,      -0.071300,      -0.071940,
       -0.072270,      -0.072270,      -0.071970,      -0.071350,      -0.070420,
       -0.069160,      -0.067570,      -0.065640,      -0.063370,      -0.060720,
       -0.057700,      -0.054260,      -0.050390,      -0.046050,      -0.044170,
       -0.042200,      -0.040140,      -0.037990,      -0.035740,      -0.033380,
       -0.030920,      -0.028280,      -0.025020,      -0.019360,      -0.014140,
       -0.012290,      -0.011120,      -0.010340,      -0.009860,      -0.009650,
       -0.009670,      -0.009900,      -0.010250,      -0.010700,      -0.012230,
       -0.014040,      -0.015640,      -0.017010,      -0.018180,      -0.019130,
       -0.019870,      -0.020410,      -0.020740,      -0.020870,      -0.020800,
       -0.020520,      -0.020040,      -0.019350,      -0.018460,      -0.017360,
       -0.016040,      -0.014500,      -0.012740,      -0.010740,      -0.008510,
       -0.006020,      -0.003280,      -0.000270,       0.003040,       0.006650,
        0.010580,       0.014870,       0.019540,       0.024630,       0.030190,
        0.036280,       0.038880,       0.041580,       0.044400,       0.047330,
        0.050380,       0.053550,       0.054910,       0.055170,       0.054680
&END
```

APPENDIX D.   QUASI-3D FLOW SOLVER FILES

A.   RVCQ3D INPUT FOR STATOR

```
'SSME HPFTP 1ST STAGE STATOR MIDSPAN CROSS SECTION'
&NL1 M=310, N=50, MTL=46, MIL=136 &END
&NL2 NSTG=4, IVDT=1, AVISC2=0, EPS=0.75,
     AVISC4=2.0, CFL=1.5, IRS=1, EPI=0.75, EPJ=0.75 &END
&NL3 IBCIN=1, IBCEX=1, ITMAX=5000, IRESTI=0,
     IRESTO=1, IRES=1, ICRNT=10000, IXRM=0 &END
&NL4 POIN=1.0, TOIN=1.0, PRAT=.87, AMLE=0.17, ALLE=0.0,
     G=1.4 &END
&NL5 ILT=0, PRNR=0.7, TW=1.0, VISPWR=.6667, RENR=564075,
     CMUTM=14, JEDGE=40, ITUR=2 &END
&NL6 OMEGA=0, NBLADE=52, NMN=2 &END
&NL7 &END
0.0000 1.5000
4.5515 4.5515
1.0000 1.0000
```

B.   RVCQ3D INPUT FOR ROTOR

```
'SSME HPFTP 1ST STAGE ROTOR MIDSPAN CROSS SECTION'
&NL1 M=330, N=50, MTL=56, MIL=143 &END
&NL2 NSTG=4, IVDT=1, AVISC2=0, EPS=0.75,
     AVISC4=2.0, CFL=2.8, IRS=1, EPI=0.75, EPJ=0.75 &END
&NL3 IBCIN=1, IBCEX=1, ITMAX=100, IRESTI=0,
     IRESTO=1, IRES=1, ICRNT=10000, IXRM=0 &END
&NL4 POIN=1.0, TOIN=1.0, PRAT=.77, AMLE=0.43, ALLE=-66,
     G=1.4 &END
&NL5 ILT=0, PRNR=0.7, TW=1.0, VISPWR=.6667, RENR=564075,
     CMUTM=14, JEDGE=40, ITUR=2 &END
&NL6 OMEGA=-.03809, NBLADE=50, NMN=2 &END
&NL7 &END
1.5000 2.6500
4.5565 4.5565
1.0000 1.0000
```

APPENDIX E.   FIND/PHASE MENU SETTINGS

A.   "FIND" CALIBRATION MENUS

I/O Port Selection:	
Traverse Controller	COM 1
Sony Position Enc.	COM 2
Printer Port	LPT 1
Proc./RMR I/O Port	COM 1
Color Link	Off

Hardware Selection:	
First Processor	IFA750
Second Processor	IFA750
Third Processor	NA
Master Interface	MI750
Rotary Encoder Type	1989

Table 4. FIND I/O Port and Processor Selection

IFA 750 Operation Parameters	Manual Override
Number of Processors	2
Number of K-Data Points	20
Data Sampling Method	TBD on
Coincidence Window Width (μsec)	1E0
DMA Time-out	999 Sec
Acquisition Mode	Coincidence
Sampling Time (μsec)	100
Filter Selections	**300K-3M Hz** **300K-3M Hz**
Number of C-Words	0
Single Measurement/Burst	Off
Transit Time Enable	Off
Minimum Threshold	10

Table 5. FIND Processor Settings

Minimum Cycles/Burst	4
Signal to Noise Ratio	Very Low
Threshold Optimization	Off

Table 6. FIND Manual Override Settings

121

	Processor 1	Processor 2
Fringe Spacing (μm)	4.7591	4.5139
Frequency Shift (MHz)	**1**	**1**
Half Angle (Deg)	3.1	3.1
Focal Length (mm)	762	762
Beam Spacing (mm)	82.5	82.5
Wavelength (nm)	514.5	488.0
Rotation x-y Plane (Degrees)		0.0
Tilt y-z Plane (Degrees)		0.0

Table 7. FIND Optics Configuration

Additional Setup Notes:

Laser Power: 1W
Seeding: 1 jet, 30 psi, 40%
Probe Volume Location: Optimized at exit of external seeding hose.

Typical Data Rates:
Green: 400-800
Blue: 400-1200
Coincidence: 220-680

B. "PHASE" OPERATION MENUS

1. Checkout Menus (1500 AND 3000 RPM)

I/O Port Selection:		Hardware Selection:	
Traverse Controller	COM 1	First Processor	IFA750
Sony Position Enc.	COM 2	Second Processor	IFA750
Printer Port	LPT 1	Third Processor	NA
Proc./RMR I/O Port	COM 1	Master Interface	MI750
Color Link	Off	Rotary Encoder Type	1989

Table 8. PHASE Checkout I/O Port and Processor Selection

IFA 750 Operation Parameters	Manual Override
Number of Processors	2
Number of K-Data Points	20
Data Sampling Method	TBD on
Coincidence Window Width (μsec)	1E0
DMA Time-out	999 Sec
Acquisition Mode	Coincidence
Sampling Time (μsec)	100
Filter Selections	**3-20 MHz** **3-20 MHz**
Number of C-Words	0
Single Measurement/Burst	Off
Transit Time Enable	Off
Minimum Threshold	30

Table 9. PHASE Checkout Processor Settings

Minimum Cycles/Burst	4
Signal to Noise Ratio	Very Low
Threshold Optimization	Off

Table 10. PHASE Checkout Manual Override Settings

123

	Processor 1	Processor 2
Fringe Spacing (Microns)	4.7591	4.5139
Frequency Shift (MHz)	1	1
Half Angle (Degrees)	3.1	3.1
Focal Length (mm)	762	762
Beam Spacing (mm)	82.5	82.5
Wavelength (Nanometers)	514.5	488.0
Rotation x-y Plane (Degrees)		0.0
Tilt y-z Plane (Degrees)		0.0

Table 11. PHASE Checkout Optics Configuration

Application	Turbo Machinery
RMR Mode of Operation	Phase Lock Loop (PLL)
Lock Detect Sensitivity	± 192 minutes
Encoder Pluses per Revolution	3600
Resolver Pulsed per Revolution	3600
Number of Sectors	50
Number of Windows	1 or 50
Window Width (points)	72
Delay to First Sector	0
Sector with Window Number 1	1

Table 12. PHASE Checkout Rotary Encoder Setup

Additional Setup Notes:

Laser: Power 0.5W
Seeding: 6 jets, 40 psi, 40%
Probe Volume: Forward Center Position

Typical Data Rates:

Green: 80-100
Blue: 120
Coincidence: 80

2. Data Run Menus (5000 RPM)

I/O Port Selection:	
Traverse Controller	COM 1
Sony Position Enc.	COM 2
Printer Port	LPT 1
Proc./RMR I/O Port	COM 1
Color Link	Off

Hardware Selection:	
First Processor	IFA750
Second Processor	IFA750
Third Processor	NA
Master Interface	MI750
Rotary Encoder Type	1989

Table 13. PHASE I/O Port and Processor Selection

IFA 750 Operation Parameters	Manual Override
Number of Processors	2
Number of K-Data Points	20
Data Sampling Method	TBD on
Coincidence Window Width (μsec)	1E0
DMA Time-out	999 Sec
Acquisition Mode	Coincidence
Sampling Time (μsec)	100
Automatic Filter Selections	**5-30 MHz** **3-20 MHz**
Number of C-Words	0
Single Measurement/Burst	Off
Transit Time Enable	Off
Minimum Threshold	30

Table 14. PHASE Processor Settings

Minimum Cycles/Burst	4
Signal to Noise Ratio	Very Low
Threshold Optimization	Off

Table 15. PHASE Manual Override Settings

125

	Processor 1	Processor 2
Fringe Spacing (Microns)	4.7591	4.5139
Frequency Shift (MHz)	**-10**	1
Half Angle (Degrees)	3.1	3.1
Focal Length (mm)	762	762
Beam Spacing (mm)	82.5	82.5
Wavelength (Nanometers)	514.5	488.0
Rotation x-y Plane (Degrees)		0.0
Tilt y-z Plane (Degrees)		0.0

Table 16. PHASE Optics Configuration

Application	Turbo Machinery
RMR Mode of Operation	Phase Lock Loop (PLL)
Lock Detect Sensitivity	$\pm$192 minutes
Encoder Pluses per Revolution	3600
Resolver Pulsed per Revolution	3600
Number of Sectors	50
Number of Windows	1 or 50
Window Width (points)	72 or as required[1]
Delay to First Sector	0 or as required[1]
Sector with Window Number 1	1

Table 17. PHASE Rotary Encoder Setup

Additional Setup notes:
Laser Power: 0.50W
Seeding: 6 jets, 60 psi, 40%
Probe Volume: As Required

1.

Probe Position	Width	Delay
Aft Inner (ai)	32	27
Aft Center (ac)	25	32
Aft Outer (ao)	25	35
Center Inner (ci)	20	70
Center Center (cc)	20	70
Center Outer	25	70
Forward (All)	72	0

126

APPENDIX F.   TTR DATA

Data Run	Tar	Cal	P2	P3	P4	vena(in-H2O)
	2/12/99					
02129fc.c01	-6.31267	135.115	121.950	121.637	12.973	138.827
	2/17/99					
02179fc.c01	-4.132	135.216	124.661	124.699	15.213	141.734
	3/5/99					
03059fo.c02	-5.83633	135.698	124.664	124.726	14.109	143.158
03059fc.c02	-7.18033	135.666	122.876	123.153	12.830	141.841
03059fi.c01	-7.722	135.684	122.437	122.404	12.155	140.759
03059ac.c01	-8.95367	135.630	122.049	121.739	11.068	140.866
03059ac.c02	-9.904	135.608	120.822	120.625	10.047	139.144
03059ao.c01	-10.9807	135.553	119.547	119.295	8.943	138.996
03059ao.c02	-11.9187	135.578	118.458	118.445	7.939	136.933
03059ai.c01	-12.7283	135.541	117.722	117.662	7.142	137.140
03059ai.c02	-13.2587	135.495	117.136	117.229	6.623	136.565
03059cc.c01	-13.8397	135.459	117.323	116.980	6.149	135.550
03059cc.c02	-14.2917	135.456	117.102	116.934	5.770	135.669
03059co.c01	-14.5507	135.431	116.457	116.442	5.392	135.229
	3/24/99					
03249fc.c01	1.279	135.166	131.920	132.027	21.268	149.303
03249cc.c01	-6.20467	135.093	124.901	124.842	13.752	143.422
03249cc.c02	-8.657	135.082	122.182	121.899	11.247	140.482
03249ci.c01	-10.6163	135.079	119.350	119.542	9.231	138.084

Table 18. TTR Data (1 of 3)

Data Run	Ref Temp (deg-C)	TT2 (deg-R)	TT3	TT4
02129fc.c01	22.90	561.99	561.30	539.74
02179fc.c01	25.36	564.62	563.55	542.15
03059fo.c02	23.79	564.10	563.53	541.59
03059fc.c02	23.93	561.83	563.72	541.97
03059fi.c01	23.97	561.78	563.84	541.80
03059ac.c01	24.08	562.89	564.12	542.09
03059ac.c02	24.16	562.87	564.28	542.35
03059ao.c01	24.23	564.01	564.36	542.43
03059ao.c02	24.32	563.98	564.33	542.28
03059ai.c01	24.37	564.34	564.77	542.56
03059ai.c02	24.45	563.89	564.52	542.45
03059cc.c01	24.54	564.23	564.68	542.36
03059cc.c02	24.60	564.40	564.72	542.48
03059co.c01	24.65	564.82	565.12	542.70
03249fc.c01	23.07	561.88	561.68	538.73
03249cc.c01	25.05	566.62	566.50	543.61
03249cc.c02	25.49	566.71	566.08	543.90
03249ci.c01	25.81	567.18	566.35	544.36

Table 19. TTR Data (2 of 3)

127

Data Run	Water Inlet	Water Outlet	Orifice Temp	RPM	GPM	Tq (in-lbs)	radial pos	swirl angle	throttle pos	atm press
02129fc.c01	539.9	549.0	572.50	5019.1	13.10	285.66	3.39	5.19	4.6371	30.15
02179fc.c01	539.1	548.1	573.66	5028.4	13.02	284.05	3.67	58.54	4.6371	30.09
03059fo.c02	540.7	549.4	571.68	5061.5	13.84	288.55	5.91	34.54	4.6371	30.03
03059fc.c02	541.0	549.7	572.09	5063.9	13.78	289.17	5.86	33.66	4.6371	30.03
03059fi.c01	540.9	549.5	572.08	5056.3	13.74	288.80	6.00	34.01	4.6371	30.03
03059ac.c01	541.9	550.7	572.81	5069.0	13.79	289.09	5.86	33.84	4.6371	30.03
03059ac.c02	541.9	550.6	572.99	5066.7	13.73	289.18	5.76	32.96	4.6371	30.00
03059ao.c01	541.4	550.2	572.78	5065.6	13.68	289.54	5.62	32.08	4.6371	30.00
03059ao.c02	540.8	549.5	572.33	5059.7	13.66	288.43	5.48	32.78	4.6371	30.00
03059ai.c01	542.7	551.4	573.71	5073.6	13.67	289.86	5.53	33.66	4.6371	30.00
03059ai.c02	541.2	549.9	572.60	5069.7	13.62	289.98	5.44	30.41	4.6371	30.00
03059cc.c01	541.2	550.0	572.54	5070.3	13.66	289.98	5.47	32.34	4.6371	30.00
03059cc.c02	541.3	550.2	572.84	5077.3	13.65	290.78	5.39	32.96	4.6371	30.00
03059co.c01	542.4	551.3	573.74	5076.7	13.62	289.45	5.35	32.17	4.6371	29.95
03249fc.c01	540.1	548.6	572.28	5057.9	14.09	288.63	5.34	38.06	4.6371	29.87
03249cc.c01	542.9	551.6	574.48	5059.6	14.01	290.09	4.61	30.15	4.6371	29.87
03249cc.c02	542.7	551.3	574.75	5058.0	13.96	289.78	4.70	27.25	4.6371	29.87
03249ci.c01	542.3	550.8	574.93	5049.9	13.98	287.84	4.59	24.79	4.6371	29.87

Table 20. TTR Data (3 of 3)

APPENDIX G.   SSME DATA

Data Run	Press Ratio	Mass Flow	Efficiency	Ref RPM	Mass Flow Vena	Ref HP	Ref Press Ratio
	2/12/99						
02129fc.c01	1.31278648	2.876	52.127	4823.346	2.263	16.533	1.322
	2/17/99						
02179fc.c01	1.31581495	2.722	51.544	4821.891	2.146	16.432	1.323
	3/5/99						
03059fo.c02	1.32057242	2.933	51.606	4854.826	2.308	16.778	1.325
03059fc.c02	1.31994656	2.758	48.486	4861.566	2.169	16.844	1.324
03059fi.c01	1.31939383	2.957	49.040	4854.119	2.327	16.804	1.324
03059ac.c01	1.32087169	2.936	49.726	4863.328	2.309	16.835	1.325
03059ac.c02	1.32075219	2.934	49.299	4860.754	2.310	16.849	1.324
03059ao.c01	1.32015887	2.987	50.539	4857.065	2.354	16.865	1.323
03059ao.c02	1.32028302	2.889	50.797	4851.623	2.277	16.779	1.323
03059ai.c01	1.32036737	2.881	51.029	4863.209	2.271	16.901	1.323
03059ai.c02	1.32067129	2.788	50.485	4860.981	2.197	16.898	1.324
03059cc.c01	1.32143113	2.925	51.138	4860.415	2.304	16.885	1.324
03059cc.c02	1.32240142	2.877	50.960	4866.718	2.265	16.941	1.325
03059co.c01	1.32235392	2.937	51.384	4864.414	2.317	16.884	1.323
	3/24/99						
03249fc.c01	1.3227426	2.882	53.418	4860.135	2.272	16.863	1.320
03249cc.c01	1.32359507	2.784	52.626	4841.198	2.203	16.873	1.321
03249cc.c02	1.32238942	2.781	51.761	4840.365	2.202	16.868	1.319
03249ci.c01	1.32137556	2.862	51.656	4831.053	2.269	16.735	1.318

Table 21. SSME Data (1of 2)

Data Run	Ref Temp ratio	HP	HP	HP
02129fc.c01	1.0406	23.275	22.749	21.387
02179fc.c01	1.0428	23.048	22.663	20.269
03059fo.c02	1.0426	23.589	23.174	22.131
03059fc.c02	1.0416	23.461	23.234	19.484
03059fi.c01	1.0417	23.437	23.169	21.101
03059ac.c01	1.0423	23.780	23.251	21.351
03059ac.c02	1.0424	23.549	23.247	21.147
03059ao.c01	1.0429	23.490	23.271	22.062
03059ao.c02	1.0429	23.437	23.155	21.455
03059ai.c01	1.0433	23.511	23.334	21.514
03059ai.c02	1.0429	23.371	23.326	20.602
03059cc.c01	1.0432	23.816	23.328	21.943
03059cc.c02	1.0433	23.757	23.425	21.570
03059co.c01	1.0436	23.766	23.316	22.214
03249fc.c01	1.0407	23.626	23.163	22.555
03249cc.c01	1.0451	23.839	23.288	21.693
03249cc.c02	1.0450	23.703	23.256	21.243
03249ci.c01	1.0453	23.386	23.063	21.777

Table 22. SSME Data (2 of 2)

129

APPENDIX H. LDV MEASUREMENT DATA

SSMEHPFTP 1st Stage Rotor LDV Data				TEST CONDITIONS:		Cp:	0.24
Data File: 03059fo.r02				Axial Position: -.16ct		V_t(m/sec):	793.4
Reduced File: 03059fo.c02				Span Position: 98%			
				N_ref:	4855		
				T_t:	563.8		

Theta	U-mean	V-mean	U-turb	V-turb	Alpha	Cuv
0.1	121.6	51.01	15.82	26.48	22.756	0.5198
0.3	121.34	51.42	15.45	25.84	22.964	0.50375
0.5	119	49.31	16.22	28.15	22.507	0.5166
0.7	114.39	48.05	16.77	29.86	22.786	0.49265
0.9	112.09	46.16	17.6	30.63	22.382	0.51376
1.1	110.34	45.81	18.36	31.37	22.549	0.41809
1.3	109.37	44.64	18.05	30.2	22.206	0.42199
1.5	110.06	44.37	18.62	29.66	21.956	0.38759
1.7	109.44	43.78	18.95	31.96	21.803	0.39165
1.9	109.76	42.62	19.09	30.25	21.221	0.35087
2.1	111.73	42.21	19.7	32.32	20.694	0.35056
2.3	114.57	42.12	19.54	30.26	20.184	0.33939
2.5	118.33	43.54	18.66	30.62	20.199	0.27928
2.7	122.12	44.03	17.38	29.28	19.828	0.33672
2.9	125.53	45.18	15.83	28.74	19.796	0.27049
3.1	129.31	45.25	14.89	27.83	19.288	0.28613
3.3	133.32	47.08	11.3	24.35	19.45	0.08748
3.5	134.63	47.62	12.18	23.57	19.479	0.12671
3.7	136.34	48.58	10.91	23.5	19.611	-0.03709
3.9	136.85	49.82	9.92	21.81	20.004	0.0534
4.1	138.21	51.73	9.07	19.56	20.522	-0.07282
4.3	137.65	52.12	10.05	20.67	20.737	-0.00682
4.5	136.51	53.02	9.61	20.81	21.226	-0.06336
4.7	137.23	54.37	8.41	19.45	21.613	-0.02297
4.9	134.53	53.92	10.24	19.83	21.84	0.11208
5.1	134.52	56.21	9.58	18.93	22.679	-0.00334
5.3	133.63	55.9	9.68	18.91	22.699	0.0708
5.5	133.06	55.49	10.31	19.23	22.637	0.19373
5.7	132.43	56.51	10.15	20.18	23.109	0.25063
5.9	132.58	56.41	10	20.33	23.048	0.20276
6.1	132.11	56.71	10.59	19.55	23.232	0.22371
6.3	131.25	56.33	11.24	19.97	23.227	0.34622
6.5	129.83	55.01	12.53	21.93	22.963	0.46626
6.7	130.17	55.66	11.86	20.57	23.152	0.38846
6.9	127.85	54.88	13.57	21.71	23.231	0.40989
7.1	125.78	53.91	14.49	23.62	23.202	0.45329

Table 23. LDV Data: (03059fo.c02)

131

SSMEHPFTP 1st Stage Rotor LDV Data		TEST CONDITIONS:			Cp:	0.24

Data File: 03059fc.r02
Reduced File: 03059fc.c02

TEST CONDITIONS:
Axial Position: -.16ct
Span Position: 93%
N_ref: 4862
T_t: 562.8

Cp: 0.24
V_t(m/sec): 792.7

Theta	U-mean	V-mean	U-turb	V-turb	Alpha	Cuv
0.1	125.81	55.52	10.81	18.47	23.81	0.29988
0.3	125.19	55.29	11.05	19.84	23.829	0.27245
0.5	125.19	56.11	10.85	20.39	24.143	0.28952
0.7	123.57	55.09	11.6	21.49	24.03	0.29669
0.9	122.96	54.73	12.37	22.3	23.994	0.29218
1.1	121.74	54.66	12.35	22.18	24.18	0.34111
1.3	120.02	54.28	12.78	24.09	24.334	0.30511
1.5	118.38	53.43	14.42	25.43	24.293	0.42258
1.7	118.01	52.44	15.08	26.97	23.96	0.43339
1.9	117.94	52.07	15.35	28.04	23.821	0.4297
2.1	118.12	54.28	16.07	25.67	24.679	0.38289
2.3	117.91	52.37	17.53	28.35	23.95	0.48533
2.5	119.23	53.15	16.47	26.76	24.028	0.43811
2.7	123.43	54.89	16.12	23.65	23.976	0.41037
2.9	123.12	56.36	17.23	24.09	24.598	0.39592
3.1	125.4	56.62	15.59	22.79	24.299	0.36971
3.3	127.68	57.72	14.94	20.69	24.326	0.35062
3.5	128.3	57.82	14.69	21	24.259	0.29907
3.7	129.91	58.08	13.77	18.87	24.087	0.24323
3.9	133.65	59.56	13.19	18.73	24.02	0.18621
4.1	136.01	59.44	11.4	18.7	23.609	0.17005
4.3	137.45	60.16	11.14	16.98	23.639	0.11617
4.5	139.14	60.09	10.14	17.76	23.359	-0.00701
4.7	139.39	58.59	10.32	17.38	22.798	0.13497
4.9	138.68	59.13	9.66	16.87	23.094	0.0738
5.1	139.4	57.74	9.42	18.4	22.499	-0.13357
5.3	138.12	56.26	8.98	19.31	22.163	-0.03038
5.5	136.53	54.58	8.97	20.49	21.789	-0.02547
5.7	135.28	55.31	9.58	19.66	22.237	-0.0616
5.9	134.42	54.63	9.16	19.7	22.117	0.07459
6.1	133.04	56.01	9.54	17.94	22.831	0.10574
6.3	132.84	55.91	9.02	18.46	22.826	-0.01026
6.5	130.45	56.25	10.31	18.25	23.325	0.15043
6.7	129.67	55.08	10.26	17.59	23.013	0.09099
6.9	128.36	55.27	10.41	18.75	23.296	0.23204
7.1	127.27	55.22	10.77	19.28	23.454	0.25541

Table 24. LDV Data: (03059fc.c02)

SSMEHPFTP 1st Stage Rotor LDV Data		TEST CONDITIONS:			Cp:	0.24

Data File: 03249fc.r01
Reduced File: 03249fc.c01

TEST CONDITIONS:
Axial Position: -.16ct
Span Position: 93%
N_ref: 4860
T_t: 561.8

Cp: 0.24
V_t(m/sec):   792.0

Theta	U-mean	V-mean	U-turb	V-turb	Alpha	Cuv
0.1	128.29	58.24	9.85	16.88	24.418	0.22926
0.3	127.95	58.56	10.5	18.49	24.593	0.12057
0.5	126.08	58.2	11.06	19.14	24.778	0.31027
0.7	124.75	57.29	11.66	20.7	24.668	0.34513
0.9	123.8	57.45	12	20.06	24.894	0.29538
1.1	122.9	57.27	12.35	21.94	24.985	0.32264
1.3	121.45	56.79	12.79	22.84	25.059	0.37165
1.5	119.12	56.18	12.86	22.16	25.249	0.34634
1.7	117.59	55.04	14.12	25.42	25.084	0.36691
1.9	119.51	56.08	13.85	25.73	25.138	0.418
2.1	116.7	54.09	14.91	27.9	24.866	0.43411
2.3	118	54.59	15.06	26.93	24.827	0.49221
2.5	118.27	56.1	16.89	26.06	25.377	0.46557
2.7	120.12	57.67	15.8	24.42	25.646	0.42004
2.9	122.23	58.35	15.3	23.3	25.517	0.33161
3.1	125.1	59.17	14.57	21.72	25.314	0.32909
3.3	126.42	59.82	14.83	21.42	25.323	0.25125
3.5	128.51	60.95	13.61	19.52	25.373	0.24981
3.7	129.81	60.03	13.81	19.1	24.82	0.24326
3.9	130.79	61.63	13.3	19.87	25.232	0.22794
4.1	133.5	62.08	12.17	17.45	24.94	0.16726
4.3	136.34	61.65	11.27	17.9	24.33	0.10266
4.5	137.98	62.5	10.08	17	24.37	0.01649
4.7	138.75	62.18	9.22	18.02	24.14	0.04901
4.9	139.88	61.38	8.88	17.15	23.691	0.04752
5.1	139.76	58.61	8.6	18.71	22.752	0.01082
5.3	139.55	58.23	8.1	18.7	22.651	-0.04032
5.5	138.25	57.38	8.61	17.71	22.542	-0.13925
5.7	137.54	56.43	8.06	18.11	22.308	-0.05887
5.9	135.66	56.63	8.39	17.83	22.659	-0.06861
6.1	134.85	56.19	8.79	18.75	22.621	0.0455
6.3	134.3	57.49	8.65	18.75	23.173	0.02327
6.5	132.27	57.01	9.18	17.38	23.318	0.07162
6.7	131.07	56.8	9.32	18.67	23.429	0.1533
6.9	130.1	57.69	9.74	17.74	23.914	0.16081
7.1	130.07	58.14	9.82	16.05	24.085	0.07916

Table 25. LDV Data: (03059fc.c01)

SSMEHPFTP 1st Stage Rotor LDV Data		TEST CONDITIONS:			Cp:	0.24

Data File: 03059fi.r01

Reduced File: 03059fi.c01

TEST CONDITIONS:

Axial Position: -.16ct

Span Position: 88%

N_ref: 4854

T_t: 562.8

Cp: 0.24

V_t(m/sec): 792.7

Theta	U-mean	V-mean	U-turb	V-turb	Alpha	Cuv
0.1	129.35	64.61	7.66	15.54	26.543	-0.03934
0.3	128.83	65.55	8.06	15.57	26.967	0.0881
0.5	128.69	66	8.36	16.21	27.154	0.11034
0.7	128.71	65.74	7.81	16.41	27.055	0.04433
0.9	128.57	67.42	7.76	15.4	27.672	0.08151
1.1	127.94	67.23	8.66	16.63	27.719	0.1784
1.3	128.55	67.17	8.61	16.91	27.587	0.19095
1.5	127.76	67.25	8.68	16.45	27.762	0.15804
1.7	127.79	68.01	9.5	17.28	28.023	0.28022
1.9	127.34	68.2	9.86	17.34	28.173	0.26254
2.1	127.11	67.96	9.66	17.44	28.133	0.33125
2.3	126.82	68.38	10.54	17.25	28.331	0.30716
2.5	127.56	69.49	10.48	16.89	28.581	0.29731
2.7	128.77	70.42	10.28	17.04	28.672	0.2955
2.9	128.5	71.14	10.51	17.2	28.968	0.3212
3.1	130.64	72.19	10.81	16.72	28.924	0.30041
3.3	132.33	72.11	10.67	16.89	28.585	0.28461
3.5	133.26	72.19	10.51	17.48	28.445	0.26403
3.7	135.28	73.83	8.74	14.59	28.623	0.11402
3.9	137.22	73.27	10.02	16.35	28.102	0.20158
4.1	137.47	72.8	9.22	16.88	27.903	0.14113
4.3	140.24	72.01	8.19	15.81	27.181	0.11303
4.5	141.63	70.39	8.05	17.09	26.427	0.13782
4.7	141.09	68.37	7.85	18.65	25.855	0.09222
4.9	141.25	66.23	8.55	19.52	25.121	0.14606
5.1	138.96	64.46	8.47	18.09	24.888	0.00918
5.3	138.72	63.82	7.99	18.88	24.706	0.06599
5.5	138.21	60.34	8.29	19.53	23.584	0.05688
5.7	135.87	61.84	8.74	18.43	24.474	-0.11739
5.9	134.27	61.46	8.34	15.31	24.595	-0.14373
6.1	133.06	61.42	8.88	17	24.776	-0.08649
6.3	133.48	61.52	8.55	17.78	24.744	-0.03716
6.5	132.08	62.19	8.6	16.57	25.215	-0.04907
6.7	130.38	63.63	7.96	15.34	26.013	-0.04692
6.9	131.29	63.77	8	16.9	25.908	-0.0587
7.1	130.64	63.89	7.72	15.69	26.062	-0.07148

Table 26. LDV Data: (03059fi.c01)

SSMEHPFTP 1st Stage Rotor LDV Data				TEST CONDITIONS:			Cp:	0.24

Data File: 03059co.r01
Reduced File: 03059co.c01

				Axial Position: .35 ct			V_t(m/sec):	794.3
				Span Position: 98%			Window	
				N_ref:	4864		Width:	2.5
				T_t:	565		Delay:	7.0

Theta(meas)	U-mean	V-mean	U-turb	V-turb	Alpha(meas)	Cuv
0.1	97.65	66.61	12.32	26.71	34.3	0.14404
0.3	103.04	69.74	17.97	21.02	34.09	-7.8696
0.5	98.28	62.32	25.3	25.28	32.378	0.20164
0.7	91	64.31	16.41	12.78	35.248	0.5698
0.9	97.05	63.39	20.13	22.87	33.151	-0.08506
1.1	96.59	62.2	17.76	25.6	32.779	0.63745
1.3	98.41	60.69	17.4	26.49	31.663	0.20779
1.5	112.98	65.74	21.02	19.16	30.195	-0.1538
1.7	101.46	57.57	24.44	25.07	29.571	0.03538
1.9	101.35	63.06	23.44	19.8	31.888	0.13534
2.1	101.57	61.83	24.55	22.84	31.333	0.37425
2.3	104.45	60.61	25.27	21.85	30.126	-0.24094
2.5	109.27	61.99	22.14	26.16	29.568	0.00063

Table 27. LDV Data: (03059co.c01)

SSMEHPFTP 1st Stage Rotor LDV Data				TEST CONDITIONS:			Cp:	0.24

Data File: 03059cc.r01
Reduced File: 03059cc.c01

				Axial Position: .35 ct			V_t(m/sec):	793.9
				Span Position: 93%			Window	
				N_ref:	4860		Width:	2.0
				T_t:	564.5		Delay:	7.0

Theta(meas)	U-mean	V-mean	U-turb	V-turb	Alpha(meas)	Cuv
0.1	92.41	64.23	6.89	13.3	34.802	-0.3831
0.3	85.84	68.08	11.8	14.68	38.42	********
0.5	79.69	63.86	4.82	12.41	38.709	0.70844
0.7	82.67	68.82	6.85	11.07	39.778	-0.08489
0.9	81.85	69.5	8.43	8.94	40.333	0.53123
1.1	77.31	67.02	4.06	11.6	40.922	0.57089
1.3	89.46	76.57	8.66	11.82	40.559	0.51821
1.5	85.13	69.21	11.18	19.13	39.11	0.49053
1.7	89.34	68.74	14.76	24.77	37.574	0.35166
1.9	101.85	67.64	24.94	18.98	33.59	0.23982

Table 28. LDV Data: (03059cc.c01)

	SSMEHPFTP 1st Stage Rotor LDV Data		TEST CONDITIONS:			Cp:	0.24

SSMEHPFTP 1st Stage Rotor LDV Data

Data File: 03059cc.r02

Reduced File: 03059cc.c02

TEST CONDITIONS:

Axial Position: .35 ct

Span Position: 93%

N_ref: 4867

T_t: 564.6

Cp: 0.24

V_t(m/sec): 794.0

Window

Width: 2.0

Delay: 7.0

Theta(meas)	U-mean	V-mean	U-turb	V-turb	Alpha(meas)	Cuv
0.1	82.36	54.29	11.13	14.56	33.39	0.97003
0.3	82.49	61.79	12.92	18.17	36.838	********
0.5	85.17	71.61	8.25	9.82	40.057	0.45243
0.7	87.91	63.34	12.98	22.71	35.774	0.70112
0.9	92.89	64.87	30.42	14.63	34.927	-0.06632
1.1	89.18	59.45	14.03	25.68	33.689	0.71292
1.3	78.09	67.75	11.67	21.87	40.944	0.78057
1.5	78.92	66.94	5.57	8.87	40.305	0.45082
1.7	96.49	71.45	17.91	18.2	36.518	0.3593
1.9	83.1	77.88	15.11	18.92	43.144	0.93605
2.1	96.58	66.56	10.57	21.94	34.572	0.04758
2.3	85.88	60.85	18.25	18.83	35.32	0.22057
2.5	91.57	65.83	28.82	14.75	35.712	0.60258
2.7	79.8	60.01	24.17	24.68	36.946	0.08063
2.9	72.93	65.38	13.83	18.81	41.875	0.55812
3.1	83.62	61.01	31.12	18.59	36.115	-0.58314
3.3	86.76	60.9	29.61	8.73	35.066	0.06123
3.5	68.66	58.92	0.85	10.04	40.633	-0.30919
3.7	91.8	56.67	30.13	18.53	31.689	-0.5743
3.9	74.38	64.56	23.34	15.24	40.96	0.0361
4.1	74.81	58.05	28.9	10.54	37.811	0.27546
4.3	70.83	56.45	16.63	13.69	38.556	-0.24498
4.5	68.36	61.66	0.88	13.86	42.047	0.05851
4.7	69.81	63.87	9.49	15.34	42.458	-0.28863
4.9	72.39	59.17	15.97	18.06	39.264	-0.54002
5.1	75.15	60.8	20.87	14.37	38.975	0.0004
5.3	69.97	62.65	9.39	14.24	41.841	0.17433
5.5	73.13	59.97	10.8	10.62	39.355	0.31894
5.7	73.35	61.88	10.4	14.27	40.154	0.10525
5.9	75.57	61.56	24.08	14.66	39.168	0.10639
6.1	77.51	64.43	14.04	14.38	39.736	-0.28994
6.3	77.29	59.25	10.32	11.63	37.475	0.01237
6.5	76.72	58.96	13.16	19.84	37.541	0.02956
6.7	80.88	58.25	11.5'	12.08	35.76	0.23884
6.9	82.68	61.99	10.73	10.03	36.863	-0.04989
7.1	80.25	61.08	8.48	12.43	37.275	0.49612

Table 29. LDV Data: (03059cc.c02)

SSMEHPFTP 1st Stage Rotor LDV Data	TEST CONDITIONS:	Cp:	0.24

Data File: 03249cc.r01
Reduced File: 03249cc.c01

TEST CONDITIONS:
Axial Position: .35 ct
Span Position: 93%
N_ref: 4841
T_t: 566.6

Cp: 0.24
V_t(m/sec):   795.4
Window
Width: 2.0
Delay: 7.0

Theta(meas)	U-mean	V-mean	U-turb	V-turb	Alpha(meas)	Cuv
0.1	87.09	66.63	14.59	14.67	37.419	********
0.3	82.61	66.83	12.16	20.57	38.973	0.69495
0.5	80.67	68.99	9.76	11.76	40.538	0.32784
0.7	82.28	71.12	6.3	11.75	40.838	0.25419
0.9	80.65	69.9	10.05	15.92	40.918	0.80771
1.1	90.56	74.74	14.12	19.14	39.532	0.37315
1.3	88.68	82.31	8.43	7.63	42.868	-0.60099
1.5	89.09	76.74	15.13	14.42	40.74	0.54132
1.7	87.45	72.05	17.92	21.32	39.486	0.78786
1.9	75.2	70.9	12.33	19.8	43.314	0.67309
2.1	81.75	67.55	19.53	29.81	39.566	0.85378
2.3	76.37	65.17	17.05	16.29	40.477	0.76802
2.5	81.31	66.56	27.67	19.56	39.307	0.34802
2.7	82.06	64.15	28.9	17.38	38.014	0.2367
2.9	74.66	62.42	19.63	10.1	39.895	0.43702
3.1	92.04	67.08	29	12.02	36.088	0.19196
3.3	79.14	62.1	30.57	18.99	38.12	-0.22925
3.5	72.29	59.37	15.23	19.28	39.395	-0.32498
3.7	84.12	63.18	31.65	14.76	36.909	0.242
3.9	69.83	60.52	15.37	13.5	40.914	-0.2834
4.1	76	60.26	29.74	17.12	38.407	-0.03822
4.3	70.63	61.23	18.79	14.94	40.921	-0.16009
4.5	71.06	59.3	19.26	14.28	39.848	-0.01146
4.7	82.82	60.21	33.77	13.76	36.019	-0.17848
4.9	76.07	57.54	26.45	21.37	37.105	-0.22977
5.1	70.24	60.99	10.66	13.64	40.966	-0.40828
5.3	74.03	61.99	23.45	15.08	39.942	0.09925
5.5	78.36	61.47	30.46	13.74	38.111	-0.16664
5.7	75.23	60.18	22.32	17.41	38.66	-0.03636
5.9	71.66	60.02	11.29	14.13	39.95	0.25336
6.1	74.64	60.48	18.3	14.61	39.015	0.34312
6.3	76.86	60.23	20.63	12.11	38.084	-0.24299
6.5	88.32	61.58	27.64	12.67	34.886	0.17726
6.7	82.82	62.03	25.94	20.34	36.831	0.16578
6.9	85.69	62.12	16.7	16.07	35.939	0.08974
7.1	83.28	63.46	17.11	17.45	37.309	0.58689

Table 30. LDV Data: (03249cc.c01)

SSMEHPFTP 1st Stage Rotor LDV Data			TEST CONDITIONS:			Cp:	0.24
Data File: 03249cc.r02			Axial Position: .35 ct			V_t(m/sec):	795.2
Reduced File: 03249cc.c02			Span Position: 93%			Window	
			N_ref:	4840		Width:	2.0
			T_t:	566.4		Delay:	7.0

Theta(meas)	U-mean	V-mean	U-turb	V-turb	Alpha(meas)	Cuv
0.1	79.64	66.91	8.77	21.19	40.033	0.65339
0.3	87.75	69.44	13.68	11.47	38.355	********
0.5	83.86	67.28	10.98	17.68	38.739	0.13
0.7	85.78	69.07	12.76	13.64	38.842	0.63124
0.9	91.99	74.34	19.03	9.83	38.942	0.39373
1.1	85.89	69.48	16.75	14.66	38.971	-0.08115
1.3	95.09	78.6	10.75	15.25	39.576	0.36667
1.5	94.74	74.37	16.93	12.31	38.13	-0.11598
1.7	86.46	74.46	14.45	20	40.735	0.74054
1.9	88.54	68.57	13.22	22.31	37.756	0.24888

Table 31. LDV Data: (03249cc.c02)

SSMEHPFTP 1st Stage Rotor LDV Data			TEST CONDITIONS:		Cp:	0.24
Data File: 03249ci.r01			Axial Position: .35 ct		V_t(m/sec):	795.5
Reduced File: 03249ci.c01			Span Position: 88%		Window	
			N_ref: 4831		Width:	2.0
			T_t: 566.8		Delay:	7.0

Theta(meas)	U-mean	V-mean	U-turb	V-turb	Alpha(meas)	Cuv
0.1	92.18	62.03	29.66	25.36	33.94	-0.10325
0.3	100.29	65.43	26.52	13.88	33.119	0.03697
0.5	107.4	65.66	23.98	21.62	31.439	-0.26095
0.7	100.34	73.6	25.46	18.44	36.261	-0.50779
0.9	80.7	72.26	13.48	19.16	41.842	0.77755
1.1	87.24	81.75	4.62	9.59	43.14	0.61318
1.3	84.78	88.67	6.5	5.64	46.284	0.93924
1.5	94	81.43	17.98	12.18	40.901	-0.44745
1.7	115.95	75.87	22	22.13	33.196	-0.84319
1.9	119.66	65.61	19.24	22.48	28.737	-0.77315
2.1	133.79	63.02	12.33	13.21	25.223	-0.31303
2.3	130.36	58.65	11.22	25.72	24.225	-0.45206
2.5	130.49	61.01	11.26	21.23	25.057	-0.45679
2.7	135.78	61.66	8.52	17.43	24.425	-0.44425
2.9	136.48	60.23	4.45	14.92	23.812	0.05577
3.1	136.08	59.77	6.61	16.78	23.711	-0.32856
3.3	138.2	62.4	6.08	14.36	24.298	0.23378
3.5	136.07	59.85	6.59	15.82	23.741	0.04643
3.7	133.8	61.87	11.68	13.6	24.815	-0.05685
3.9	131.68	61.01	15.05	14.65	24.861	-0.14756
4.1	133.77	60.27	11.11	15.53	24.254	0.18253
4.3	131.47	59.24	14.77	15.25	24.256	0.04644
4.5	131.92	60.6	15.65	13.5	24.673	-0.04874
4.7	129.99	61.17	17.38	14.29	25.199	0.17246
4.9	125.58	58.92	19.59	15.42	25.136	-0.07092
5.1	120.9	60.19	23.72	15.08	26.467	-0.07601
5.3	118.78	61.46	25.38	14.26	27.358	-0.07307
5.5	121.32	61.47	24.14	14.14	26.871	0.11315
5.7	120.58	59.55	24.5	13.37	26.282	0.03803
5.9	116.26	59.69	27.69	13.95	27.175	-0.03024
6.1	106.13	59.78	31.24	16.63	29.391	0.15438
6.3	105.32	60.95	33.59	14.36	30.06	0.08558
6.5	109.59	60.49	30.26	15.69	28.895	-0.0085
6.7	112.7	60.19	28.81	16.04	28.107	0.01441
6.9	108.77	61.58	28.96	14.56	29.516	-0.16648
7.1	100.58	65.46	29.31	20.87	33.056	-0.42596

Table 32. LDV Data: (03249ci.c01)

139

SSMEHPFTP 1st Stage Rotor LDV Data			TEST CONDITIONS:			Cp:	0.24
Data File: 03059ao.r01			Axial Position: .84 ct			V_t(m/sec):	793.7
Reduced File: 03059ao.c01			Span Position: 98%			Window	
			N_ref:	4857		Width:	7.2
			T_t:	564.2		Delay:	3.5

Theta(meas)	U-mean	V-mean	U-turb	V-turb	Alpha(meas)	Cuv
0.1	116.13	30.15	12.98	44.09	14.553	0.33649
0.3	128.01	68.3	21.37	22.4	28.081	0.51115
0.5	128.63	65.91	15.07	39.12	27.13	0.20038
0.7	122.72	44.39	11.93	72.24	19.887	0.2429
0.9	130.61	63.66	17.57	32.34	25.984	0.36337
1.1	119.54	63.47	17.96	42.76	27.967	-0.19953
1.3	132.35	50.38	18.14	57.56	20.839	0.74377
1.5	120.11	54.14	19.34	39.83	24.263	0.12457
1.7	132.22	50.45	14.48	44.67	20.886	0.1208
1.9	111.86	48.56	23	47.26	23.468	0.03149
2.1	125.59	56.15	14.33	36.64	24.089	0.03572
2.3	127	51.26	15.52	38.17	21.979	0.37614
2.5	119.3	52.22	18.69	36.17	23.639	0.2991
2.7	120.83	50.31	21.33	33.34	22.607	0.14344
2.9	122.54	57.56	17.91	31.59	25.161	-0.19741
3.1	130.94	57.94	10.33	24.63	23.869	0.50701
3.3	127.85	58.61	15.81	15.95	24.628	0.20441
3.5	124.23	58.77	19.21	23.33	25.319	-0.00068
3.7	122.56	58.85	22.09	17.34	25.649	0.12425
3.9	123.57	59.97	20.41	20.75	25.888	0.26657
4.1	124.93	59.5	20.27	18.42	25.469	0.00153
4.3	125.98	60.7	21.34	16.61	25.724	0.07482
4.5	124.28	60.91	21.52	16.92	26.11	-0.09478
4.7	124.45	59.64	20.83	16.19	25.607	-0.03661
4.9	127.16	61.04	20.1	15.18	25.642	0.06166
5.1	125.81	60.65	21.27	14.1	25.738	-0.06994
5.3	122.28	61.01	22.85	14.35	26.515	-0.11759
5.5	118.03	62.15	26.67	16.86	27.769	-0.07071
5.7	119.73	60.36	24.41	15.32	26.754	-0.03718
5.9	111.97	60.21	28.78	17.98	28.267	-0.20527
6.1	116.69	62.94	27.72	16.54	28.34	-0.04468
6.3	121.76	61.99	21.84	21.71	26.979	0.22268
6.5	123.62	60.22	23.41	20.81	25.972	0.27697
6.7	116.7	60.15	27.39	34.87	27.268	0.13545
6.9	119.31	61.53	24.77	24.39	27.28	0.35599
7.1	125.43	72.21	26.09	30.75	29.93	0.38897

Table 33. LDV Data: (03059ao.c01)

SSMEHPFTP 1st Stage Rotor LDV Data			TEST CONDITIONS:			Cp:	0.24
Data File: 03059ao.r02			Axial Position: .84 ct			V_t(m/sec):	793.7
Reduced File: 03059ao.c02			Span Position: 98%			Window	
			N_ref: 4852			Width:	2.5
			T_t: 564.2			Delay:	3.5

Theta(meas)	U-mean	V-mean	U-turb	V-turb	Alpha(meas)	Cuv
0.1	131.04	67.62	18.53	35.39	27.294	0.24828
0.3	131.19	64.63	14.99	38.79	26.225	0.19059
0.5	126.76	54.39	20.99	52.35	23.224	0.33799
0.7	123.32	48.73	16.57	27.94	21.562	0.10227
0.9	117.18	54.01	25.19	37.68	24.744	0.36859
1.1	125.91	40.7	15.33	55.35	17.915	0.57204
1.3	127.41	55.28	14.87	42.78	23.453	0.27325
1.5	126	51.7	18.34	54.45	22.311	0.16841
1.7	115.66	54.34	20.18	38.39	25.167	0.2724
1.9	120.65	47.66	19.26	45.51	21.556	0.2036
2.1	123.64	50.04	22.31	38.26	22.034	0.27361
2.3	119.37	49.24	19.58	37.62	22.418	0.32399
2.5	118.53	51.42	22.07	34.92	23.454	0.14757

Table 34. LDV Data: (03059ao.c02)

SSMEHPFTP 1st Stage Rotor LDV Data			TEST CONDITIONS:			Cp:	0.24
Data File: 03059ac.r01			Axial Position: .84 ct			V_t(m/sec):	793.2
Reduced File: 03059ac.c01			Span Position: 93%			Window	
			N_ref: 4863			Width:	2.5
			T_t: 563.5			Delay:	3.2

Theta(meas)	U-mean	V-mean	U-turb	V-turb	Alpha(meas)	Cuv
0.1	123.88	86.43	6.66	7.82	34.902	-0.15186
0.3	124.58	80.05	12.14	14.68	32.724	-0.11122
0.5	131.76	84.19	8.76	10.7	32.576	0.25729
0.7	128.1	77.39	18.95	14.82	31.139	0.09896
0.9	147.25	80.26	3.25	15.91	28.592	0.99011
1.1	125.85	70.18	10.8	14.78	29.144	0.17076
1.3	113.37	54.2	18.27	15.61	25.551	0.71391
1.5	120.09	70.53	21.29	26.14	30.425	0.47635
1.7	115.85	70.79	22.22	14.93	31.425	0.72846
1.9	119.78	63.12	24.49	23.77	27.789	0.50639
2.1	117.71	66.26	28.81	21.78	29.375	0.33776
2.3	111.92	57.34	27.82	28.08	27.128	0.43483
2.5	111.27	63.11	30.33	21.31	29.562	0.1131

Table 35. LDV Data: (03059ac.c01)

SSMEHPFTP 1st Stage Rotor LDV Data		TEST CONDITIONS:			Cp:	0.24
Data File: 03059ac.r02		Axial Position: .84 ct			V_t(m/sec):	793.3
Reduced File: 03059ac.c02		Span Position: 93%			Window	
		N_ref:	4861		Width:	2.5
		T_t:	563.6		Delay:	3.2

Theta(meas)	U-mean	V-mean	U-turb	V-turb	Alpha(meas)	Cuv
0.1	122.22	87.92	12	5.62	35.729	-0.20234
0.3	125.99	81.77	18.34	23.64	32.985	-0.45322
0.5	118.31	82.78	12.83	20.37	34.981	0.95043
0.7	123.47	88.88	13.82	6.72	35.749	-0.82488
0.9	129.98	74.27	8.81	12.67	29.744	0.27182
1.1	123.67	65.19	15.36	27.92	27.796	0.04294
1.3	118.29	66.86	25.47	30.87	29.477	-0.16541
1.5	116.53	61.73	22.72	9.64	27.912	0.67872
1.7	112.95	57.09	29.53	38.58	26.815	0.00833
1.9	121.73	63.97	20.14	12.83	27.721	-0.07287
2.1	90.12	56.85	27.97	14.1	32.244	-0.08042
2.3	110.17	63.11	27.16	24.11	29.806	0.07546
2.5	110.5	66.34	25.69	20.02	30.979	0.07018
2.7	105.74	60.72	27.49	23.27	29.868	0.10318
2.9	92.86	59.63	31.74	23.69	32.706	0.14003
3.1	96.44	60.78	33.62	15.57	32.223	-0.14907
3.3	108.72	61.06	31.07	15.72	29.319	0.12129
3.5	105.2	61.81	32.68	12.92	30.439	-0.08417
3.7	87.19	62.14	32.81	15.63	35.477	0.24012
3.9	96.71	61.72	33.95	16.8	32.547	0.0865
4.1	102.58	60.76	32.6	14.22	30.638	-0.01052
4.3	98.25	60.12	35.08	14.99	31.462	-0.06306
4.5	100.65	61.38	33.62	16.57	31.376	-0.05461
4.7	101.73	60.6	33.8	14.62	30.78	0.1191
4.9	95.83	61.49	35.1	15.03	32.684	-0.03519
5.1	94.49	62.48	35.38	14.71	33.476	-0.0544
5.3	85.5	61.05	34.94	14.11	35.525	-0.00367
5.5	85.2	62.1	35.57	15.3	36.089	-0.02103
5.7	86.34	64	34.09	15.96	36.547	0.10417
5.9	86.68	63.24	34.11	15.94	36.115	0.17262
6.1	102.64	67.2	29.93	17.58	33.214	0.10024
6.3	97.98	65.85	29.06	18.74	33.904	0.30646
6.5	94.85	65.77	28.74	17.86	34.738	0.68724
6.7	107.86	68.37	24.33	18.81	32.37	0.3356
6.9	106.04	75.14	21.76	17.88	35.324	0.63163
7.1	113.2	80.38	17.98	14.19	35.376	-0.59093

Table 36. LDV Data: (03059ac.c02)

SSMEHPFTP 1st Stage Rotor LDV Data		TEST CONDITIONS:				Cp:	0.24
Data File: 03059ai.r01		Axial Position: .84 ct				V_t(m/sec): 794.0	
Reduced File: 03059ai.c01		Span Position: 88%				Window	
		N_ref: 4863				Width:	3.2
		T_t: 564.6				Delay:	2.7

Theta(meas)	U-mean	V-mean	U-turb	V-turb	Alpha(meas)	Cuv
0.1	118.2	69.98	15.85	17.36	30.629	-0.02707
0.3	120.04	71.51	14.44	14.23	30.782	0.05894
0.5	121.8	72.06	8.16	17.93	30.609	-0.16487
0.7	117.72	74.18	18.57	18.7	32.215	0.29515
0.9	123.39	74.1	10.66	15.82	30.985	0.35694
1.1	119.94	69.68	13.88	16.8	30.158	0.25284
1.3	117.23	77.42	8.07	15.66	33.44	-0.25034
1.5	114.5	76.99	16.76	17.28	33.918	-0.16294
1.7	124.75	72.49	9.2	23.14	30.162	-0.79277
1.9	107.78	66.08	28.93	23.69	31.515	0.3794
2.1	123.14	52.67	9.73	37.64	23.159	-0.88719
2.3	116.71	65.94	26.42	21.84	29.464	0.19031
2.5	112.85	61.27	29.64	18.36	28.499	-0.0756
2.7	105.49	62.31	30.6	23.18	30.571	0.12272
2.9	100.05	60.36	34.42	21.43	31.101	-0.05797
3.1	104.18	60.83	32.91	17.9	30.282	0.15279
3.3	98.68	58.3	34.17	15.84	30.573	-0.09357
3.5	97.13	58.47	35.1	17.37	31.045	0.00143
3.7	93.45	60.85	36.73	16.34	33.071	-0.14819
3.9	93.46	60.53	36.35	14.34	32.931	-0.0395
4.1	90.65	60.9	36.03	14.2	33.893	-0.01307
4.3	94.43	60.28	36.1	15.61	32.552	0.02568
4.5	93.92	60.37	36.42	15.65	32.73	0.02268
4.7	90.99	60.89	36.35	15.16	33.789	0.04013
4.9	92.74	60.35	36.42	15.11	33.057	-0.01019
5.1	92.5	60.33	35.68	14.2	33.111	0.004
5.3	95.83	61.34	35.74	15.52	32.623	0.00431
5.5	89.41	60.98	35.95	15.21	34.295	0.02476
5.7	94.55	60.98	35.81	14.55	32.82	-0.03039
5.9	97.35	61.28	35.38	15.5	32.189	0.07065
6.1	99.06	61.77	33.96	15.58	31.947	0.04014
6.3	103.57	61.83	32.32	17.41	30.835	0.08755
6.5	100.07	62.66	32.69	16.55	32.053	0.00332
6.7	101.52	61.92	31.09	16.6	31.38	0.13157
6.9	110.83	65.72	24.78	16.22	30.667	0.24001
7.1	114.91	64.9	22.27	18.41	29.458	0.11713

Table 37. LDV Data: (03059ai.c01)

143

SSMEHPFTP 1st Stage Rotor LDV Data			TEST CONDITIONS:			Cp:	0.24
Data File: 03059ai.r02			Axial Position: .84 ct			V_t(m/sec):	793.7
Reduced File: 03059ai.c02			Span Position: 88%			Window	
			N_ref: 4861			Width:	3.2
			T_t: 564.2			Delay:	2.7

Theta(meas)	U-mean	V-mean	U-turb	V-turb	Alpha(meas)	Cuv
0.1	120.09	68.11	14.71	16.86	29.558	0.09282
0.3	121.59	71.52	11.67	17.01	30.464	-0.03972
0.5	121.57	71.71	12.14	15.48	30.536	-0.22974
0.7	122.74	75.32	12.81	15.95	31.536	-0.07647
0.9	121.19	71.51	15.94	16.23	30.544	0.44524
1.1	117.35	73.19	16.69	19.56	31.95	0.28678
1.3	120.11	62.14	17.53	13.87	27.355	0.53201
1.5	113.52	77.22	20.24	18.08	34.227	0.38634
1.7	115.52	72.25	17.3	25.94	32.021	0.10002
1.9	118.24	57.86	20.57	23.65	26.075	0.12929
2.1	109.59	63.46	21.66	33.31	30.076	0.3328
2.3	115.33	69.53	22.62	18.44	31.084	0.30504
2.5	100.53	57.31	31.93	28.43	29.685	-0.10954
2.7	103.17	58.93	32.62	27.45	29.735	0.10407
2.9	103.36	59.21	33.1	25.66	29.806	-0.27455
3.1	100.12	59.49	34.21	18.77	30.717	-0.04467

Table 38. LDV Data: (03059ai.c02)

144

APPENDIX I.   TTR EXPERIMENT CHECKLISTS

A.   TTR PRE-START CHECKLIST
1. **Axial Compressor** (A/C): START WARMING OIL (2 hours prior to running TTR by shop technician only)
2. **Shop air** (Small Compressor in A/C room):
   a. Drain Hose- PLACE OUTSIDE DOOR
   b. Outlet Valve– CLOSE (green handle)
   c. Compressor Switch- ON
   d. Tank Drain Valve– OPEN (red handle)
   e. Tank Drain Valve– CLOSED (after bleeding)
   f. Output Hose to green piping- CHECK CONNECTED
   g. Outlet Valve- OPEN
3. **TTR shop air** (test cell):
   a. Dynamometer valves (2)- CHECK FULL OPEN
   b. Air valve – OPEN (bayonet valve green pipe)
   c. Oil Mist Filters (2)- PRESS TO BLEED
   d. Oil Mist Regulator- OFF
   e. Seeding Regulators (2)- OFF (6 handles flat)
   f. Plenum Manual Inlet Valve - CHECK CLOSED (green wheel handle)
   g. Alternate Source Air Hose- ROUTE AND CONNECT (from compressor test cell to seeding regulators using T-fitting. Air supplied by bayonet valve on wall in upper control room)
4. **Cobra Probe**- CHECK RETRACTED (if installed)
5. **Calibration air** – CHECK REGULATOR PRESSURE (upper control room- 25 psi)
6. **Dynamometer cooling water:**
   a. Cooling Water- CHECK ON (A/C room)
   b. Water Supply Valve- OPEN AND VERIFY PRESSURE RISE (red handle in A/C room)
   c. Water Outlet Valve - OPEN AND VERIFY PRESSURE DROP (green handle in A/C room)
   d. Heat Exchanger Cooling Water Supply Valve- CHECK OPEN (Red handle aligned with PVC pipe in test cell)
   e. Pump Outlet Valve-CHECK OPEN (2nd Red handle aligned)
   f. Holding Tank Water Level - CHECK (wire indicator between marks)

CAUTION: ENSURE PUMP OUTLET VALVE AND BOTH DYNAMOMETER VALVES ARE OPEN PRIOR TO TURNING

145

ON SCAVENGE PUMP.

      g.   Scavenge Pump- ON (switch on cell wall)

      h.   Dynamometer Water Seal Valve- CHECK OPEN (silver knurled knob on dynamometer inlet valve)

7.   Set-up TTR Control Panel in upper control room:

      a.   Panel Breaker- ON (below shelf)

      b.   RPM read out- CHECK ZERO RPM (top of console)

      c.   #1 and #2 Dump Valves- CHECK FULL OPEN

      d.   TTR Valve (#5)- CHECK CLOSED

      e.   TTR Run Log- START

8.   Data Acquisition System Hardware Wiring:

      a.   GPIB Cables- CHECK (connected from PC to DVM, SDIU to DVM, Universal Counter to DVM, & Scanner #2 to DVM.

      b.   Universal Counter Channels A & B- CHECK (wire labeled "TTR RPM" to channel A, and wire labeled "TTR Flow Rate" to channel B)

      c.   Scanivalve #1 Cable- CHECK (black cable with large connector to junction box 'Scanivalve' position, and small gray wire cannon plug to SCU channel 20 (upper plug)

      d.   Scanivalve Pigtail- CHECK (connected between Scanivalve cable and transducer in test cell)

      e.   SDIU Cable- CHECK (gray cable with small black wire attached connected to junction box 'SDIU' position)

      f.   Solenoid Controller Wire Bundle –CHECK (white bundle connected to junction box 'CTLR2' position)

      g.   50-Pin Ribbon Cable- CHECK (connected to upper slot on back of 486 PC)

      h.   Turbine Torque Cannon Plug- CHECK (gray wire connected to SCU channel 33, upper plug)

      i.   Cobra Probe Cannon Plug- CHECK (white wire bundle connected to control box)

      j.   Mass Flow Differential Pressure Transducer (DPT)- CHECK (gray wire connected to SCU channel 24, upper plug)

9.   Instrumentation Master Power Switch- ON

10.   Instrumentation Power- ON (for all components)

11.   Calibrate Mass Flow DPT Wheatstone Bridge:

      a.   Jumper Cable- CONNECT (SCU chan 24 to DVM)

      b.   Bridge Zero- ADJUST UPPER KNOB (DVM reads zero volts)

      c.   Check Line Hose- CONNECT (blue hose to either side of DPT on wall of A/C room)

Note: If Allis Chalmers Compressor operating, disconnect other DPT line.

    d.   Check 'Gage' Switch- ON

    e.   Check 'A/C Orifice and Transducer Cal' Switch- ON

    f.   Calibration Pressure- SET 5 IN HG

    g.   Bridge Span- ADJUST LOWER KNOB (DVM to read 6.785E-3 volts)

    h.   Calibration Air- OFF (Close 'A/C Orifice and Transducer Cal' switch and open bleed valve behind console)

    i.   Iterate- REPEAT STEPS G AND H AS REQUIRED

    j.   'A/C Orifice and Transducer Cal' switch- OFF

    k.   Check Line Hose- DISCONNECT FROM DPT AND RECONNECT ORIGINAL HOSE (A/C room)

12.   Calibrate Scanivalve DPT Wheatstone Bridge:

    a.   Calibration Pressure- SET TO 10 IN HG

    b.   'Turbine' switch- ON

    c.   Jumper Cable- CONNECT (SCU chan 20 to DVM)

    d.   Scanivalve Port No. 1- ADJUST (check remote off, select #1, select port, and adjust upper knob so DVM reads zero)

    e.   Scanivalve Port No. 2- ADJUST (select and adjust lower knob so DVM reads 13.609E-3)

    f.   Iterate- REPEAT STEPS D AND E AS REQUIRED

    g.   Jumper Cable- DISCONNECT

Note: Leave 10 in Hg pressure set and 'Turbine' Switch On.

13.   Cobra Probe DPT- (if required) SET CH. 22 TO ZERO

14.   Calibrate Lebow Load Cell: (if required)

    a.   Jumper Cable- CONNECT (ch. 33 to DVM)

    b.   Bridge Zero- ADJUST (ch. 33 upper knob so DVM reads zero)

    c.   Calibration Arm- ATTACH TO DYNAMOMETER

    d.   Weights- APPLY(31.44 lb. at 2 ft from center)

    e.   Bridge Span- SET (2.197E-3 volts)

    f.   Iterate- AS REQUIRED

    g.   Weights/Arm- REMOVE

    h.   Jumper Cable- REMOVE

15.   Set up LabVIEW software on 486 PC:

    a.   C:\labview\ttr\ssme_ttr.vi- OPEN AND SET AMBIENT PRESSURE

    b.   OPEN USING NOTEPAD AND ENTER DATE AT BOTTOM OF EACH DATA FILE:

             C:\labview\ttr\TTRdata.dat,

             C:\labview\ttr\SSMEdata.dat

             C:\labview\ttr\vel_prfl.dat, (if req'd)

    c.   TTR_test.vi- OPEN

d.   Actuator.vi- OPEN (if required) Run to get read
out of Cobra probe position
    e.   Velprfl.vi- OPEN (if required)
16. **Dynamometer Outlet Water Temperature Gauge-**
     CHECK (T3 box, top of instrumentation console)
17. **Dynamometer Outlet Valve-** SET TO 50% (using TTR
     Auto Control Panel in upper control room; select
     manual mode "M", press up arrow, right button,
     set with horizontal indicator)
WARNING: ENSURE DYNAMOMETER OUTLET VALVE REMAINS
AT LEAST 10% OPEN.
NOTE: 0% IS FULL OPEN AND 100% IS FULL CLOSED.
18. **Plenum Inlet Sump Valve-** BLEED OFF WATER/DIRT
19. **Plenum Manual Inlet Valve -** OPEN
20. **Recirculation Water Pressure-** CHECK
     APPROXIMATELY 65 PSIG (Gauge on wall side of TTR)
21. **Oil mist:** (just prior to starting turbine)
     a.   Regulator- SET 30 PSI
     b.   Oil Drop Rate- CHECK AT ONE PER SECOND and
             adjust pressure as required
22. **Outside Gate-** SHUT AND LATCH

B.   LDV SYSTEM OPERATION CHECKLIST
1.   **Laser Safety Signs-** POST AT DOOR ENTRANCE AND
     WINDOW
2.   **Hardware Connections-** VERIFY CORRECT
     Note: 3-phase AC power breaker in A/C Room, Panel A
3.   **Cooling Water Discharge Hose-** ROUTE AND
     CONNECT
4.   **Beam Attenuator-** OPEN
5.   **Lens Cover-** REMOVE
6.   **Laser Start:**
     a.   Power supply Switch Bar- ON
     b.   Key Control- ON
     c.   Water Flow Rate- ADJUST (all indicator
             lights on, then open valve 1/2 turn more)
7.   **Laser Power Supply:**
     a.   Laser Power Meter Select Dial- 3 WATTS
     b.   Line Current Meter Select Dial- 50 AMPS
     c.   Light Control- CHECK FULL CCW
     d.   Current Control- CHECK FULL CCW
     e.   Control Selector- 'CURRENT'
     f.   Power On- PRESS
     g.   Power INTLK Light- CHECK ON
     h.   Ready Light- CHECK ON IN 45-60 SECONDS
     i.   Laser Start- PRESS

      j.   Current Control- SET 0.5 WATTS (eye safe)

      k.   Laser Log- START ENTRY

8.   **Traverse Table setup:**

      a.   Hand Control/Computer Control Switch-
            COMPUTER CONTROL

      b.   Power Supply Switch- ON

      c.   Sony Position Encoder- CHECK ON
            NOTE: DO NOT TURN OFF POWER OR
            REFERENCE POSITION WILL BE LOST.

9.   **Photomultiplier Power Supply set-up:**

      a.   Power Switches- ON

      b.   Current Control Knob- ONE O'CLOCK POSITION

10.   **Frequency Shifter set-up:**

      a.   Power Switches- ON

      b.   Shift Select- SET AS REQUIRED
      (Both: 1 MHz down for external seeding checkout)
      NOTE: Into flow; green up; blue down

11.   **IFA 750 Power**-ON

12.   **RMR Power**- ON

13.   **Oscilloscope Set-up** (OPR signal/burst signal):

      a.   Power- ON

      b.   Vertical Mode- ALT (dual trace)

      c.   Trigger- SLOPE

      d.   X10 Mag- PRESS OUT

      e.   Ch 1 Volts/Div (vertical scale)- 2/0.1

      f.   Ch 2 Volts/Div(horizontal scale)- 5/20m

      g.   A & B Sec/Div- 10ms/0.1μs

14.   **286 Computer (test cell):**

      a.   Video Monitor- ON

      b.   CPU- ON

      c.   Change Directory- C:\>cd FIND4

      d.   Start Program- 'FIND'

      e.   Program Menus- SET FOR LASER OPTICS CHECK

15.   **Check Laser Optics:**

      a.   Beam Crossing- CHECK (using microscope
            objective)

      b.   External Seeding- SET UP
            (attach external pipe, 30 psi, 40%, top jet on
            one seeder)

      c.   Laser- SET UP (1 W, 1 MHz shift down (both))

      d.   Beam- FOCUS IN SEEDING OUTPUT

      e.   Photomultipliers- SET ADJUST SCREWS FOR
            MAXIMUM DATA RATE (if required)

16.   **286 Computer**

      a.   Change Directory- C:\>cd PHASE

      b.   Start program- C:\PHASE>PHASE

       c.   Program Menus- SET AS REQUIRED FOR DATA
17.   Beam Reference Position- set
18.   386 Computer (Upper control room):
       a.   Video Monitor- ON
       b.   CPU- ON
       c.   Change Directory- C:\>cd PHASE
       d.   Start program- C:\PHASE>PHASE
       e.   Program Menus- SET AS REQUIRED FOR DATA
19.   Measurement Preparation
       a.   Laser Blank/Window- CLEAN
       b.   End Wall- CLEAN

C.   TTR START WITH LDV MEASUREMENT CHECKLIST

1.   TTR_test.vi- RUN (click arrow and switch)
2.   Adjust TTR Speed to 1500 RPM
       a.   No. 5 valve- OPEN TO 20% (~ 800 rpm)
       b.   Dump Valve No. 2- CLOSE (~ 1500 rpm)
      NOTE: MASS FLOW RATE NOW ACCURATE.
       c.   Test Cell- CHECK
       d.   Take LDV Measurements as necessary
           i.   Regulators- 40 TO 60 PSI
           ii.   Jet Valves- ALL OPEN
           iii.   LPM Air- 40%
           iv.   Laser Power Control- SET AS REQUIRED
           v.   SSME_TTR.VI- RUN CONCURRENT WITH LASER DATA SETS
3.   Adjust TTR Speed to 3000 RPM
       a.   No. 5 TTR valve- OPEN TO 50%
       b.   No. 1 Dump valve- CLOSE AS REQUIRED (Approximately 65%)
WARNING: CHANGE DUMP VALVE POSITIONS SLOWLY TO MAINTAIN COMPRESSOR SPEED AT 3950 ±50.
       c.   Test Cell- CHECK
       d.   Take LDV Measurements as necessary
       e.   Shift LDV Computer Ctrl to Upper Ctrl Room
       f.   Make instrumentation adjustments in test cell as necessary.
       g.   Increase Oil Mist Regulator Pres (Approx. 40 psi)
CAUTION: AVOID ENTERING TEST CELL ABOVE 3K RPM.
4.   Adjust TTR Speed to 5000 RPM
       a.   No. 5 valve- OPEN TO 80%
       b.   #1 Dump Valve- CLOSE AS REQUIRED (Approximately 45%)
       c.   Take LDV Measurements as necessary
5.   Accelerometers, Water and Bearing Temps- MONITOR FOR NORMAL INDICATIONS

6. **Log-** RECORD TTR OPERATING COND's EACH HOUR
LIMITATIONS: DYNAMOMETER WATER TEMP < 125 DEG C
BEARING TEMP < 130 DEG C
ACCELEROMETERS CHECK NORMAL

D. ***TTR EMERGENCY SHUTDOWN CHECKLIST***
1. **DUMP VALVES- BOTH OPEN**
2. **NO. 5 VALVE- CLOSE**
3. **SCAVENGE PUMP- OFF**

E. TTR SHUT-DOWN CHECKLIST
1. **Cobra Probe-** RETRACT
2. **Dump Valve No. 1-** OPEN
3. **Valve No. 5-** CLOSE TO 20%
4. **Dump Valve No. 2-** OPEN
5. **Test Cell-** CHECK
6. **Valve No. 5-** CLOSE
7. **Dynamometer Exit Valve-** FULL OPEN
8. **Manual Plenum Inlet Valve-** CLOSE
9. **Scavenge Pump-** OFF
10. **Shop Air in Test Cell-** SECURE
11. **A/C and cooling water-** ADVISE SHOP TECHNICIAN TO SECURE
12. **Red and green cooling water valves-** CLOSED
13. **Complete post run inspection**
14. **Instrumentation master switch-** OFF
15. **Console switch-** OFF
16. **Calibration air-** SET ZERO
17. **LabVIEW programs-** CLOSE

F. LDV SHUTDOWN CHECKLIST
1. **Current Control-** FULL CCW
2. **TTS**
   a. MOVE TO REFERENCE POSITION
   b. COMPUTER CONTROL
3. **Laser Power Supply:**
   a. Power Off- PRESS
   b. Key Control- OFF
   c. Power Supply Switch Bar- OFF
4. **Cooling Water-** SECURE
5. **Water Hose-** SECURE
6. **Laser Safety Sign-** STOW

APPENDIX J.   MISCELLANEOUS SOFTWARE PROGRAMS

1.   RVCQ3Dmod1

```
**********************************************************
'qin' and 'bcio' subroutine mods referred to RVCQ3Dmod1.
**********************************************************
      subroutine bcio
c     inlet, exit, and cut b.c.
      include 'commz1'
      real qbe(2),cu1(200),cu2(200),cu3(200),cu4(200),tal(200)
      real r0in(200)


*----------------------------------------------------------------
c     inlet b.c.
c     ibcin = 1: inlet r*vth specified (default)
c     ibcin = 2: inlet bc fixed at ic (no change)
c     ibcin = 3: inlet angle specified
c     note that vin & alin are set by q3dic

      if(ibcin.ne.2)then

      rgm =1./gm
      gdgm=g/gm
c
c

      if(ibcin.eq.1)then
      do i=mil,mir
            r0in(i)=p0in(i)/t0in(i)
            tal(i)=tan(alin(i))
            cu3(i) =gp
            cu1(i) =gp*(4.*t0in(i)/gm-2.*vin(i)**2)
            cu2(i) =2.*gm
      enddo
      else
      do i=mil,mir
            r0in(i)=p0in(i)/t0in(i)
            tal(i)=tan(alin(i))
            cu3(i) =gp+2.*tal(i)**2
            cu1(i) =cu3(i)*4.*t0in(i)/gm
            cu2(i) =2.*gm*(1.+tal(i)**2)
        enddo
      endif

c     store rminus in a(i)
      do 10 i=mil,mir
      j=n2
      r2=1./qq(1,i,j)
      u2=qq(2,i,j)*r2
      v2=qq(3,i,j)*r2
      c2=sqrt(max(0.,g*p(i,j)*r2))
      rmi2=u2-2.*rgm*c2
   10 a(i)=rmi2

c     force periodicity between (mil,n) & (mir,n) by averaging rminus
      a(mil)=.5*(a(mil)+a(mir))
      a(mir)=a(mil)

c     update solution on boundary using new rminus
      j=nm
      do 20 i=mil,mir
      rmi1=a(i)
```

```fortran
         cu4(i)=max(0.,cu1(i)-cu2(i)*rmi1**2)
c        write(*,*)cu1(i),cu2(i),cu3(i),cu4(i),a(i)
         u1 =max(.01,(gm*rmi1+sqrt(cu4(i)))/cu3(i))
         if(ibcin.eq.1)v1=vin(i)
         if(ibcin.eq.3)v1=u1*tal(i)
         q1sq=u1**2+v1**2
         c1sq=t0in(i)-gmd2*q1sq
         beta=1.+gmd2*q1sq/c1sq
         p1  =p0in(i)/(g*beta**gdgm)
         rho1=r0in(i)/beta**rgm
         p(    i,j)=p1
         qq(1,i,j)=rho1
         qq(2,i,j)=rho1*u1
         qq(3,i,j)=rho1*v1
   20    qq(4,i,j)=rgm*p1+.5*rho1*q1sq

c        reset dummy grid lines
         do 25 k=1,4
         do 25 i=mil,mir
   25    qq(k,i,n)=qq(k,i,nm)
c  25    qq(k,i,n)=2.*qq(k,i,nm)-qq(k,i,n2)

         do 26 i=mil,mir
   26    p(i,n)=gm*(qq(4,i,n)-.5*(qq(2,i,n)**2+qq(3,i,n)**2)/qq(1,i,n))

         endif
*-----------------------------------------------------------------------
c        exit b.c.
c        ibcex = 1: exit pressure ratio specified (default)
c        ibcex = 2: reset energy by extrapolation
c        ibcex = 3: Giles' exit bc sets average prat using characteristics

         do 30 i=1,m,mm
         if(i.eq.1)then
         i2=2
         i3=3
         else
         i2=mm
         i3=m2
         endif

         do 30 j=1,n
c        extrapolate q1 - q3
         qq(1,i,j)=2.*qq(1,i2,j)-qq(1,i3,j)
         qq(2,i,j)=2.*qq(2,i2,j)-qq(2,i3,j)
         qq(3,i,j)=2.*qq(3,i2,j)-qq(3,i3,j)

         if(ibcex.eq.1)then
c        prat specified
         qq(4,i,j)=prat/gm+.5*(qq(2,i,j)**2+qq(3,i,j)**2)/qq(1,i,j)

         else if(ibcex.eq.2)then
c        extrapolate q4
         qq(4,i,j)=2.*qq(4,i2,j)-qq(4,i3,j)
         endif

   30    p(i,j)=gm*(qq(4,i,j)-.5*(qq(2,i,j)**2+qq(3,i,j)**2)/qq(1,i,j))

         if(ibcex.eq.3)then
c        find average exit density and velocity
         qbe(1)=0.
         qbe(2)=0.
         do 40 i=1,m,mm
         do 40 j=2,nm
         dy=abs(y(i,j)-y(i,j-1))
         dj=qq(1,i,j)
         dm=qq(1,i,j-1)
         uj=qq(2,i,j)   /dj
         um=qq(2,i,j-1)/dm
```

154

```
      qbe(1)=qbe(1)+.5*dy*(dj+dm)
   40 qbe(2)=qbe(2)+.5*dy*(dj*uj**2+dm*um**2)
      ubar=sqrt(qbe(2)/qbe(1))
      rbar=qbe(1)/(ubar*abs(pitch))
      cbar=sqrt(g*prat/rbar)

c     rescale exit pressure using dp=rho*c*du; reset q4
      do 50 i=1,m,mm
      do 50 j=1,n
      u1=qq(2,i,j)/qq(1,i,j)
      ps=prat*(1.+g*(u1-ubar)/cbar)
      p(    i,j)=ps
   50 qq(4,i,j)=ps/gm+.5*(qq(2,i,j)**2+qq(3,i,j)**2)/qq(1,i,j)
      endif
*------------------------------------------------------------------------
c     averaged solution along cut
      if(mtl-1.lt.2)return
      do 60 k=1,4
cdir$ ivdep
      do 60 il=2,mtl-1
      ir=mp-il
      qbar=.5*(qq(k,il,2)+qq(k,ir,2))
c     qbar=(4.*(qq(k,il,2)+qq(k,ir,2))-(qq(k,il,3)+qq(k,ir,3)))/6.
      qq(k,il,1)=qbar
   60 qq(k,ir,1)=qbar

      do 65 il=2,mtl-1
      ir=mp-il
      ps=gm*(qq(4,il,1)-.5*(qq(2,il,1)**2+qq(3,il,1)**2)/qq(1,il,1))
      p(il,1)=ps
   65 p(ir,1)=ps

      return
      end


************************

      subroutine qin
c     reads plot3d compatible restart files in relative frame
      include 'commz1'
      real qqin(200,4)

c     save inlet b.c.
      j=nm
      do 10 k=1,4
      do 10 i=mil,mir
   10 qs(k,i,j)=qq(k,i,j)

c     read plot3d-compatable file
      if(ich.eq.0)nj=nm
      if(ich.eq.1)nj=n
      read(2)im,jn

      if(im.ne.m.or.jn.ne.nj)then
      write(6,600)m,nj,im,jn
      stop
      endif

      read(2)dum,dum,dum,time
      read(2)(((qq(k,i,j),i=1,m),j=1,nj),k=1,4)
      read(2)idum,idum,idum,nres,idum,dum,dum,dum
      read(2)((resd(nr,l),nr=1,nres),l=1,5)
      read(2)((qq(k,i,n),i=1,m),k=1,4)

c     reset residual history if ires < 0
      if(ires.ge.0)then
      iter=int(time)
      else
      ires=abs(ires)
```

155

```fortran
      iter=0
      nres=0
      endif

c     convert to absolute system
      do 20 j=1,n
      do 20 i=1,m
      ruq=qq(2,i,j)**2
      rcvt=qq(4,i,j)-.5*(ruq+qq(3,i,j)**2)/qq(1,i,j)
      qq(3,i,j)=qq(3,i,j)+r(i,j)*omega*qq(1,i,j)
      qq(4,i,j)=rcvt+.5*(ruq+qq(3,i,j)**2)/qq(1,i,j)
   20 p(    i,j)=gm*(qq(4,i,j)-.5*(qq(2,i,j)**2+qq(3,i,j)**2)/qq(1,i,j))
c
      OPEN(UNIT=65,FILE='qin.dat',STATUS='UNKNOWN')
      do i=mil,mir
            read(65,*)(qqin(i,k),k=1,4)
c           write(*,*)(qqin(i,k),k=1,4)
      enddo
c
      gdgm=g/gm
c
      do i=mil,mir
      uin=qqin(i,2)/qqin(i,1)
      vin(i)=qqin(i,3)/qqin(i,1)
      tsin=qqin(i,4)/qqin(i,1)-.5*(uin**2+vin(i)**2)
      tsi=g*gm*tsin
      psi=qqin(i,1)*tsi
      vsq=uin**2+vin(i)**2
      t0in(i)=tsi+gmd2*vsq
      csi=sqrt(tsi)
      emi=(sqrt(vsq))/csi
      p0in(i)=psi*(1.+gmd2*emi**2)**gdgm
c      psin=gm*(qqin(i,4)-.5*(qqin(i,2)**2+qqin(i,3)**2)/qqin(i,1))
c      tsin=psin/qqin(i,1)
c      sosin=sqrt(g*gm*tsin)
c     vin(i)=qqin(i,3)/qqin(i,1)
c      win=sqrt((qqin(i,2)**2+qqin(i,3)**2)/qqin(i,1)**2)
c      amachin=win/sosin
c      t0in(i)=tsin*(1.+(gm/2.)*amachin**2)
c      p0in(i)=psin*(t0in(i)/tsin)**(g/gm)
      alin(i)=atan2(qqin(i,3),qqin(i,2))
      enddo

c     reset inlet b.c. if iresti = 2
      if(iresti.eq.2)then
      j=nm
      do 30 k=1,4
      do 30 i=mil,mir
   30 qq(k,i,j)=qs(k,i,j)
      endif

  600 format(/,' ***** fatal error (qin.600) *****',/,
     &' m,  n read from input           ',2i5,' do not match',/,
     &' m,  n read from restart file ',2i5)

      return
      end
```

156

2. Wake_Interpolation.m

```
%File for linear interpolation of output wake grids from RVCQ3D Q-files
%to be used as input Q-files for downstream solutions.

%C. Scott Anderson
clear all
close all
delete qin.dat


%q format [y_coordinate, rho, rho_u, rho_v, e]
%Run script 'stator_out.m'
load qout0.mat

[m_out,n_out]=size(qout0);
qout=qout0;

%grid coordinates for rotor input q vector
%Run script 'rotor_in.m'
load yin.mat

[m_in,n_in]=size(yin);
qin(:,1)=yin;
yqin=yin(m_in,1)-yin(1,1);


%Timestep qout
timesteps=1;        %Input # of timesteps
step=0.02;            %Input size of timestep in grid units

%Determine wake passings
steps_per_pass=floor(yqin/step)
wake_passes=ceil(timesteps/steps_per_pass)

for p=1:wake_passes             %Set up wake passes

for t=1:steps_per_pass          %Set up timesteps per wake pass

    %Stretch stator wake to match rotor
    yqout0=qout0(m_out,1)-qout0(1,1);
    yqin=yin(m_in,1)-yin(1,1);
    yratio =yqin/yqout0;
    qoutstretch=qout0;
    qoutstretch(:,1)=yratio*qout0(:,1);

    %Shift qout(:,1) to qin
    yshift=yin(1,1)-qoutstretch(1,1);
    qoutshift=qoutstretch;
    qoutshift(:,1)=qoutstretch(:,1)+yshift;
    qout=qoutshift;

    %Timestep qout
    qout_temp=qout;
    qout_temp(:,1)=qout(:,1)+(t*step);
    qgrtr=find(qout_temp(:,1)>yin(m_in,1));
    [m_qgrtr,n_qgrtr]=size(qgrtr);
    for s=(m_qgrtr+1):m_out
        qout(s,:)=qout_temp((s-m_qgrtr),:);
    end
    for s=1:m_qgrtr
        qout(s,:)=qout_temp((s+m_out-m_qgrtr),:);
        qout(s,1)=qout(s,1)-yqin;
    end

    %Stretch timestepped stator wake to match rotor
    yqout=qout(m_out,1)-qout(1,1);
```

```
        yratio =yqin/yqout;
        qoutstretch=qout;
        qoutstretch(:,1)=yratio*qout(:,1);
        qout=qoutstretch;

        %Shift timestepped stator wake to match rotor
        yshift=yin(1,1)-qout(1,1);
        qout(:,1)=qout(:,1)+yshift;

%Perform interpolation from qout to qin
jless=0;
jgrtr=0;

for i=1:m_in                                    %Size qin
    jequal=find(qout(:,1)==qin(i,1));


    if isempty(jequal)==0
        numequal=size(jequal);
        for e=1:numequal
        qin(i,2)=qout(jequal(e),2);
        qin(i,3)=qout(jequal(e),3);
        qin(i,4)=qout(jequal(e),4);
        qin(i,5)=qout(jequal(e),5);
        end
    else
        jless=max(find(qout(:,1)<qin(i,1)));
        if isempty(jless)==1
            jless=0;
        else
        end
        jgrtr=min(find(qout(:,1)>qin(i,1)));
        if isempty(jgrtr)==1
            jgrtr=0;
        else
        end
        dy=qout(jgrtr,1)-qout(jless,1);

        drho=qout(jgrtr,2)-qout(jless,2);
        m=drho/dy;
        b=qout(jless,2)-m*qout(jless,1);
        qin(i,2)=m*qin(i,1)+b;

        drho_u=qout(jgrtr,3)-qout(jless,3);
        m=drho_u/dy;
        b=qout(jless,3)-m*qout(jless,1);
        qin(i,3)=m*qin(i,1)+b;


        drho_v=qout(jgrtr,4)-qout(jless,4);
        m=drho_v/dy;
        b=qout(jless,4)-m*qout(jless,1);
        qin(i,4)=m*qin(i,1)+b;


        d_e=qout(jgrtr,5)-qout(jless,5);
        m=d_e/dy;
        b=qout(jless,5)-m*qout(jless,1);
        qin(i,5)=m*qin(i,1)+b;

    end
end                         %Interpolation Loop

%Ensure symmetry in qin
qin(m_in,2:5)=qin(1,2:5);

%PRACTICE PLOTS FOR COMPARISON
figure(1)
pause
```

```
plot(qin(:,1),qin(:,2),'y',qout(:,1),qout(:,2),'c')




    end                 %Timesteps per pass

    end                 %Wake passes

figure(2)
plot(qin(:,1),qin(:,2),'y',qin(:,1),qin(:,3),'m',...
qin(:,1),qin(:,4),'c',qin(:,1),qin(:,5),'r')
hold on
plot(qout(:,1),qout(:,2),'y',qout(:,1),qout(:,3),'m',...
qout(:,1),qout(:,4),'c',qout(:,1),qout(:,5),'r')
hold off

diary qin.dat
qin(:,2:5)
diary off
```

LIST OF REFERENCES

1. Pratt and Whitney Website, http://www.pratt-whitney.com/engines/gallery/turbopump.cut.html, United Technologies Corp., April 10, 1999.

2. Sutton, G.P., "Rocket Propulsion Elements, An Introduction to the Engineering of Rockets", Sixth Edition, John Wiley & Sons Inc., 1992.

3. Chima, R.V., "TCGRID 3-D Grid Generator for Turbomachinery", User's Manual and Documentation, Version 202, October 1, 1996.

4. Chima, R.V., "SWIFT version 107", Preliminary Documentaion, July 1, 1997.

5. Chima, R.V., "RVCQ3D-Rotor Viscous Code 3-D", User's Manual and Documentation, Version 303, March 1, 1999.

6. McKee, J.R., "Experimental and Computational Investigation of Cold-Flow Through the Turbine of the Space-Shuttle Main Engine High Pressure Fuel Turbopump", Master's Thesis, Naval Postgraduate School, Monterey, California, March 1998.

7. Durst, F., Melling, A., and Whitelaw, J.H., "Principles and Practice of Laser Doppler Anemometry", Academic Press, Inc., 1976.

8.   Zaccaria, M.A. and Lakshminarayana, B., "Unsteady Flow Field Due to Nozzle Wake Interaction with the Rotor in an Axial Flow Turbine: Part I- Rotor Passage Flow Field", Journal of Turbomachinery, Volume 119, Number 2, pages 201-224, April 97.

9.   Zaccaria, M.A. and Lakshminarayana, B., "Unsteady Flow Field Due to Nozzle Wake Interaction with the Rotor in an Axial Flow Turbine: Part II- Rotor Exit Flow Field", Journal of Turbomachinery, Volume 119, Number 2, pages 214-224, April 97.

10. Studevan, C.C., "Design of a Cold-Flow Test Facility for the High-Pressure Fuel Turbopump Turbine of the Space Shuttle Main Engine", Master's Thesis, Naval Postgraduate School, Monterey, California, December 1993.

11. Rutkowski, R.J., "Cold-flow Simulation of the Alternate Turbopump Development Turbine of the Space Shuttle Main Engine High Pressure Fuel Turbopump", Master's Thesis, Naval Postgraduate School, Monterey, California, March 1994.

12. Greco, P.A., "Turbine Performance Mapping of the Space-Shuttle Main Engine High-Pressure Fuel Turbopump", Master's Thesis, Naval Postgraduate School, Monterey, California, September 1995.

13. Southward, J.D., "Laser Doppler Velocimetry in the Space-Shuttle Main Engine High-Pressure Fuel Turbopump", Master's Thesis, Naval Postgraduate School, Monterey, California, March 1998.

14. Wendt, John F., "Computational Fluid Dynamics", 2nd edition, Springer-Verlag, Berlin, Germany, 1996.

15. TSI, "Phase Resolved Software (PHASE)", Instruction Manual, Part Number 1990564, Preliminary Revision 2, March 1992.

16. Chima, R.V., "Revised Grape Code Input for Cascades", User's Manual, June 1990.

17. Sorenson, R.L., "A computer Program to Generate Two-Dimensional Grids about Airfoils and Other Shapes by Use of Poisson's Equations", NASA Technical Memorandum-81198, 1980.

18. Chima, R.V., "TCGRID (Turbomachinery C GRID)", User's Manual, November 1990.

19. Chima, R.V., "RVCQ3D (Rotor Viscous Code Quasi 3D) Documentation", August 1990.

20. Chima, R.V., "Calculation of Multistage Turbomachinery Using Steady Characteristic Boundary Condtions", NASA Technical Memorandum-206613, 1998.

21. Chima,R.V., "RVC3D (Rotor Viscous Code 3D)", User's manual, March, 1992.

22. TSI, "Laser Doppler Velocimetry Components", TSI, Incorporated, 1998.

23. TSI, "Flow Information Display Software (FIND)", Instruction Manual, Part Number 1990585, Version 3.5, January 1992.

INITIAL DISTRIBUTION LIST

No. of Copies

1. Defense Technical Information Center.................................. 2
    8725 John J. Kingman Rd., Ste 0944
    Ft. Belvoir, VA 22060-6218

2. Dudley Knox Library 2
    Naval Postgraduate School
    411 Dyer Rd.
    Monterey, CA 93943-5101

3. Department Chairman, Code AA 1
    Department of Aeronautics and Astronautics
    Naval Postgraduate School
    699 Dyer Road, Rm. 137
    Monterey, CA 93943-5107

4. Dr. Garth V. Hobson, Code AA/HG 5
    Department of Aeronautics and Astronautics
    Naval Postgraduate School
    699 Dyer Road, Rm. 137
    Monterey, CA 93943-5107

5. Dr. Raymond P. Shreeve, Code AA/SF................................. 1
    Department of Aeronautics and Astronautics
    Naval Postgraduate School
    699 Dyer Road, Rm. 137
    Monterey, CA 93943-5107

6. Naval Air Warfare Center 1
    AIR-4.4.T (Attn: Mr. C. Gorton)
    Propulsion and Power Engineering, Building 106
    Patuxent River, MD 20670-5304

7. Naval Air Warfare Center 1
    AIR-4.4.3 (Attn: Mr. J. Zidzik)
    Propulsion and Power Engineering, Building 106
    Patuxent River, MD 20670-5304

8. Naval Warfare Center Aircraft Division 1
    AIR-4.4.3.1 (Attn: D. Parish)
    Propulsion and Power Engineering, Building 106
    Patuxent River, MD 20670-5304

9. C. Scott Anderson 2
    4604 Oceanfront Ave.
    Virginia Beach, VA 23454